Cell Stem Cell

Resource

A suite of new Dre recombinase drivers markedly expands the ability to perform intersectional genetic targeting

Graphical Abstract

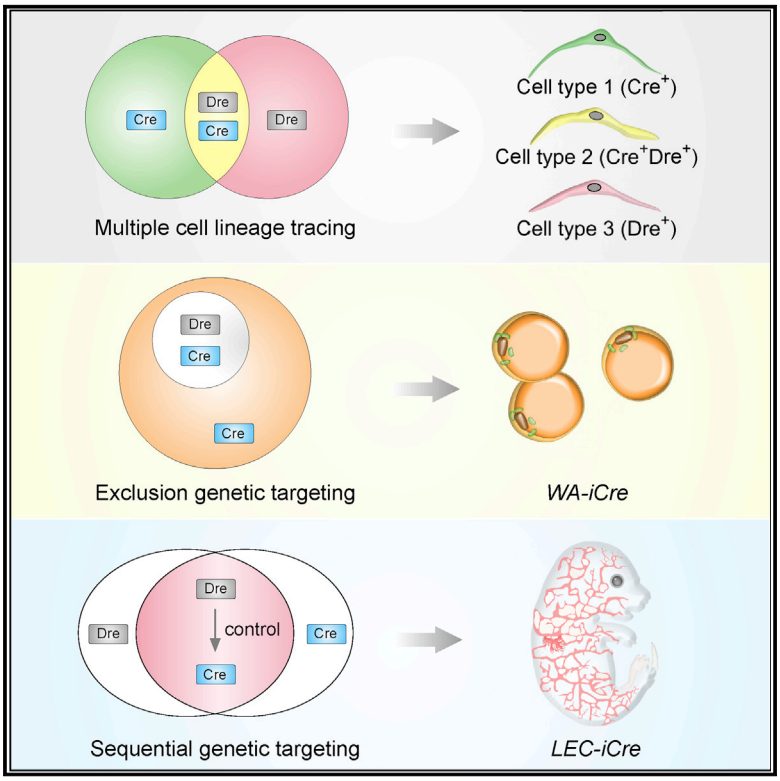

Highlights

- More than 70 new Dre driver lines are provided as a resource for intersectional genetics
- PDGFRa^{+}PDGFRb^{+} or PDGFRa^{+} perivascular cells contribute to *de novo* adipocytes
- "Exclusion" dual recombinase enables gene deletion in white but not brown adipocytes
- Sequential dual recombinase enables gene deletion in lymphatic endothelial cells

Authors

Ximeng Han, Zhenqian Zhang, Lingjuan He, ..., Lixin Wang, Ben He, Bin Zhou

Correspondence

drheben@126.com (B.H.), zhoubin@sibs.ac.cn (B.Z.)

In Brief

The combinatory use of Dre and Cre recombinase-mediated intersectional genetics significantly enhances the precision of *in vivo* lineage tracing and gene targeting. Han et al. developed more than 70 new intersectional drivers to target diverse cell lineages. Highlighting their application, Han et al. used these new tools to study perivascular progenitors of adipocytes and performed gene knockout in white adipocytes (WAs) and lymphatic endothelial cells (LECs).

Han et al., 2021, Cell Stem Cell *28*, 1–17
June 3, 2021 © 2021 Elsevier Inc.
https://doi.org/10.1016/j.stem.2021.01.007

CellPress

Please cite this article in press as: Han et al., A suite of new Dre recombinase drivers markedly expands the ability to perform intersectional genetic targeting, Cell Stem Cell (2021), https://doi.org/10.1016/j.stem.2021.01.007

Cell Stem Cell

CellPress

Resource

A suite of new Dre recombinase drivers markedly expands the ability to perform intersectional genetic targeting

Ximeng Han,[1,10,13] Zhenqian Zhang,[1,13] Lingjuan He,[1,13] Huan Zhu,[1,13] Yan Li,[1] Wenjuan Pu,[1] Maoying Han,[10] Huan Zhao,[1] Kuo Liu,[1,11] Yi Li,[1,2] Xiuzhen Huang,[1] Mingjun Zhang,[1] Hengwei Jin,[1] Zan Lv,[1] Juan Tang,[1] Jinjin Wang,[3] Ruilin Sun,[3] Jian Fei,[3] Xueying Tian,[4] Shengzhong Duan,[5,6] Qing-Dong Wang,[7] Lixin Wang,[8,9] Ben He,[2,*] and Bin Zhou[1,10,11,12,14,*]

[1]State Key Laboratory of Cell Biology, Shanghai Institute of Biochemistry and Cell Biology, Center for Excellence in Molecular Cell Science, Chinese Academy of Sciences, University of Chinese Academy of Sciences, Shanghai 200031, China

[2]Department of Cardiology, Shanghai Chest Hospital, Shanghai Jiaotong University, Shanghai, China

[3]Shanghai Engineering Research Center for model organizations, Shanghai Model Organisms Center, Inc., Shanghai, China

[4]Key Laboratory of Regenerative Medicine of Ministry of Education, College of Life Science and Technology, Jinan University, Guangzhou, China

[5]Laboratory of Oral Microbiota and Systemic Diseases, Shanghai Ninth People's Hospital, College of Stomatology, Shanghai Jiao Tong University School of Medicine, Shanghai 200125, China

[6]National Clinical Research Center for Oral Diseases, Shanghai Key Laboratory of Stomatology & Shanghai Research Institute of Stomatology, Shanghai 200011, China

[7]Bioscience Cardiovascular, Research and Early Development, Cardiovascular, Renal and Metabolism (CVRM), BioPharmaceuticals R&D, AstraZeneca, Gothenburg, Sweden

[8]Department of Vascular Surgery, Zhongshan Hospital, Fudan University, Shanghai, China

[9]Department of Vascular Surgery, Xiamen Branch, Zhongshan Hospital, Fudan University, Xiamen, China

[10]School of Life Science and Technology, ShanghaiTech University, 100 Haike Road, Shanghai 201210, China

[11]School of Life Science, Hangzhou Institute for Advanced Study, University of Chinese Academy of Sciences, Hangzhou 310024, China

[12]Institute for Stem Cell and Regeneration, Chinese Academy of Sciences, Beijing 100101, China

[13]These authors contributed equally

[14]Lead contact

*Correspondence: drheben@126.com (B.H.), zhoubin@sibs.ac.cn (B.Z.)

https://doi.org/10.1016/j.stem.2021.01.007

SUMMARY

The use of the dual recombinase-mediated intersectional genetic approach involving Cre-loxP and Dre-rox has significantly enhanced the precision of *in vivo* lineage tracing, as well as gene manipulation. However, this approach is limited by the small number of Dre recombinase driver constructs available. Here, we developed more than 70 new intersectional drivers to better target diverse cell lineages. To highlight their applicability, we used these new tools to study the *in vivo* adipogenic fate of perivascular progenitors, which revealed that PDGFRa^{+} but not PDGFRa^{-}PDGFRb^{+} perivascular cells are the endogenous progenitors of adult adipocytes. In addition to lineage tracing, we used members of this new suite of drivers to more specifically knock out genes in complex tissues, such as white adipocytes and lymphatic vessels, that heretofore cannot be selectively targeted by conventional Cre drivers alone. In summary, these new transgenic tools expand the intersectional genetic approach while enhancing its precision.

INTRODUCTION

Unraveling the cellular and molecular mechanisms that underlie the generation of specialized cell types and their coordinated functions is critical for deepening our understanding of organ development, tissue homeostasis, and regeneration. Recombinase-mediated genetic targeting provides an important platform to track cellular origins and fates *in vivo*, while also elucidating the genetic regulation of cell behavior in multiple biological processes, such as embryogenesis, tumorigenesis, and tissue regeneration (Kretzschmar and Watt, 2012; Jensen and Dymecki, 2014; Baron and van Oudenaarden, 2019; Liu et al., 2020). Over the past three decades, among many types of recombinases, the Cre-loxP system represents the most widely used approach for *in vivo* molecular and cellular study in animal models (Sauer and Henderson, 1988; Lakso et al., 1992; Schwenk et al., 1995). The linchpin of this system for precise genetic manipulation depends on the specificity of the genetic promoter used to express Cre (Molkentin and Houser, 2013; Tian et al., 2015). However, many of the Cre drivers used are not sufficiently specific, inadvertently resulting in inaccurate data interpretation and thus sometimes in contradictory conclusions regarding cell fate

Please cite this article in press as: Han et al., A suite of new Dre recombinase drivers markedly expands the ability to perform intersectional genetic targeting, Cell Stem Cell (2021), https://doi.org/10.1016/j.stem.2021.01.007

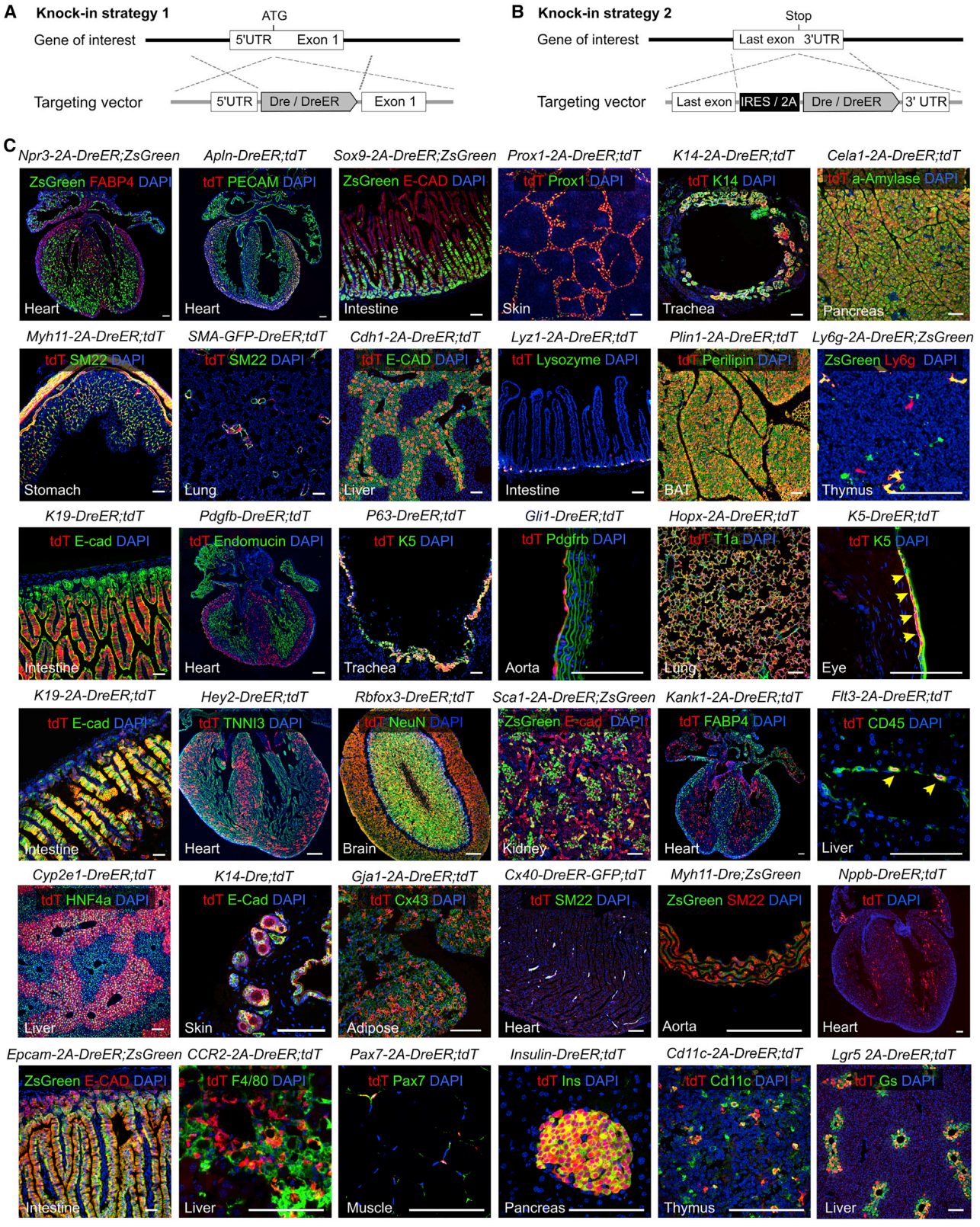

(legend on next page)

Please cite this article in press as: Han et al., A suite of new Dre recombinase drivers markedly expands the ability to perform intersectional genetic targeting, Cell Stem Cell (2021), https://doi.org/10.1016/j.stem.2021.01.007

and gene function analyses (Eschenhagen et al., 2017; He et al., 2020). Indeed, this lack of specificity of single promoters to drive Cre expression is highlighted by recent single-cell RNA sequencing (scRNA-seq) technology that has identified the genetic complexity of numerous cell populations within a given tissue (Cohen et al., 2018; Di Talia and Poss, 2016; Aran et al., 2019).

One important way to understand newly identified cell subtypes requires their *in vivo* manipulation at both the cellular and molecular levels, so that one can understand if the cells play critical function(s) during normo- and pathophysiology. Although many new markers have been identified to define these subpopulations of cells, most often it is technically challenging to use a single marker to genetically target a specific sub-type of cells *in vivo*. It has been reported that other orthogonal recombinases could be combined with Cre-loxP (Jensen et al., 2008; Kim et al., 2009; He et al., 2016) to enhance the specificity of targeting a subpopulation of cells that would otherwise not be achievable with reliance on a single recombinase. Recently, a suite of diverse reporters that respond to the recombinases Cre, Dre, and Flpe has permitted enhanced cell type targeting and functionality *in vivo* (Daigle et al., 2018; Li et al., 2018). However, the demand for genetic tools with enhanced specificity and performance still far exceeds their current availability (Zhao and Zhou, 2019). We therefore aimed to generate a diverse set of cell type-specific mouse lines for the Dre recombinase, which is orthogonal to the Cre-loxP system (Anastassiadis et al., 2009; Hermann et al., 2014). In the present study, we generated more than 70 new Dre lines, which, together with several distinct types of intersectional genetic approaches also reported here, provide an invaluable genetic tool of broad utility in multiple diverse life science fields.

Several decades of pioneering research into adipogenesis have consistently suggested that *de novo* formation of adipocytes takes place close to the vessel wall, leading to the inference of the existence of perivascular stem cells or progenitors (Gesta et al., 2007; Tang et al., 2008; Berry et al., 2014; Vishvanath et al., 2016; Min et al., 2016). However, the exact nature of such perivascular stem cells remains incompletely known and even controversial in the field (Guimarães-Camboa et al., 2017; Vishvanath et al., 2017; Guimarães-Camboa and Evans, 2017; Cano et al., 2017). Previous studies using lineage tracing on the basis of *Pdgfrb-Cre* or inducible *Pdgfrb-rtTA* revealed pericytes as perivascular progenitor cells of adipocytes (Tang et al., 2008; Vishvanath et al., 2016). Additional studies using different Cre drivers support a mural cell origin of adipocytes in the adult stage (Long et al., 2014; Jiang et al., 2014; Berry et al., 2017). However, another recent study showed that pericytes or smooth muscle cells labeled by *Tbx18-CreER* maintained their identity in diverse pathological settings without contributing to other cell lineages (e.g., adipocytes) (Guimarães-Camboa et al., 2017), challenging the current view of endogenous pericytes as perivascular progenitors of adipocytes. Studies using Pdgfra labeling reported that perivascular PDGFRa$^+$ cells make a significant contribution to mature adipocytes in adult fat depots (Lee et al., 2012; Berry and Rodeheffer, 2013; Jeffery et al., 2015; Cattaneo et al., 2020). Despite reported specific and efficient labeling of mural cells by the aforementioned markers, such as PDGFRb (Vishvanath et al., 2017), PDGFRb is also reported to be expressed in a subset of adventitial fibroblasts (Guimarães-Camboa and Evans, 2017; Cattaneo et al., 2020). Here we used intersectional genetic approach to reassess the contribution of perivascular stem cells marked by distinct gene signatures to adipocytes in adult tissues.

In addition to enhancing the precision of genetic lineage tracing, intersectional genetics enables more specific gene deletion in cell lineages that is not achievable with previous Cre-loxP strategies. Here we provided two examples on how to use NOT or AND logic to perform any flox gene deletion specifically in tissues that have not been previously achieved using singular Cre drivers. By developing NOT-logic sequential intersectional genetics, we successfully delete genes specifically in white adipocytes (WAs). Using AND-logic sequential intersectional genetics, we generated the first authentic Cre driver for both lineage tracing and gene deletion exclusively in lymphatic vessels. Our expansion here of the available Dre driver suite increases the ability to genetically manipulate cell lineages of interest more precisely, allowing a deeper understanding of cell behaviors and gene functions in multiple life science disciplines.

RESULTS

Generation and characterization of new Dre or DreER drivers

To enable the broader application of intersectional approaches in multiple fields, we developed more than 70 new genetic drivers, each of which was based mainly on a Dre or DreER strategy. In these new mouse lines, cDNA encoding Dre or DreER was knocked into the endogenous gene locus by replacing the translational start codon (ATG) using CRISPR-Cas9 (Figure 1A). For some alleles, it is critical to keep the endogenous gene intact, as the heterozygote state might have functional effects on cells. For this purpose, cDNA encoding Dre or DreER linked downstream to an internal ribosome entry site (IRES) or self-cleaved 2A peptide was then knocked into the translational stop codon just upstream of the 3′ UTR (Figure 1B). For the first strategy, we named the mouse line *gene name-Dre* or *gene name-DreER*, and for the second strategy we named the lines *gene name-2A/IRES-Dre* or *gene name-DreER*. The nomenclatures reflect the different targeting strategies in this study. Of all these knockin mouse lines, the majority were generated by homologous recombination using CRISPR-Cas9, while a few were generated by a conventional embryonic stem cell (ESC)-based strategy using positive and negative selection of correct targeted clones.

To systematically characterize the Dre or DreER drivers, we crossed each of these mice with Dre-rox-responsive tdTomato or ZsGreen reporter lines (Madisen et al., 2015; He et al., 2017b).

Figure 1. Generation and characterization of new Dre or DreER mouse alleles

(A and B) Schematic diagram illustrating the knockin strategies of Dre or DreER into the 5′ UTR or 3′ UTR of genes of interest by homologous recombination. (C) Examples of immunostaining images on tissue sections collected from 36 new mouse lines. Nuclei are stained with DAPI. BAT, brown adipose tissue. Scale bars, 100 μm. Each image is representative of five individual biological samples. Information for more mouse lines is listed in Table S1. See also Figure S1 and Tables S1 and S2.

Please cite this article in press as: Han et al., A suite of new Dre recombinase drivers markedly expands the ability to perform intersectional genetic targeting, Cell Stem Cell (2021), https://doi.org/10.1016/j.stem.2021.01.007

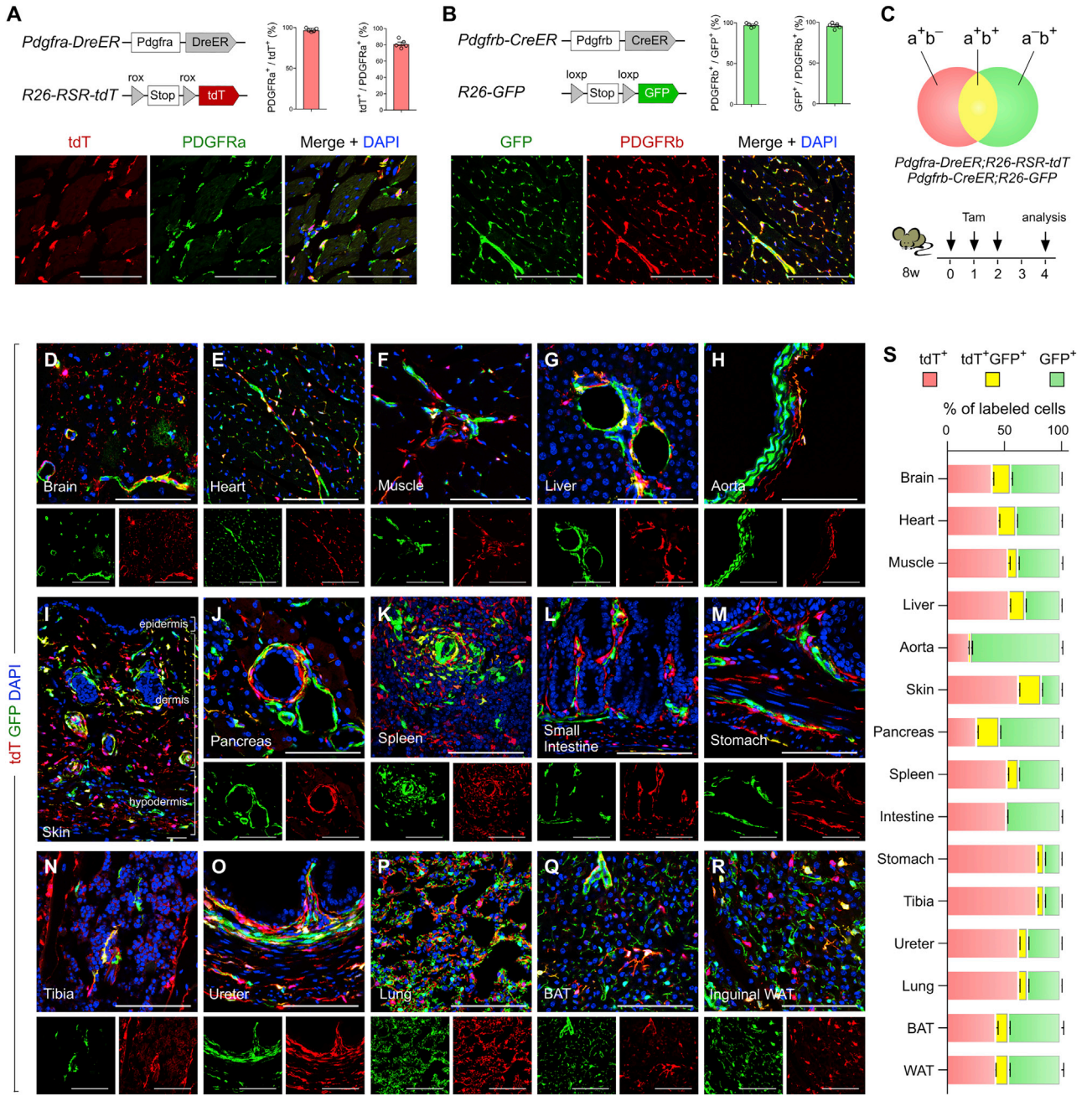

Figure 2. Generation of intersectional genetic strategies for labeling of PDGFRa$^+$ and/or PDGFRb$^+$ perivascular cells

(A) Schematic diagram illustrating genetic labeling of PDGFRa$^+$ cells by *Pdgfra-DreER* and its reporter *R26-RSR-tdT*. Lower panel shows immunostaining on heart sections for tdT and PDGFRa. Right panel shows quantification of the percentage of tdT$^+$ cells expressing PDGFRa (specificity) and the percentage of PDGFRa$^+$ cells expressing tdT (efficiency).

(B) Schematic diagram illustrating the genetic labeling of PDGFRb$^+$ cells by *Pdgfrb-CreER* and its reporter *R26-GFP*. Lower panel shows immunostaining on heart sections for GFP and PDGFRb. Right panel shows quantification of the percentage of GFP$^+$ cells expressing PDGFRb (specificity) and the percentage of PDGFRb$^+$ cells expressing GFP (efficiency).

(C) Schematic diagram illustrating intersectional genetic labeling of PDGFRa$^+$ cells (tdT$^+$), PDGFRb$^+$ cells (GFP$^+$), and PDGFRa$^+$PDGFRb$^+$ cells (tdT$^+$GFP$^+$) by *Pdgfra-DreER;R26-RSR-tdT;Pdgfrb-CreER;R26-GFP* mice (top) and the tamoxifen (Tam) induction strategy and tissue collection (bottom).

(D–R) Immunostaining for tdT and GFP on tissue sections collected from multiple organs. The lower panel images in each organ are split channels. BAT, brown adipose tissue; WAT, white adipose tissue.

(S) Quantification of the percentage of labeled cells expressing tdT, GFP, or both in the indicated tissues. Data are mean ± SEM; n = 5.

Scale bars, 100 μm. Each image is representative of five individual biological samples. See also Figure S2.

Please cite this article in press as: Han et al., A suite of new Dre recombinase drivers markedly expands the ability to perform intersectional genetic targeting, Cell Stem Cell (2021), https://doi.org/10.1016/j.stem.2021.01.007

CellPress

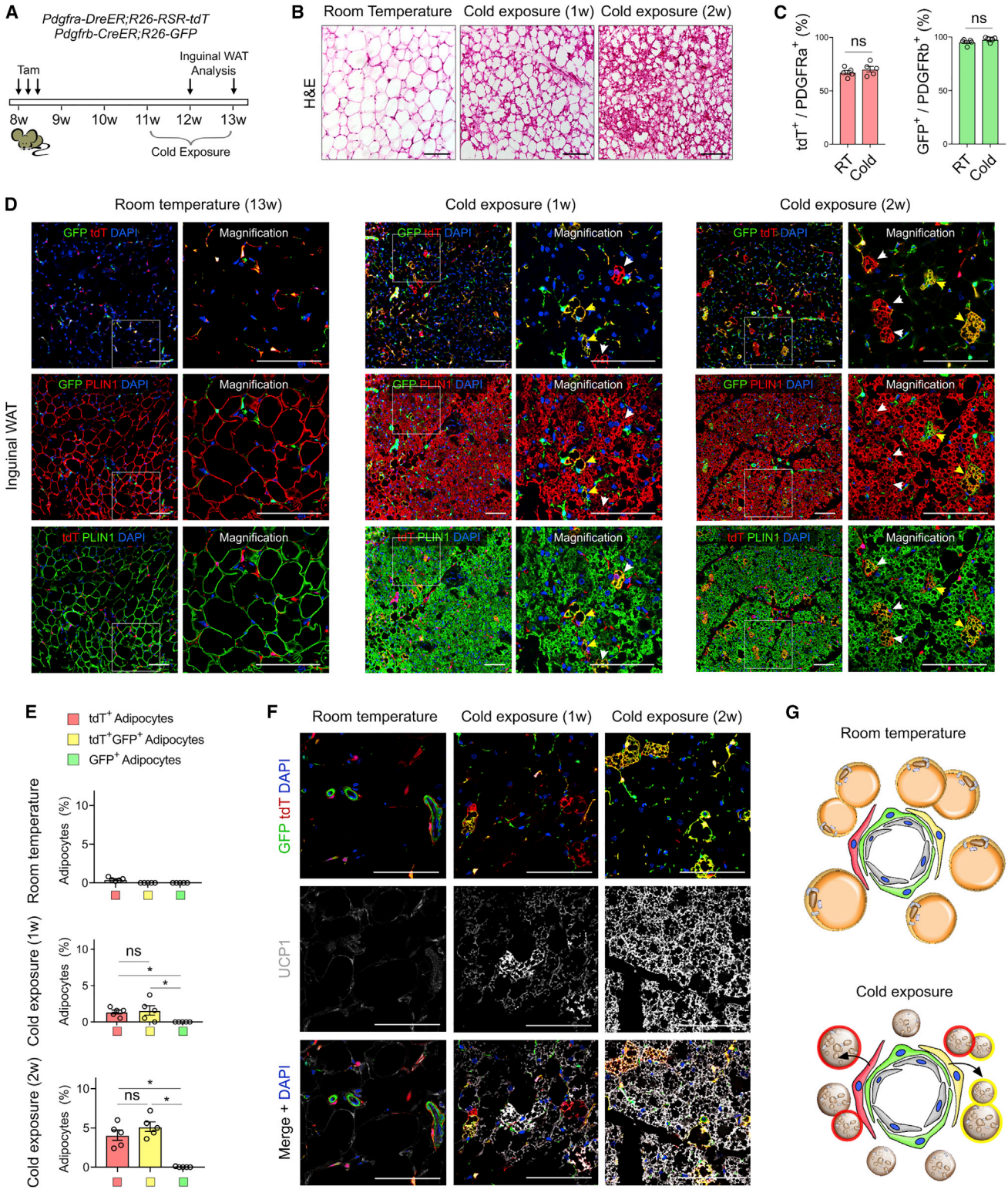

Figure 3. Contribution of PDGFRa$^+$ and/or PDGFRb$^+$ cells to adipocytes after cold exposure

(A) Schematic diagram illustrating the experimental design.

(B) H&E-stained tissue sections collected from inguinal WAT of mice under room temperature (RT) or during cold exposure for 1 or 2 weeks.

(C) Quantification of the percentage of PDGFRa$^+$ cells expressing tdT or PDGFRb$^+$ cells expressing GFP in RT or cold exposure for 2 weeks. Data are mean ± SEM; n = 5; ns, non-significant.

(legend continued on next page)

Please cite this article in press as: Han et al., A suite of new Dre recombinase drivers markedly expands the ability to perform intersectional genetic targeting, Cell Stem Cell (2021), https://doi.org/10.1016/j.stem.2021.01.007

For example, we found that endocardial cells in the trabecular myocardium were labeled mainly by *Npr3-2A-DreER* but not by *Apln-DreER*, while FABP4$^+$ coronary endothelial cells in the compact myocardium were traced mainly by *Apln-DreER* but not by *Npr3-2A-DreER* (Figure 1C, first two images), consistent with previous fate mapping results on the basis of *Npr3-CreER* and *Apln-CreER* drivers (Zhang et al., 2016; Tian et al., 2013). Similarly, we generated Dre or DreER drivers on the basis of different promoters, such as *Sox9*, *Prox1*, *K14*, *Cela1*, *Myh11*, *SMA*, *Cdh1*, *Lyz1*, *Plin1*, *Ly6g*, *Sca1*, *Hopx*, *P63*, and *K5*, and crossed these lines with Dre-responding ZsGreen or tdTomato reporters. After sectioning of the relevant tissues, we performed immunostaining for ZsGreen or tdTomato along with cell lineage markers for each tissue, and we found that most of the drivers exhibited high specificity for targeting the expected cell lineage (Figure 1C).

In addition to the Dre and DreER drivers, we also generated some Cre-induced Dre drivers that contained a Stop cassette flanked by two loxP sites (LSL) upstream of the Dre allele (Figure S1A). The strategy of placing LSL before Dre for Cre induction was recently reported to be useful in detecting transient gene activity in specific cell lineages *in vivo*, including epithelial-to-mesenchymal (EMT)-related gene activity during tumor growth and metastasis (Li et al., 2020). We therefore included additional Cre-responsive Dre drivers such as *Twist*, *Zeb1*, *Snai1*, *Sma*, *Pdgfrb*, *TP63*, *Krt5*, and *Cx40-LSL-Dre* lines in the Dre tool resource (Figure S1B). We then tested the *Twist-LSL-Dre* or *Zeb1-LSL-Dre* lines in combination with a *Kit-CreER* driver (Figure S1C) and found that we could successfully fate map their transient gene activity in mammary epithelial cells during tumor growth (Figures S1D–S1J) using MMTV-PyMT mouse model (Guy et al., 1992). The information for all these Dre, DreER, and LSL-Dre knockin lines appears in Table S1, listing mouse line name, gene targeting strategies, targeting tissues or cell lineages, and available stock number deposited in Shanghai Model Organism company mouse database (https://www.modelorg.com/en/). Genotyping PCR primers were provided in Table S2.

Generation of intersectional genetics for tracing perivascular adipocyte progenitors

With the full suite of new genetic drivers in place, we wanted to begin to use a few of them to resolve some unsettled issues in the stem cell field. In particular, over the past decade there has been an intense debate regarding whether pericytes or adventitial fibroblasts behave as *in vivo* mesenchymal stem cells. PDGFRa is a marker used for perivascular adventitial cells or fibroblasts, and by examining heart and adipose tissue sections collected from *Pdgfra-DreER;R26-rox-Stop-rox (RSR)-tdT*, we found that PDGFRa$^+$ cells were specifically and efficiently labeled (Figure 2A; Figures S2A–S2C). These labeled cells also expressed fibroblast marker FSP1 (Figure S2D). Of note, we also found that *Pdgfra-DreER* efficiently labels PDGFRa$^+$ cells in other organs or tissues collected from *Pdgfra-DreER;R26-RSR-tdT;Pdgfrb-CreER;R26-GFP* mice (Figures S2E and S2F), and the various mosaicism is likely due to the different recombination efficiencies by tamoxifen. PDGFRb is a marker reported to be expressed in pericytes and by examining heart and adipose tissue sections from *Pdgfrb-CreER;R26-GFP*, we found that PDGFRb$^+$ cells were also specifically and efficiently labeled (Figure 2B; Figures S2G–S2I). These labeled cells also expressed pericyte marker NG2 (Figure S2J).

Lineage-tracing studies based on individual traditional markers for fibroblasts or pericytes may have unintentionally traced a subset of cells that express both of these markers, therefore confounding the interpretation of the fate mapping results. Taking advantage of Dre drivers in combination with Cre lines, we developed an intersectional genetic approach to labeling three populations of perivascular cells simultaneously *in vivo*: PDGFRa$^+$, PDGFRb$^+$, and PDGFRa$^+$PDGFRb$^+$ cells (Figure 2C). We performed immunostaining for tdT, GFP, and DAPI, on multiple tissue sections from *Pdgfra-DreER;R26-RSR-tdT;Pdgfrb-CreER;R26-GFP* mice treated with Tam 2 days before tissue collection (Figure 2C). For a brief period after Tam treatment ($\leq$48 h), the tdT or GFP labeling represented PDGFRa and PDGFRb expression in those labeled cells, most of which were found close to vascular endothelial cells in examined organs and tissues (Figures 2D–2R). We found that tdT$^+$ and GFP$^+$ cells were largely two distinct cell populations in most organs or tissues (Figures 2D–2R). A subset of fluorescent cells did express both tdT and GFP, indicating PDGFRa$^+$PDGFRb$^+$ cells in the perivascular niche (Figures 2D–2R). For example, ~15% of all labeled perivascular cells expressed both tdT and GFP in the brain and heart, and ~10% in the brown adipose tissue (BAT) or white adipose tissue (WAT), while the majority of labeled cells express either tdT or GFP alone in these tissues (Figure 2S). Quantification data of all examined tissues revealed that different percentages of labeled cells were tdT$^+$GFP$^+$ (Figure 2S). For example, we detected tdT$^+$GFP$^+$ cells in the adventitia (outermost layer) of the aorta (Figure 2H), consistent with results from a previous study based on PDGFRa and PDGFRb antibody staining of the aortic wall (Cattaneo et al., 2020). Therefore, this intersectional genetic approach enables simultaneous genetic tracing of three molecularly distinct cell populations *in vivo*, namely, PDGFRa$^+$, PDGFRa$^+$PDGFRb$^+$, and PDGFRb$^+$ perivascular cells.

PDGFRa$^+$PDGFRb$^+$ cells preferentially contribute to *de novo* adipogenesis in adult mice

Having established the genetic labeling of perivascular cell populations, we next exposed mice to cold conditions to induce the beiging of adipocytes in the WAT, which has been reported to occur at least partly through *de novo* differentiation from perivascular adipocyte progenitors (Wang et al., 2013). By combining such stimulation with our intersectional genetic fate mapping

(D) Immunostaining for tdT, GFP, and Perilipin 1 (PLIN1) on inguinal WAT sections from mice housed at RT for 13 weeks (left) or cold exposed for 1 week (middle) or 2 weeks (right). All tdT, GFP, and PLIN1 are pseudo-colored in images as indicated. White arrowheads, tdT$^+$PLIN1$^+$ adipocytes; yellow arrowheads, tdT$^+$GFP$^+$PLIN1$^+$ adipocytes.

(E) Quantification of percentage of adipocytes expressing tdT, GFP, or both in inguinal WAT under different conditions. Data are mean ± SEM; n = 5; *p < 0.05; ns, non-significant.

(F) Immunostaining for tdT, GFP, and UCP1 on inguinal WAT sections from mice under different conditions.

(G) Illustration showing *de novo* adipogenesis from PDGFRa$^+$ and PDGFRa$^+$PDGFRb$^+$ under cold exposure condition.

Scale bars, 100 μm. Each image is representative of five individual biological samples. See also Figures S2–S4.

Please cite this article in press as: Han et al., A suite of new Dre recombinase drivers markedly expands the ability to perform intersectional genetic targeting, Cell Stem Cell (2021), https://doi.org/10.1016/j.stem.2021.01.007

CellPress

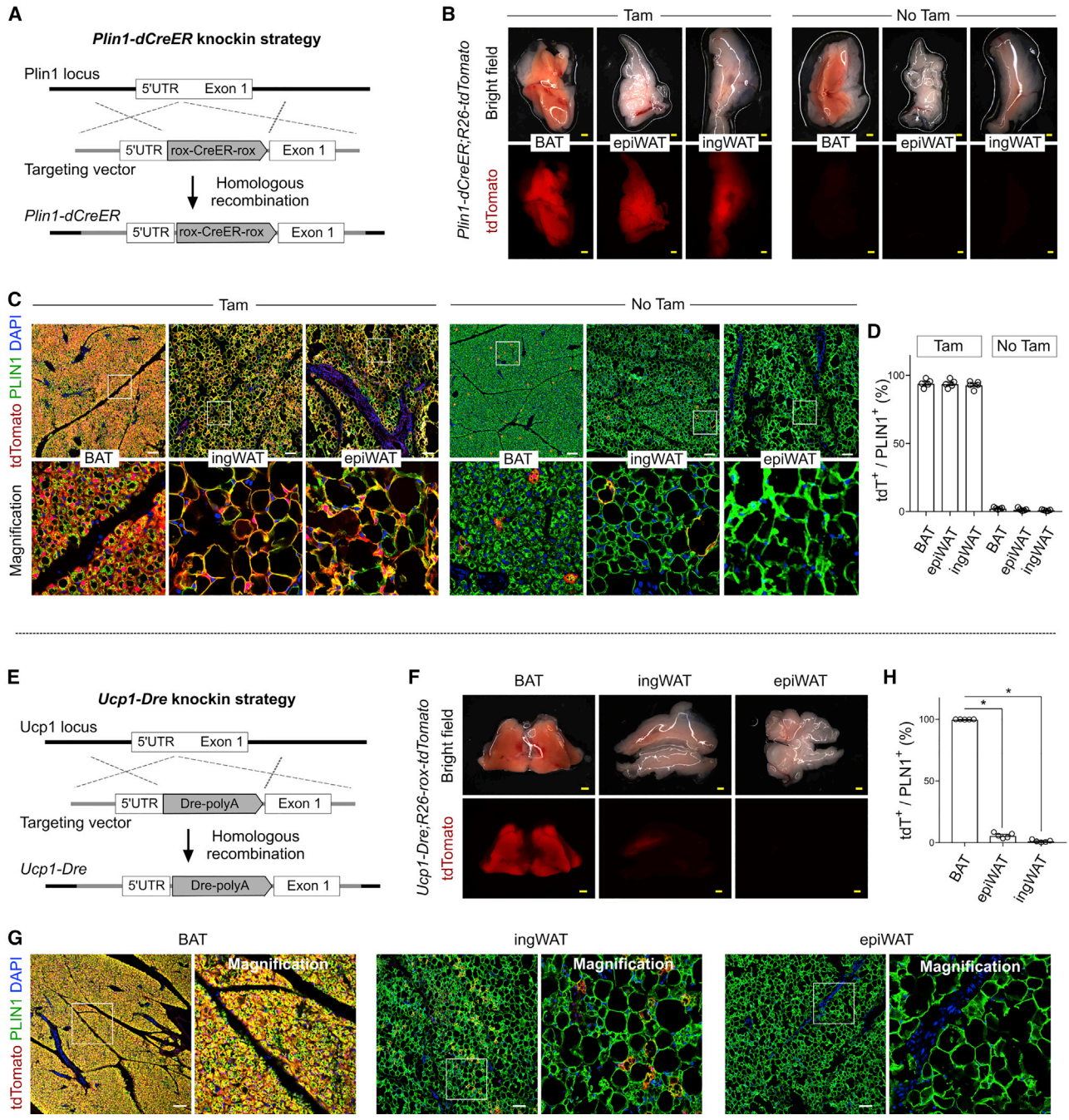

Figure 4. Generation and characterization of *Plin1-dCreER* and *Ucp1-Dre* mouse lines

(A) Schematic diagram illustrating the generation of *Plin1-dCreER* by homologous recombination using CRISPR-Cas9.

(B) Whole-mount bright-field and fluorescence images of intracapsular brown adipose tissue (BAT), inguinal white adipose tissue (ingWAT), and epididymal white adipose tissue (epiWAT) from adult *Plin1-dCreER;R26-tdTomato* mice treated with tamoxifen (Tam) or without tamoxifen (No Tam).

(C) Immunostaining for tdTomato and PLIN1 on BAT, ingWAT, and epiWAT tissue sections.

(D) Quantification of the percentage of PLIN1$^+$ adipocytes expressing tdTomato (tdT) in Tam or No Tam-treated groups. Data are mean ± SEM; n = 5.

(E) Schematic diagram illustrating the generation of *Ucp1-Dre* by homologous recombination using CRISPR-Cas9.

(F) Whole-mount bright-field and fluorescence images of BAT, ingWAT, and epiWAT collected from *Ucp1-Dre;R26-rox-tdTomato* mice.

(G) Immunostaining for tdTomato and PLIN1on BAT, ingWAT, and epiWAT tissue sections.

(H) Quantification of the percentage of PLIN1$^+$ adipocytes expressing tdTomato (tdT) in BAT, epiWAT, and ingWAT tissues. Data are mean ± SEM; n = 5; *p < 0.05.

Scale bars, 1 mm (yellow); 100 μm (white). See also Figure S5.

Please cite this article in press as: Han et al., A suite of new Dre recombinase drivers markedly expands the ability to perform intersectional genetic targeting, Cell Stem Cell (2021), https://doi.org/10.1016/j.stem.2021.01.007

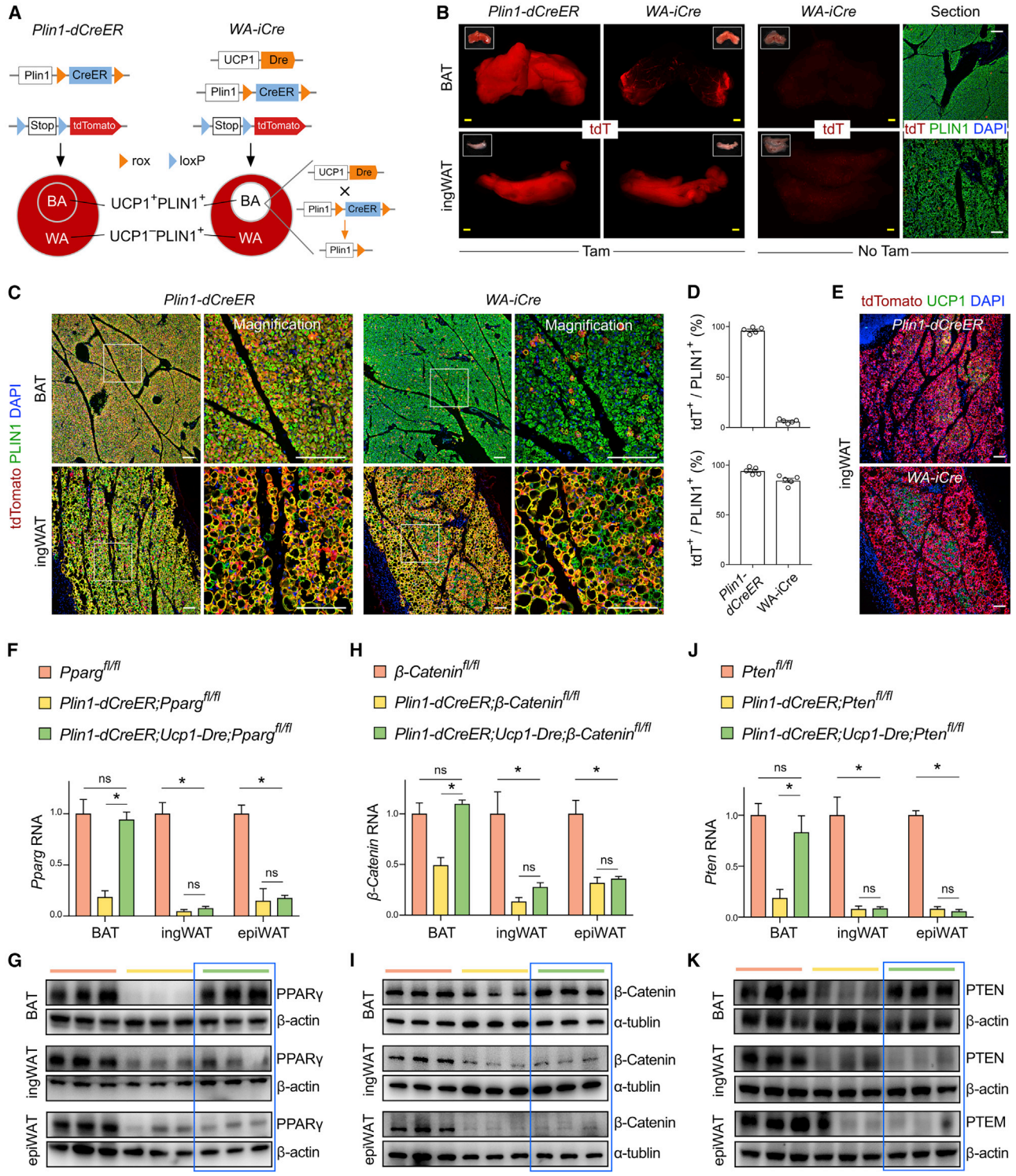

Figure 5. White adipocyte-inducible Cre (*WA-iCre*) targets mainly white but not brown adipose tissue

(A) Schematic diagram illustrating the strategy for targeting white adipocytes (WAs) but not brown/beige adipocytes (BAs) using dual recombinases.

(B) Whole-mount fluorescence of BAT and ingWAT from *Plin1-dCreER;R26-tdTomato* or *WA-iCre;R26-tdTomato* mice treated with Tam (B) or no Tam. Right panel shows immunostaining images of BAT and ingWAT sections of *WA-iCre;R26-tdTomato* mice without Tam. Insets, bright-field images.

(C) Immunostaining for tdTomato and PLIN1 on BAT or ingWAT sections from *Plin1-dCreER;R26-tdTomato* or *WA-iCre;R26-tdTomato* mice (Tam).

(D) Quantification of the percentage of PLIN1^{+} adipocytes expressing tdTomato. Data are mean ± SEM; n = 5.

(E) Immunostaining for tdTomato and UCP1 on ingWAT sections from *Plin1-dCreER;R26-tdTomato* or *WA-iCre;R26-tdTomato* mice treated with Tam.

(legend continued on next page)

Please cite this article in press as: Han et al., A suite of new Dre recombinase drivers markedly expands the ability to perform intersectional genetic targeting, Cell Stem Cell (2021), https://doi.org/10.1016/j.stem.2021.01.007

strategy, we aimed to determine whether, and to what extent, perivascular progenitor cells contribute to new adipocytes in inguinal WAT (ingWAT) after cold exposure (Figure 3A). Hematoxylin and eosin (H&E) staining of ingWAT sections revealed a striking change in adipocyte morphology over the course of the 2-week cold challenge, with a vast increase in beige cell-like structures (Figure 3B). Quantification of immunostained sections revealed that the percentage of PDGFRa$^+$ cells expressing tdT did not change significantly among the mice kept at room temperature or at 6°C for 1 or 2 weeks (Figure 3C). Additionally, the GFP labeling percentage of PDGFRb$^+$ cells were statistically similar among these groups (Figure 3C), suggesting that the abundance of differentially labeled cell populations does not appear to be significantly regulated by cold exposure in our models.

We next examined the contribution of different perivascular cell populations to adipocytes in mice kept at room temperature and those kept at 6°C for 1 or 2 weeks. By immunostaining for tdT, GFP, and the adipocyte marker PLIN1 on ingWAT sections, we found that most of the tdT$^+$, GFP$^+$, or tdT$^+$GFP$^+$ perivascular cells did not express PLIN1 in mice housed at room temperature (Figure 3D). Except for rare tdT$^+$ adipocytes indicative of a PDGFRa$^+$ cell origin, we did not detect any appreciable GFP$^+$ or GFP$^+$tdT$^+$ adipocytes in ingWAT at room temperature (Figure 3E). In the groups of mice exposed to cold for 1 or 2 weeks, we found readily detectable tdT$^+$ and tdT$^+$GFP$^+$ adipocytes in the midst of non-labeled adipocytes in the ingWAT (Figure 3D). Notably, several small clusters of tdT$^+$ multilocular beige adipocytes were detected in samples of mice housed in the cold for 2 weeks. Quantitatively, 1.38% ± 0.27%, 1.59% ± 0.65%, and 0.0036% ± 0.0023% of PLIN1$^+$ adipocytes were tdT$^+$, tdT$^+$GFP$^+$, and GFP$^+$, respectively, in ingWAT after 1 week of cold exposure, while 4.08% ± 0.67%, 5.16% ± 0.61%, and 0.023% ± 0.011% of such adipocytes were tdT$^+$, tdT$^+$GFP$^+$, and GFP$^+$, respectively, after 2 weeks of cold exposure (Figure 3E). Although the number of tdT$^+$ perivascular mesenchymal cells was 4 times greater than that of tdT$^+$GFP$^+$ cells at the time initial labeling (Figure 2S), there was no significant difference between their contributions to new adipocytes after cold exposure (Figure 3E), indicating that PDGFRa$^+$PDGFRb$^+$ perivascular mesenchymal cells were more potent in their contribution to new adipocytes after cold exposure, compared with those of PDGFRa$^+$ cells. Immunostaining for the beige cell marker UCP1 confirmed that most of the labeled adipocytes began to express UCP1 after cold exposure (Figure 3F), indicating their beige cell fate after differentiation from adipocyte progenitors (Figure 3G). Of note, a substantial number these UCP1$^+$ multilocular adipocytes were derived from pre-existing adipocytes labeled by *Plin1-CreER* (Figures S2K–S2M). Additionally, we used an alternative model of skin wound healing for adipogenesis as previously reported (Plikus et al., 2017). After skin injury, we found that PDGFRa$^+$ and PDGFRa$^+$PDGFRb$^+$ mesenchymal cells, but not PDGFRb$^+$ cells, regenerate fat cells during wound healing process (Figure S3).

To characterize the gene profiles of these distinct perivascular cell populations in adipose tissues, we next performed scRNA-seq analysis of cells isolated from ingWAT of 8-week-old wild-type C57BL/6 mice (Figure S4). Clustering and UMAP visualization of the cells revealed at least eight cell molecularly distinct cell populations, which we annotated as fibroblasts, pericytes, macrophages, endothelial cells, T cells, B cells, natural killer (NK) cells, and neutrophils (Figures S4A and S4B). Re-clustering of 5,044 fibroblasts identified two unique stromal cell populations with distinct molecular signatures (Figures S4C–S4E). One of them expresses *Pdgfra* transcripts, and the second population expresses both *Pdgfra* and *Pdgfrb*; they constitute 72.48% and 27.52% of fibroblasts, respectively. Indeed, PDGFRa$^+$ single-positive cells are molecularly distinct from PDGFRa$^+$PDGFRb$^+$ double-positive cells at molecular levels (530 differentially expressed genes). PDGFRa$^+$ cells express *Pi16*, *Sbsn*, and *Dpp4*, whereas double-positive cells express *Cxcl14*, *Steap4*, and *Col15a1* (Figure S4D). Of note, we found that CD81, a newly identified adipocyte progenitor cell marker (Oguri et al., 2020), was expressed in both populations (Figure S4D). Gene Ontology (GO) enrichment pathways analysis revealed that upregulated genes in PDGFRa$^+$PDGFRb$^+$ are related to extracellular structure organization, response to wounding, and positive regulation of fat cell differentiation (Figure S4F).

The increased specificity of gene knockout in white adipocytes by intersectional genetics

Having shown the utility of intersectional genetics for more accurate lineage tracing, we next used some of the new drivers for gene manipulation in cell types that has not previously been achieved by traditional Cre drivers. For functional study of genes, investigators generally use floxed alleles from the currently available mouse resources. Here, we explored two different but complementary sequential intersectional genetic approaches that permit Dre-controlled Cre targeting for *in vivo* gene functional study in cell lineages that are previously difficult to specifically target; notably, WAs and lymphatic endothelial cells (LECs). For the former we used a so-called NOT strategy, while for the latter we used a so-called AND strategy.

There are two distinct types of adipose tissues in mammals: WAT and BAT. Despite their significant differences in function and associated gene regulation, the current main approach for gene knockout mainly uses pan-adipose Cre driver, such as *adiponectin-Cre* (Eguchi et al., 2011). But such genetic drivers are not specific for WAs, so to date all gene knockout strategies to target WAT also delete the gene of interest in BAT. To specifically delete genes in WAs, we took advantage of intersectional genetic approach and generated a Dre-controlled Cre driver to restrict Cre activity specifically in WAs. In this design, we used two markers: PLIN1 and UCP1, which are a pan-adipocyte marker and a brown adipocyte (BA) marker, respectively. Therefore, PLIN1$^+$UCP1$^+$ cells are specific to BAT, while PLIN1$^+$UCP1$^-$ cells are more enriched in WAT.

(F, H, and J) qRT-PCR analysis of Pparg (F), β-catenin (H), and Pten (J) expression in the three indicated flox homozygous mouse strains containing no Cre, *Plin1-dCreER*, or *WA-iCre* allele. Data are mean ± SEM; n = 4 or 5; ns, non-significant; *p < 0.05.

(G, I, and K) Western blotting of PPARγ (G), β-catenin (I), and PTEN (K) and control α-tubulin or β-actin in BAT, ingWAT, and epiWAT of the three mice groups used in (F)–(J). n = 3 biological repeats.

Scale bars, 1 mm (yellow), 100 μm (white). See also Figure S6.

Please cite this article in press as: Han et al., A suite of new Dre recombinase drivers markedly expands the ability to perform intersectional genetic targeting, Cell Stem Cell (2021), https://doi.org/10.1016/j.stem.2021.01.007

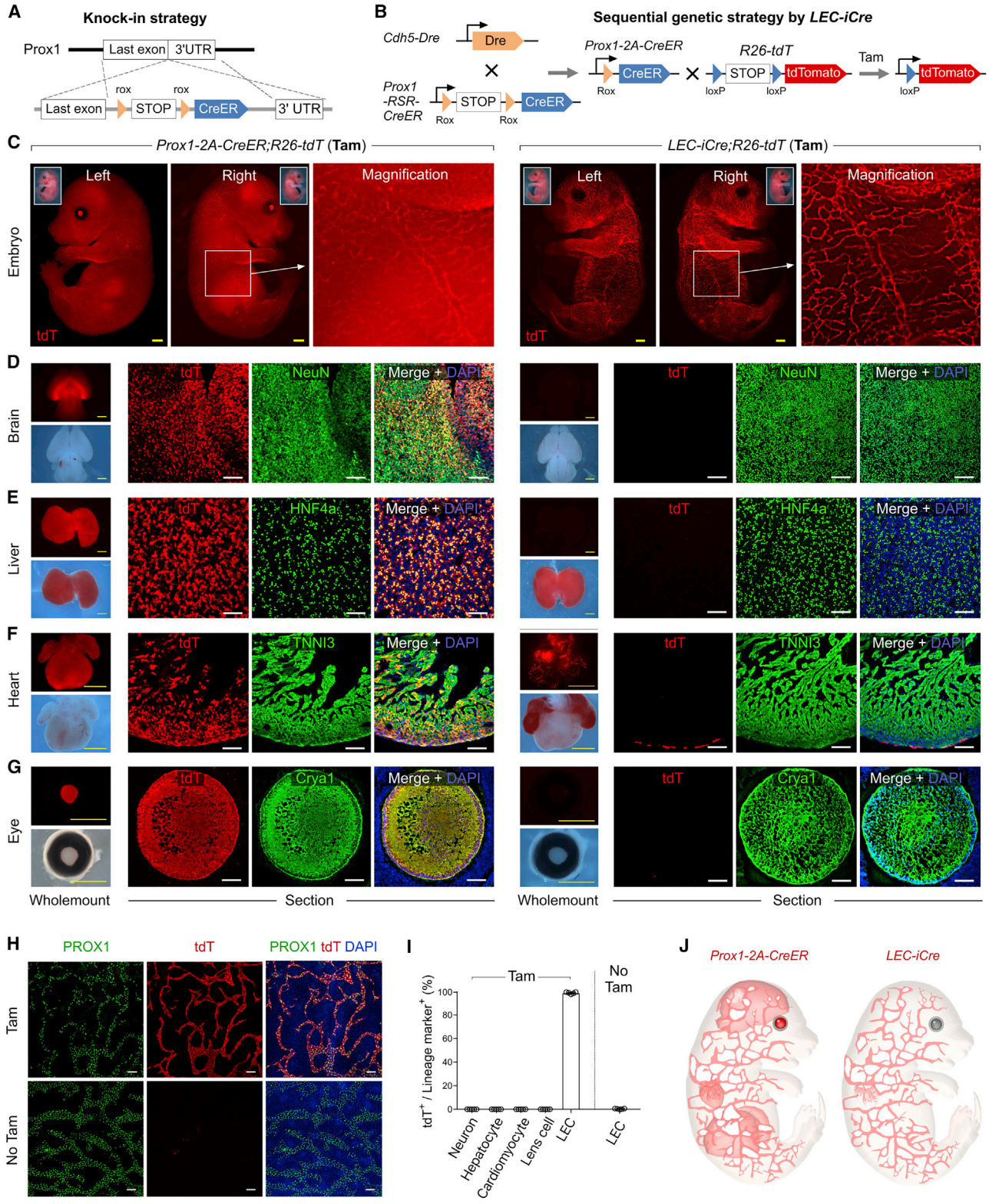

Figure 6. Generation of lymphatic endothelial cell-specific inducible Cre (*LEC-iCre*)

(A) Schematic diagram illustrating the knockin strategy for generation of *Prox1-rox-Stop-rox-CreER (Prox1-RSR-CreER)* mice.

(B) Schematic diagram illustrating the strategy for generation of *LEC-iCre* mice using sequential intersectional genetics.

(C) Whole-mount fluorescence images of E15.5–E16.5 *Prox1-2A-CreER;R26-tdT* (left) and *LEC-iCre;R26-tdT* (right) embryos treated with Tam.

(legend continued on next page)

Please cite this article in press as: Han et al., A suite of new Dre recombinase drivers markedly expands the ability to perform intersectional genetic targeting, Cell Stem Cell (2021), https://doi.org/10.1016/j.stem.2021.01.007

We first generated *Plin1-rox-CreER-rox* mice, in which CreER could be deleted by Dre recombinase (Figure 4A). We named this mouse *Plin1-dCreER* to indicate deletion of CreER in the presence of Dre recombinase. We crossed *Plin1-dCreER* mice with an *R26-tdTomato* reporter mouse strain and treated the offspring *Plin1-dCreER;R26-tdTomato* mice with Tam. As expected, tdT^+ signals were detected in intracapsular BAT, ingWAT, and epididymal WAT (epiWAT) in the Tam-treated groups (Figure 4B). Additionally, *Plin1-dCreER* did not target organs or tissues other than adipose tissues (Figure S5). Very rare tdT^+ signals could be detected in adipose tissues or other organs of mice without Tam treatment (Figures 4B–4D; Figure S5). Immunostaining for tdT and PLIN1 on BAT, ingWAT, and epiWAT sections confirmed the high efficiency of pan-adipocyte labeling (Figures 4C and 4D). These data indicate that in the absence of Dre, *Plin1-dCreER* worked as a general pan-adipocyte-inducible Cre driver. We next generated a Dre driver to specifically remove CreER from *Plin1-dCreER* in BAs. We generated *Ucp1-Dre* mice (Figure 4E) and crossed them with *R26-rox-tdTomato* reporter mice, finding strong tdT^+ signals in BAT and weak tdT^+ signals in ingWAT or epiWAT (Figure 4F). Immunostaining for tdTomato and PLIN1 confirmed that *Ucp1-Dre* mainly targeted BAs in the BAT and minimally targeted WAs in the WAT (Figures 4G and 4H).

Having successfully generated *Plin1-dCreER* and *Ucp1-Dre* drivers, we crossed mice harboring these alleles to develop an inducible Cre driver for WAs (*WA-iCre*; Figure 5A). In this design of intersectional genetics (i.e., the NOT-logic strategy), *WA-iCre* mainly targets $UCP1^-PLIN1^+$ WAs but not $UCP1^{+-}$ $PLIN1^+$ BAs, as CreER in *Plin1-dCreER* allele has already been removed by *Ucp1-Dre* in BAs (Figure 5A). Different from *Plin1-dCreER* or any other previous pan-adipocyte Cre drivers that target both BAs and WAs, *WA-iCre* mainly targeted WAs but not BAs (Figure 5A). Whole-mount fluorescence images showed that ingWAT but not BAT exhibited bright tdT^+ signals in *WA-iCre* mice, while both BAT and ingWAT have bright tdT^+ signals in *Plin1-dCreER* littermates (Figure 5B). We detected very rare tdT^+ cells in BAT or ingWAT of WA-iCre mice without Tam treatment (Figure 5B). Immunostaining for tdT and PLIN1 on tissue sections revealed that the majority of adipocytes in the BAT and ingWAT of *Plin1-dCreER* mice were tdT^+ (Figures 5C and 5D). In *WA-iCre* mice, although the majority of adipocytes in ingWAT were tdT^+, there were minimal tdT^+ cells in BAT (Figures 5C and 5D). Noticeably, a subset of unlabeled adipocytes in the ingWAT of *WA-iCre* mice were small in size and morphologically unlike generally large WAs containing large lipid droplet (Figure 5C). In the consecutive sections stained with tdT and UCP1, we detected that these few unlabeled adipocytes in the ingWAT of *WA-iCre* mice were $UCP1^+$ (Figure 5E). In contrast, these $UCP1^+$ adipocytes were labeled by *Plin1-dCreER* (Figure 5E). Of note, we also detected some tdT^+ multilocular adipocytes in ingWAT of *WA-iCre* mice in both homeostasis and after cold exposure (Figures S6A–S6C), suggesting that some beige adipocytes may maintain thermogenic activity via UCP1-independent pathways (Roesler and Kazak, 2020; Ikeda et al., 2017; Jun et al., 2020).

As this intersectional genetic approach resulted in Cre activity as the ultimate readout in WAs, we next examined whether *WA-iCre* could specifically delete genes in WAs. We crossed *WA-iCre* mice with peroxisome proliferator-activated receptor gamma (*Pparg*)-flox mice, as Pparg is an important transcriptional modulator of adipocyte fate (Cristancho and Lazar, 2011), and generated *Plin1-dCreER;Ucp1-Dre;*$Pparg^{fl/fl}$ mice (Figure 5F). As technical controls, we included littermates *Plin1-dCreER;*$Pparg^{fl/fl}$ mice and $Pparg^{fl/fl}$ mice in the following experiments (Figure 5F). qRT-PCR analysis showed a significant lower expression of Pparg mRNA in the BAT, ingWAT, and epiWAT of *Plin1-dCreER;*$Pparg^{fl/fl}$ mice compared with those of $Pparg^{fl/fl}$ mice (Figure 5F). Although *Pparg* mRNA in ingWAT and epiWAT was significantly lower in *Plin1-dCreER;Ucp1-Dre;*$Pparg^{fl/fl}$ mice compared with those in $Pparg^{fl/fl}$ mice, there was no significant difference of Pparg mRNA in the BAT between the these two groups (Figure 5F). Western blotting analysis showed that PPARγ protein expression was significantly reduced in *Plin1-dCreER;*$Pparg^{fl/fl}$ mice compared with $Pparg^{fl/fl}$ in BAT, ingWAT, and epiWAT (Figure 5G). Although PPARγ protein in ingWAT or epiWAT was noticeably reduced in *Plin1-dCreER;Ucp1-Dre;*$Pparg^{fl/fl}$ mice compared with that of $Pparg^{fl/fl}$ mice, PPARγ protein expression in BAT was comparable between these two groups (Figure 5G), indicating specific Pparg deletion in WAs but not BAs. Phenotypically, we found smaller volumes of adipose tissues and larger adipocyte size in both *Plin1-dCreER;Ucp1-Dre;*$Pparg^{fl/fl}$ and *Plin1-dCreER;*$Pparg^{fl/fl}$ mice compared with $Pparg^{fl/fl}$ in the ingWAT and epiWAT (Figures S6D–S6F). Of note, larger adipocyte size in BAT were noticed in the *Plin1-dCreER;*$Pparg^{fl/fl}$ mice but not in *Plin1-dCreER;Ucp1-Dre;*$Pparg^{fl/fl}$ mice (Figure S6F). We next tested if Wnt signaling or Pten is required for adipose tissue homeostasis by crossing *WA-iCre* with *β-Catenin-flox* and *Pten-flox* alleles. We found similar results by *β-Catenin-* or *PTEN*-mediated gene deletion by qRT-PCR (Figures 5H and 5J) and western blotting analysis (Figures 5I and 5K). However, we did not detect strong phenotypic change in adipose tissues in these two mutants (Figures S6G–S6J). Taken together, the intersectional genetics (i.e., the NOT-logic strategy) enables gene manipulation in a subset of cell populations, such as WAs, that would otherwise be unachievable using a simple Cre-loxp strategy.

Generation of Dre-controlled Cre line for specific targeting of LECs

In addition to the NOT-logic strategy outlined above, we also applied an AND-logic strategy for intersectional genetics by Dre-controlled Cre activity in the intersectional common part of two genes. Although the most widely used Cre tools for targeting LECs are *Prox1-CreER* lines (Srinivasan et al., 2007; Bazigou

(D–G) Whole-mount fluorescence and bright-field images of brain, liver, heart, and eye. Immunostaining for tdT and difference cell lineage markers NeuN, HNF4a, TNNI3, and Crya1 on tissue sections from *Prox1-2A-CreER;R26-tdT* (left) and *LEC-iCre;R26-tdT* (right).
(H) Immunostaining for tdT and PROX1 on *LEC-iCre;R26-tdT* embryos treated with tamoxifen (Tam) or no Tam.
(I) Quantification of the percentage of specific type of cells expressing tdT. Data are mean ± SEM; n = 5.
(J) Illustration indicating the genetic targeting by *Prox1-2A-CreER* and *LEC-iCre* mouse line.
Scale bars: yellow, 1 mm; white, 100 μm. Each image is representative of five individual biological samples. See also Figure S7.

Please cite this article in press as: Han et al., A suite of new Dre recombinase drivers markedly expands the ability to perform intersectional genetic targeting, Cell Stem Cell (2021), https://doi.org/10.1016/j.stem.2021.01.007

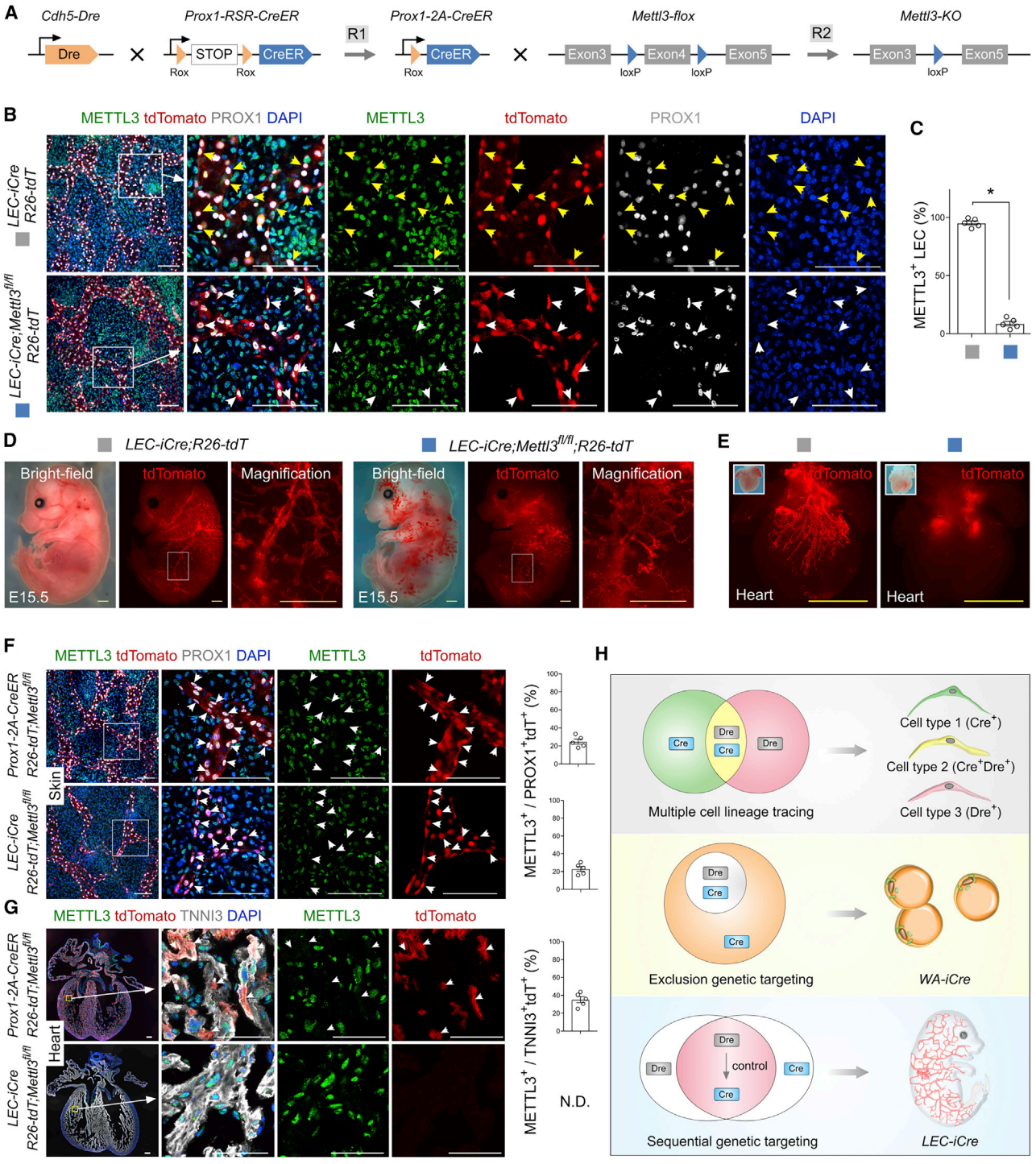

Figure 7. Specific gene knockout in lymphatic vessels by *LEC-iCre*

(A) Schematic diagram illustrating the strategy for *LEC-iCre* mediated Mettl3 gene knockout.

(B) Immunostaining for METTL3, PROX1, and tdTomato on *LEC-iCre;R26-tdT* (top) and *LEC-iCre;Mettl3$^{fl/fl}$;R26-tdT* (bottom) embryo skin. Yellow arrowheads, METTL3^{+}PROX1^{+}tdTomato^{+} LECs; white arrowheads, METTL3^{-}PROX1^{+}tdTomato^{+} LECs.

(C) Quantification of the percentage of tdTomato^{+} LECs expressing METTL3. Data are mean ± SEM; n = 5; *p < 0.05.

(D) Whole-mount bright-field and fluorescence images of *LEC-iCre;R26-tdT* (left) and *LEC-iCre;Mettl3$^{fl/fl}$;R26-tdT* (right) embryos.

(E) Whole-mount fluorescence images of *LEC-iCre;R26-tdT* (left) and *LEC-iCre;Mettl3$^{fl/fl}$;R26-tdT* (right) hearts. Insets are bright-field images.

(legend continued on next page)

Please cite this article in press as: Han et al., A suite of new Dre recombinase drivers markedly expands the ability to perform intersectional genetic targeting, Cell Stem Cell (2021), https://doi.org/10.1016/j.stem.2021.01.007

et al., 2011), they actually target other cell lineages, as *Prox1* expression is more broadly expressed in tissues beyond lymphatic vessels. For example, *Prox1* is expressed and also functionally required in differentiation of neural stem cells (Torii et al., 1999), cardiomyocytes in the developing heart (Risebro et al., 2009), hepatocyte maturation during liver development (Sosa-Pineda et al., 2000), and epithelial cells and fiber cells in the lens (Wigle et al., 1999). Thus, from our new suite of intersectional genetic drivers, we developed a specific Cre driver for lymphatic vessels using a sequential intersectional genetics-based AND-logic strategy.

Similar to the previously reported *Prox1-IRES-CreER* knockin line (Srinivasan et al., 2007), we inserted a CreER cassette into the *Prox1* gene locus after the last coding exon to maintain the endogenous *Prox1* expression while allowing simultaneous CreER expression using a self-cleaved 2A peptide. But we also included an additional rox-Stop-rox (RSR) cassette upstream of CreER, therefore preventing basal CreER expression from the *Prox1* locus (Figure 6A). This rox-flanked Stop cassette allows the introduction of another set of genetic control by Dre drivers, such as the endothelial cell-specific driver *Cdh5-Dre*. As lymphatic vessels originate mainly from venous endothelial cells (Srinivasan et al., 2007), the intersectional part of *Cdh5* and *Prox1* was expected to restrict the Cre activity in the endothelial cell-derived PROX1$^+$ lymphatic vessels, but not in any other non-endothelial cell lineages or derivatives, such as PROX1$^+$ neurons, cardiomyocytes, hepatocytes, or epithelial cells in lens. We therefore crossed *Cdh5-Dre* mice with *Prox1-RSR-CreER* mice to generate an LEC-specific Cre (*LEC-iCre*). In this design, Dre-rox recombination switches *Prox1-RSR-CreER* into a *Prox1-2A-CreER* genotype. Tam-induced Cre-loxP recombination would subsequently result in genetic targeting in all organs and tissues of LECs only (Figure 6B).

To first examine if *Prox1-2A-CreER* after Dre-rox recombination worked in the same way as previously reported *Prox1-IRES-CreER* drivers, we conducted germline removal of RSR by *CAG-Dre* (Anastassiadis et al., 2009) and generated a *Prox1-2A-CreER* mouse strain for crossing with *R26-tdT* reporter mice (Madisen et al., 2010) (Figure S7A). We used the previously reported *Prox1-IRES-CreER* mice (Srinivasan et al., 2007) for a side-by-side comparison. Whole-mount fluorescence images of E15.5 *Prox1-2A-CreER;R26-tdT* embryos showed lymphatic vascular patterning of tdT$^+$ signals on the skin, consistent with that of E15.5 *Prox1-IRES-CreER;R26-tdT* embryos (Figure S7B). Whole-mount fluorescence images of individual organs, such as brain, liver, heart, and eye, of the two groups mice revealed tdT$^+$ signals in these examined organs (Figures S7C–S7F). Immunostaining for tdT and different lineage markers confirmed the wide expression of Prox1 gene in neurons, hepatocytes, cardiomyocytes, and lens cells in the embryos (Figures S7C–S7F), albeit with different recombination efficiency between different lines. These data demonstrate *Prox1-RSR-CreER* could be switched to *Prox1-2A-CreER*, which worked similarly as the previously reported *Prox1-IRES-CreER* approach in broadly targeting multiple tissues in addition to LECs.

Having validated the *Prox1-2A-CreER* allele, we next restricted the RSR-CreER to CreER genotype switch only in the endothelial cells by using a *Cdh5-Dre* (Figure 6B). We compared the efficiency and specificity of lymphatic vessel labeling between *Prox1-2A-CreER* and *LEC-iCre* using the *R26-tdT* reporter (Figure 6B). Whole-mount fluorescence images of E15.5–E16.5 embryos revealed a significant difference in the tdT$^+$ signal patterns between the *Prox1-2A-CreER;R26-tdT* and *LEC-iCre;R26-tdT* groups (Figure 6C). We could detect noticeable tdT$^+$ signals from some organs, such as the brain, liver, and eye, in addition to the lymphatic vessel pattern on the skin in *Prox1-2A-CreER;R26-tdT* mice (Figure 6C). In contrast, a typical lymphatic vessel pattern was readily detectable in *LEC-iCre;R26-tdT* mice without any tdT$^+$ signal from the brain, liver, or eye (Figure 6C). Examination of individual organs by whole-mount fluorescence and sectional immunostaining confirmed that there was no tdT$^+$ neurons in the brain, hepatocytes in liver, cardiomyocytes in heart, or epithelial cells in the eye lens in *LEC-iCre;R26-tdT* mice (Figures 6D–6G). Immunostaining for PROX1 and tdT in the skin revealed that virtually all PROX1$^+$ cells expressed tdT (Figure 6H). Quantification data showed that the labeling efficiency of PROX1$^+$ lymphatic vessels was 99.08% ± 0.36%, while there was no labeling of non-LECs in the examined organs (Figure 6I), highlighting the specificity of *LEC-iCre*. As technical controls, we detected very rare tdT$^+$ LECs in *LEC-iCre;R26-tdT* or *Prox1-2A-CreER;R26-tdT* embryos without Tam treatment (Figures 6H and 6I; Figures S7G and S7H) or in *Prox1-RSR-CreER;R26-tdT* embryos with Tam treatment (Figure S7I). Therefore, on the basis of intersectional genetics (i.e., the AND-logic strategy), we generated a high-efficiency LEC-specific Cre driver (Figure 6J).

Finally, we used this *LEC-iCre* strain to perform gene deletion specifically in LECs. Modification of mRNA has been recently reported to play essential roles in mRNA metabolism and affect various cellular processes, including endothelial cell fate and functions. N6-methyladenosine (m^{6}A) is one of the key mRNA modifications (Roundtree et al., 2017), which is methylated by methyltransferase-like protein 3 (METTL3) (Fu et al., 2014). Genetic ablation of Mettl3 in endothelial cells leads to aberrant gene expression and malfunction of endothelial cells in embryos (Zhang et al., 2017; Lv et al., 2018). Here we examined if Mettl3 plays functional roles in regulating lymphogenesis during embryonic development. We crossed *LEC-iCre* mice with flox allele for Mettl3, a gene encoding a key RNA methyltransferase (Lin et al., 2017). We analyzed the Mettl3 gene knockout efficiency and specificity and also the LEC phenotype of *LEC-iCre;-Mettl3$^{fl/fl}$;R26-tdT* (mutant), in comparison with *LEC-iCre;R26-*

(F) Immunostaining for METTL3, tdTomato, and PROX1 on E15.5 *Prox1-2A-CreER;R26-tdT;Mettl3$^{fl/fl}$* (upper panel) and *LEC-iCre;R26-tdT;Mettl3$^{fl/fl}$* (lower panel) skins. Arrowheads, METTL3$^-$PROX1$^+$tdT$^+$ LECs. Right panel shows quantitation of the percentage of PROX1+tdT+ LECs expressing METTL3. Data are mean ± SEM; n = 5.

(G) Immunostaining for METTL3, tdTomato, and TNNI3 on E15.5 *Prox1-2A-CreER;R26-tdT;Mettl3$^{fl/fl}$* (upper panel) and *LEC-iCre;R26-tdT;Mettl3$^{fl/fl}$* (lower panel) heart sections. Arrowheads, METTL3$^-$TNNI3$^+$tdT$^+$ cardiomyocytes. Right panel shows quantitation of the percentage of TNNI3$^+$tdT$^+$ cardiomyocytes expressing METTL3. Data are mean ± SEM; n = 5.

(H) Illustration showing strategies for genetic lineage tracing and gene knockout using intersectional genetic system.

Scale bars: yellow, 1 mm; white, 100 μm. Each image is representative of five individual biological samples.

Please cite this article in press as: Han et al., A suite of new Dre recombinase drivers markedly expands the ability to perform intersectional genetic targeting, Cell Stem Cell (2021), https://doi.org/10.1016/j.stem.2021.01.007

tdT littermate controls (Figure 7A). Immunostaining for METT3, tdTomato, and PROX1 on E15.5 embryos showed that METTL3 was expressed in PROX1$^+$tdTomato$^+$ LECs of control mice (Figures 7B and 7C, yellow arrowheads). However, METTL3 was not detected in most PROX1$^+$tdTomato$^+$ LECs in mutant mice (Figures 7B and 7C, white arrowheads), while METTL3 was readily detectable in other cell lineages (non-LECs), suggesting efficient and specific Mettl3 gene knockout by *LEC-iCre*. Whole-mount fluorescence images of E15.5 embryos and hearts revealed irregular lymphatic vessel patterning in the skin and defective cardiac lymphatic vessel growth in the mutants, compared with those of littermate controls (Figures 7D and 7E), indicating that Mettl3 was functionally required for lymphatic vessel growth during embryogenesis. To further illustrate the advantage of using *LEC-iCre* for gene functional study, we compared the specificity of Mettl3 gene deletion by *Prox1-2A-CreER* and *LEC-iCre*. In the skin lymphatic vessels, both Cre drivers specifically and efficiently deleted Mettl3 (Figure 7F). While *Prox1-2A-CreER*targeted cardiomyocytes and deleted most Mettl3 expression in the myocardium in addition to LECs, *LEC-iCre* specifically targeted LECs without any recombination in the cardiomyocytes (Figure 7G). The above results also highlight the importance of using a more specific Cre driver for precisely deleting genes and deciphering their functions in biological processes.

DISCUSSION

Precise genetic targeting is the basis for understanding specific cell type behavior and gene function in development, homeostasis, and disease. Although most studies mainly use a singular Cre recombinase for cell lineage tracing or gene functional study, there is increased demand for precision in genetic targeting by using two or more recombinases. Although previous efforts have generated some forms of Dre+Cre combination for cell lineage tracing and gene deletion (Hermann et al., 2014; Madisen et al., 2015; Liu et al., 2019; Pu et al., 2018), the broad utility of Dre+Cre is still in its infancy because of the very few Dre drivers currently available. In this study, we provide a suit of transgenic Dre drivers to facilitate the broader utility of combining Dre and Cre for intersectional genetic studies.

In addition to the list of more than 70 new Dre lines reported here, this study also provided an example on how dual recombinase-mediated lineage tracing permits simultaneous fate mapping of a cell type that heretofore has been difficult to target with use of only a single Cre driver. In particular, we used the dual-recombinase system to explore the fate of multiple perivascular cell types during adult adipogenesis in response to homeostasis, cold stress, and injury. We also used a few Dre lines to show their application with modified Cre drivers to more specifically delete genes in tissues, such as WAs and lymphatic vessels, which have not hitherto been achieved (Figure 7H). We expect that these different Dre drivers, when used in combination with Cre, would enable more precise genetic lineage tracing and gene functional analysis in specific cell lineages in the future.

One of the fundamental questions in adipogenesis is the origin of new adipocytes in adult tissues. However, there are currently different views on the perivascular stem cells that generate new adipocytes *in vivo* (Vishvanath et al., 2017; Guimarães-Camboa and Evans, 2017). Previously, the widely used mural cell marker PDGFRb was reported to be non-specific to mural cells, as it could also be expressed by some PDGFRa$^+$ fibroblasts in adipose tissues (Cattaneo et al., 2020). In this study, our dual recombinase-mediated lineage-tracing strategy allowed us to map the fate of three perivascular cell populations, namely, PDGFRa$^+$, PDGFRb$^+$, and PDGFRa$^+$PDGFRb$^+$ cells. Their fate mapping suggested that PDGFRa$^+$ and PDGFRa$^+$PDGFRb$^+$ perivascular cells have the potential to generate new adipocytes during cold exposure, while they contribute minimally to adipocytes during homeostasis. Of note, we found that PDGFRa^{+-} PDGFRb$^+$ cells have more significant potential in generating adipocytes than PDGFRa$^+$ cells during cold exposure, highlighting the heterogeneity of PDGFRa$^+$ cells in their potentiality for adipogenesis. Alternatively, these results could also be interpreted as indicating that among PDGFRb$^+$ cells, only those co-expressing PDGFRa have the potential to generate new adipocytes, partially explaining the previous PDGFRb lineage-tracing results for adipogenesis (Tang et al., 2008; Vishvanath et al., 2016). These fate mapping results based on our intersectional genetic approach not only reconcile some of the previous controversial lineage tracing data based on singular PDGFRa or PDGFRb Cre drivers but also provide new insights on which subset of the heterogeneous cell populations has the potential to regenerate new adipocytes in adult tissues.

Further iterations of intersectional genetic approaches would promote the power of dual recombinase-mediated genetic technology in not only solving unsettled scientific questions but also opening a new window for exploring *in vivo* cell fate plasticity and their molecular regulations in biological processes. Furthermore, with the advent of scRNA-seq technology, further sub-types of new cell lineages could be identified; thus subsequent elucidation of their function *in vivo* would require precise genetic lineage tracing and gene functional study. The many new Dre drives provided here, when used in combination with Cre lines, would enable us to dissect the potential functions of newly identified cell (sub)populations in multiple fields. These potential demands, in turn, would also promote the advancement of new technology in genetic approaches, enlarging the pools of multiple recombinases mouse lines and creating new strategies to more precisely probe cell behaviors and manipulate their functions.

Limitations of study

Although inducible Dre drivers are temporally controlled, their recombination efficiencies are not high for some DreER lines in our study. For adipocyte progenitor study, we performed scRNA-seq analysis of the isolated cells from ingWAT to characterize the gene profile of different perivascular cells. Although we identify different gene expression in PDGFRa$^+$PDGFRb$^+$ or PDGFRa$^+$ cells, this study does not provide the underlying molecular mechanisms that account for their different ability to generate new adipocytes. The scRNA-seq data revealed several new markers that could be used to generate new Cre drivers to specifically target these two distinct cell populations such that gene functional analysis could be done in future. In this scRNA-seq analysis, we failed to detect population of adipocytes, likely because of the low density and fragility of adipocytes during gel beads-in-emulsion generation in the 10x Chromium Controller. It merits further investigation to understand whether adipocytes from different perivascular progenitors (e.g.,

Please cite this article in press as: Han et al., A suite of new Dre recombinase drivers markedly expands the ability to perform intersectional genetic targeting, Cell Stem Cell (2021), https://doi.org/10.1016/j.stem.2021.01.007

CellPress

PDGFRa$^+$PDGFRb$^+$ or PDGFRa$^+$ cells) may exhibit different molecular profiles and functions in future.

STAR★METHODS

Detailed methods are provided in the online version of this paper and include the following:

- KEY RESOURCES TABLE
- RESOURCE AVAILABILITY
  - Lead contact
  - Materials availability
  - Data and code availability
- EXPERIMENTAL MODEL AND SUBJECT DETAILS
  - Mice generation and breeding
- METHOD DETAILS
  - Genomic PCR
  - Cold exposure and skin wound injury model
  - Whole-mount fluorescence microscopy
  - Whole-mount immunostaining
  - Section immunostaining
  - Inguinal stromal cell preparation
  - Single-cell RNA sequencing preparation and analysis
  - H&E staining
  - Western blotting
  - Quantitative real-time PCR (qRT-PCR) analysis
- QUANTIFICATION AND STATISTICAL ANALYSIS
  - Statistics analysis

SUPPLEMENTAL INFORMATION

Supplemental Information can be found online at https://doi.org/10.1016/j.stem.2021.01.007.

ACKNOWLEDGMENTS

This study was supported by the National Key Research & Development Program of China (2019YFA0110400, 2019YFA0802000, 2018YFA0108100, 2018YFA0107900, and 2017YFC1001303), the Strategic Priority Research Program of the Chinese Academy of Sciences (CAS; XDA16010507 and XDB19000000), the National Science Foundation of China (31730112, 91849202, 31625019, 31730112, 31922032, 81872241, 31900625, 8208810001, 32050087, and 31900625), the Key Project of Frontier Sciences of the CAS (QYZDB-SSW-SMC003), the Shanghai Science and Technology Commission (19JC1415700, 19YF1455300, 19ZR1479800, and 20QC1401000), the Collaborative Innovation Program of the Shanghai Municipal Health Commission (2020CXJQ01), the Major Program of Development Fund for Shanghai Zhangjiang National Innovation Demonstration Zone (ZJ2018-ZD-004), the Pearl River Talent Recruitment Program of Guangdong Province (2017ZT07S347), the Young Elite Scientists Sponsorship Program Grant of the CAS, a Youth Innovation Promotion Association grant, the Shanghai Yangfan Project, the Shanghai Rising Star Project, the China Postdoctoral Science Foundation, the China Postdoctoral Innovative Talent Support Program, the Royal Society Newton Advanced Fellowship, AstraZeneca, the Sanofi-SIBS Fellowship, and the XPLORER PRIZE. We thank Shanghai Model Organisms Center, Inc. (SMOC), and GemPharmatech Co., Ltd., for mouse generation. We thank Astrid Gillich for editing the manuscript and Ralf Adams, Hongkui Zeng, and Minghan Tong for mice sharing. We also thank members of National Center for Protein Science Shanghai for assistance in microscopy and the animal facility for assistance of mice experiments.

AUTHOR CONTRIBUTIONS

X. Han, Z.Z., L.H., and H. Zhu designed the study, performed experiments, and analyzed the data. Yan Li, W.P., M.H., H. Zhao, K.L., Yi Li, X. Huang, M.Z., H.J., Z.L., J.T., X.T., S.D., Q.-D.W., L.W., and B.H. bred the mice, performed experiments, and provided intellectual input. J.W., R.S., and J.F. directed the generation of mouse lines. B.Z. conceived and supervised the study and wrote the manuscript.

DECLARATION OF INTERESTS

The authors declare no competing interests.

Received: August 4, 2020
Revised: December 6, 2020
Accepted: January 11, 2021
Published: February 9, 2021

REFERENCES

Akiyama, T.E., Sakai, S., Lambert, G., Nicol, C.J., Matsusue, K., Pimprale, S., Lee, Y.H., Ricote, M., Glass, C.K., Brewer, H.B., Jr., and Gonzalez, F.J. (2002). Conditional disruption of the peroxisome proliferator-activated receptor gamma gene in mice results in lowered expression of ABCA1, ABCG1, and apoE in macrophages and reduced cholesterol efflux. Mol. Cell. Biol. *22*, 2607–2619.

Anastassiadis, K., Fu, J., Patsch, C., Hu, S., Weidlich, S., Duerschke, K., Buchholz, F., Edenhofer, F., and Stewart, A.F. (2009). Dre recombinase, like Cre, is a highly efficient site-specific recombinase in E. coli, mammalian cells and mice. Dis. Model. Mech. *2*, 508–515.

Aran, D., Looney, A.P., Liu, L., Wu, E., Fong, V., Hsu, A., Chak, S., Naikawadi, R.P., Wolters, P.J., Abate, A.R., et al. (2019). Reference-based analysis of lung single-cell sequencing reveals a transitional profibrotic macrophage. Nat. Immunol. *20*, 163–172.

Baron, C.S., and van Oudenaarden, A. (2019). Unravelling cellular relationships during development and regeneration using genetic lineage tracing. Nat. Rev. Mol. Cell Biol. *20*, 753–765.

Bazigou, E., Lyons, O.T., Smith, A., Venn, G.E., Cope, C., Brown, N.A., and Makinen, T. (2011). Genes regulating lymphangiogenesis control venous valve formation and maintenance in mice. J. Clin. Invest. *121*, 2984–2992.

Berry, R., and Rodeheffer, M.S. (2013). Characterization of the adipocyte cellular lineage in vivo. Nat. Cell Biol. *15*, 302–308.

Berry, R., Jeffery, E., and Rodeheffer, M.S. (2014). Weighing in on adipocyte precursors. Cell Metab. *19*, 8–20.

Berry, D.C., Jiang, Y., Arpke, R.W., Close, E.L., Uchida, A., Reading, D., Berglund, E.D., Kyba, M., and Graff, J.M. (2017). Cellular aging contributes to failure of cold-induced beige adipocyte formation in old mice and humans. Cell Metab. *25*, 166–181.

Cano, E., Gebala, V., and Gerhardt, H. (2017). Pericytes or mesenchymal stem cells: is that the question? Cell Stem Cell *20*, 296–297.

Cattaneo, P., Mukherjee, D., Spinozzi, S., Zhang, L., Larcher, V., Stallcup, W.B., Kataoka, H., Chen, J., Dimmeler, S., Evans, S.M., and Guimarães-Camboa, N. (2020). Parallel lineage-tracing studies establish fibroblasts as the prevailing in vivo adipocyte progenitor. Cell Rep. *30*, 571–582.e2.

Cohen, M., Giladi, A., Gorki, A.-D., Solodkin, D.G., Zada, M., Hladik, A., Miklosi, A., Salame, T.-M., Halpern, K.B., David, E., et al. (2018). Lung single-cell signaling interaction map reveals basophil role in macrophage imprinting. Cell *175*, 1031–1044.e18.

Cristancho, A.G., and Lazar, M.A. (2011). Forming functional fat: a growing understanding of adipocyte differentiation. Nat. Rev. Mol. Cell Biol. *12*, 722–734.

Daigle, T.L., Madisen, L., Hage, T.A., Valley, M.T., Knoblich, U., Larsen, R.S., Takeno, M.M., Huang, L., Gu, H., Larsen, R., et al. (2018). A suite of transgenic driver and reporter mouse lines with enhanced brain-cell-type targeting and functionality. Cell *174*, 465–480.e22.

Di Talia, S., and Poss, K.D. (2016). Monitoring tissue regeneration at single-cell resolution. Cell Stem Cell *19*, 428–431.

Please cite this article in press as: Han et al., A suite of new Dre recombinase drivers markedly expands the ability to perform intersectional genetic targeting, Cell Stem Cell (2021), https://doi.org/10.1016/j.stem.2021.01.007

Eguchi, J., Wang, X., Yu, S., Kershaw, E.E., Chiu, P.C., Dushay, J., Estall, J.L., Klein, U., Maratos-Flier, E., and Rosen, E.D. (2011). Transcriptional control of adipose lipid handling by IRF4. Cell Metab. *13*, 249–259.

Eschenhagen, T., Bolli, R., Braun, T., Field, L.J., Fleischmann, B.K., Frisén, J., Giacca, M., Hare, J.M., Houser, S., Lee, R.T., et al. (2017). Cardiomyocyte regeneration: a consensus statement. Circulation *136*, 680–686.

Fu, Y., Dominissini, D., Rechavi, G., and He, C. (2014). Gene expression regulation mediated through reversible m^6A RNA methylation. Nat. Rev. Genet. *15*, 293–306.

Gerl, K., Miquerol, L., Todorov, V.T., Hugo, C.P.M., Adams, R.H., Kurtz, A., and Kurt, B. (2015). Inducible glomerular erythropoietin production in the adult kidney. Kidney Int. *88*, 1345–1355.

Gesta, S., Tseng, Y.H., and Kahn, C.R. (2007). Developmental origin of fat: tracking obesity to its source. Cell *131*, 242–256.

Guimarães-Camboa, N., and Evans, S.M. (2017). Are perivascular adipocyte progenitors mural cells or adventitial fibroblasts? Cell Stem Cell *20*, 587–589.

Guimarães-Camboa, N., Cattaneo, P., Sun, Y., Moore-Morris, T., Gu, Y., Dalton, N.D., Rockenstein, E., Masliah, E., Peterson, K.L., Stallcup, W.B., et al. (2017). Pericytes of multiple organs do not behave as mesenchymal stem cells in vivo. Cell Stem Cell *20*, 345–359.e5.

He, M., Tucciarone, J., Lee, S., Nigro, M.J., Kim, Y., Levine, J.M., Kelly, S.M., Krugikov, I., Wu, P., Chen, Y., et al. (2016). Strategies and tools for combinatorial targeting of GABAergic neurons in mouse cerebral cortex. Neuron *91*, 1228–1243.

Guy, C.T., Cardiff, R.D., and Muller, W.J. (1992). Induction of mammary tumors by expression of polyomavirus middle T oncogene: a transgenic mouse model for metastatic disease. Molecular and Cellular Biology *12*, 954–961.

He, L., Huang, X., Kanisicak, O., Li, Y., Wang, Y., Li, Y., Pu, W., Liu, Q., Zhang, H., Tian, X., et al. (2017a). Preexisting endothelial cells mediate cardiac neovascularization after injury. J. Clin. Invest. *127*, 2968–2981.

He, L., Li, Y., Li, Y., Pu, W., Huang, X., Tian, X., Wang, Y., Zhang, H., Liu, Q., Zhang, L., et al. (2017b). Enhancing the precision of genetic lineage tracing using dual recombinases. Nat. Med. *23*, 1488–1498.

He, L., Nguyen, N.B., Ardehali, R., and Zhou, B. (2020). Heart regeneration by endogenous stem cells and cardiomyocyte proliferation: controversy, fallacy, and progress. Circulation *142*, 275–291.

Hermann, M., Stillhard, P., Wildner, H., Seruggia, D., Kapp, V., Sánchez-Iranzo, H., Mercader, N., Montoliu, L., Zeilhofer, H.U., and Pelczar, P. (2014). Binary recombinase systems for high-resolution conditional mutagenesis. Nucleic Acids Res. *42*, 3894–3907.

Huelsken, J., Vogel, R., Erdmann, B., Cotsarelis, G., and Birchmeier, W. (2001). beta-Catenin controls hair follicle morphogenesis and stem cell differentiation in the skin. Cell *105*, 533–545.

Ikeda, K., Kang, Q., Yoneshiro, T., Camporez, J.P., Maki, H., Homma, M., Shinoda, K., Chen, Y., Lu, X., Maretich, P., et al. (2017). UCP1-independent signaling involving SERCA2b-mediated calcium cycling regulates beige fat thermogenesis and systemic glucose homeostasis. Nat. Med. *23*, 1454–1465.

Jeffery, E., Church, C.D., Holtrup, B., Colman, L., and Rodeheffer, M.S. (2015). Rapid depot-specific activation of adipocyte precursor cells at the onset of obesity. Nat. Cell Biol. *17*, 376–385.

Jensen, P., and Dymecki, S.M. (2014). Essentials of recombinase-based genetic fate mapping in mice. Methods Mol. Biol. *1092*, 437–454.

Jensen, P., Farago, A.F., Awatramani, R.B., Scott, M.M., Deneris, E.S., and Dymecki, S.M. (2008). Redefining the serotonergic system by genetic lineage. Nat. Neurosci. *11*, 417–419.

Jiang, Y., Berry, D.C., Tang, W., and Graff, J.M. (2014). Independent stem cell lineages regulate adipose organogenesis and adipose homeostasis. Cell Rep. *9*, 1007–1022.

Jun, H., Ma, Y., Chen, Y., Gong, J., Liu, S., Wang, J., Knights, A.J., Qiao, X., Emont, M.P., Xu, X.Z.S., et al. (2020). Adrenergic-independent signaling via CHRNA2 regulates beige fat activation. Dev. Cell *54*, 106–116.e5.

Kim, J.C., Cook, M.N., Carey, M.R., Shen, C., Regehr, W.G., and Dymecki, S.M. (2009). Linking genetically defined neurons to behavior through a broadly applicable silencing allele. Neuron *63*, 305–315.

Kretzschmar, K., and Watt, F.M. (2012). Lineage tracing. Cell *148*, 33–45.

Lakso, M., Sauer, B., Mosinger, B., Jr., Lee, E.J., Manning, R.W., Yu, S.H., Mulder, K.L., and Westphal, H. (1992). Targeted oncogene activation by site-specific recombination in transgenic mice. Proc. Natl. Acad. Sci. U S A *89*, 6232–6236.

Lee, Y.H., Petkova, A.P., Mottillo, E.P., and Granneman, J.G. (2012). In vivo identification of bipotential adipocyte progenitors recruited by β3-adrenoceptor activation and high-fat feeding. Cell Metab. *15*, 480–491.

Li, Y., He, L., Huang, X., Bhaloo, S.I., Zhao, H., Zhang, S., Pu, W., Tian, X., Li, Y., Liu, Q., et al. (2018). Genetic lineage tracing of nonmyocyte population by dual recombinases. Circulation *138*, 793–805.

Li, Y., Lv, Z., Zhang, S., Wang, Z., He, L., Tang, M., Pu, W., Zhao, H., Zhang, Z., Shi, Q., et al. (2020). Genetic fate mapping of transient cell fate reveals N-cadherin activity and function in tumor metastasis. Dev. Cell *54*, 593–607.e5.

Lin, Z., Hsu, P.J., Xing, X., Fang, J., Lu, Z., Zou, Q., Zhang, K.J., Zhang, X., Zhou, Y., Zhang, T., et al. (2017). Mettl3-/Mettl14-mediated mRNA N^6-methyladenosine modulates murine spermatogenesis. Cell Res. *27*, 1216–1230.

Liu, Q., Liu, K., Cui, G., Huang, X., Yao, S., Guo, W., Qin, Z., Li, Y., Yang, R., Pu, W., et al. (2019). Lung regeneration by multipotent stem cells residing at the bronchioalveolar-duct junction. Nat. Genet. *51*, 728–738.

Liu, K., Jin, H., and Zhou, B. (2020). Genetic lineage tracing with multiple DNA recombinases: A user's guide for conducting more precise cell fate mapping studies. J. Biol. Chem. *295*, 6413–6424.

Long, J.Z., Svensson, K.J., Tsai, L., Zeng, X., Roh, H.C., Kong, X., Rao, R.R., Lou, J., Lokurkar, I., Baur, W., et al. (2014). A smooth muscle-like origin for beige adipocytes. Cell Metab. *19*, 810–820.

Lv, J., Zhang, Y., Gao, S., Zhang, C., Chen, Y., Li, W., Yang, Y.-G., Zhou, Q., and Liu, F. (2018). Endothelial-specific m^6A modulates mouse hematopoietic stem and progenitor cell development via Notch signaling. Cell Res. *28*, 249–252.

Madisen, L., Zwingman, T.A., Sunkin, S.M., Oh, S.W., Zariwala, H.A., Gu, H., Ng, L.L., Palmiter, R.D., Hawrylycz, M.J., Jones, A.R., et al. (2010). A robust and high-throughput Cre reporting and characterization system for the whole mouse brain. Nat. Neurosci. *13*, 133–140.

Madisen, L., Garner, A.R., Shimaoka, D., Chuong, A.S., Klapoetke, N.C., Li, L., van der Bourg, A., Niino, Y., Egolf, L., Monetti, C., et al. (2015). Transgenic mice for intersectional targeting of neural sensors and effectors with high specificity and performance. Neuron *85*, 942–958.

Min, S.Y., Kady, J., Nam, M., Rojas-Rodriguez, R., Berkenwald, A., Kim, J.H., Noh, H.L., Kim, J.K., Cooper, M.P., Fitzgibbons, T., et al. (2016). Human 'brite/beige' adipocytes develop from capillary networks, and their implantation improves metabolic homeostasis in mice. Nat. Med. *22*, 312–318.

Molkentin, J.D., and Houser, S.R. (2013). Are resident c-Kit+ cardiac stem cells really all that are needed to mend a broken heart? Circ. Res. *113*, 1037–1039.

Oguri, Y., Shinoda, K., Kim, H., Alba, D.L., Bolus, W.R., Wang, Q., Brown, Z., Pradhan, R.N., Tajima, K., Yoneshiro, T., et al. (2020). CD81 controls beige fat progenitor cell growth and energy balance via FAK signaling. Cell *182*, 563–577.e20.

Plikus, M.V., Guerrero-Juarez, C.F., Ito, M., Li, Y.R., Dedhia, P.H., Zheng, Y., Shao, M., Gay, D.L., Ramos, R., Hsi, T.C., et al. (2017). Regeneration of fat cells from myofibroblasts during wound healing. Science *355*, 748–752.

Pu, W., He, L., Han, X., Tian, X., Li, Y., Zhang, H., Liu, Q., Huang, X., Zhang, L., Wang, Q.D., et al. (2018). Genetic targeting of organ-specific blood vessels. Circ. Res. *123*, 86–99.

Risebro, C.A., Searles, R.G., Melville, A.A.D., Ehler, E., Jina, N., Shah, S., Pallas, J., Hubank, M., Dillard, M., Harvey, N.L., et al. (2009). Prox1 maintains muscle structure and growth in the developing heart. Development *136*, 495–505.

Roesler, A., and Kazak, L. (2020). UCP1-independent thermogenesis. Biochem. J. *477*, 709–725.

Roundtree, I.A., Evans, M.E., Pan, T., and He, C. (2017). Dynamic RNA modifications in gene expression regulation. Cell *169*, 1187–1200.

Please cite this article in press as: Han et al., A suite of new Dre recombinase drivers markedly expands the ability to perform intersectional genetic targeting, Cell Stem Cell (2021), https://doi.org/10.1016/j.stem.2021.01.007

Sauer, B., and Henderson, N. (1988). Site-specific DNA recombination in mammalian cells by the Cre recombinase of bacteriophage P1. Proc. Natl. Acad. Sci. U S A *85*, 5166–5170.

Schwenk, F., Baron, U., and Rajewsky, K. (1995). A cre-transgenic mouse strain for the ubiquitous deletion of loxP-flanked gene segments including deletion in germ cells. Nucleic Acids Res. *23*, 5080–5081.

Sosa-Pineda, B., Wigle, J.T., and Oliver, G. (2000). Hepatocyte migration during liver development requires Prox1. Nat. Genet. *25*, 254–255.

Srinivasan, R.S., Dillard, M.E., Lagutin, O.V., Lin, F.J., Tsai, S., Tsai, M.J., Samokhvalov, I.M., and Oliver, G. (2007). Lineage tracing demonstrates the venous origin of the mammalian lymphatic vasculature. Genes Dev. *21*, 2422–2432.

Suzuki, A., Yamaguchi, M.T., Ohteki, T., Sasaki, T., Kaisho, T., Kimura, Y., Yoshida, R., Wakeham, A., Higuchi, T., Fukumoto, M., et al. (2001). T cell-specific loss of Pten leads to defects in central and peripheral tolerance. Immunity *14*, 523–534.

Tang, W., Zeve, D., Suh, J.M., Bosnakovski, D., Kyba, M., Hammer, R.E., Tallquist, M.D., and Graff, J.M. (2008). White fat progenitor cells reside in the adipose vasculature. Science *322*, 583–586.

Tian, X., Hu, T., Zhang, H., He, L., Huang, X., Liu, Q., Yu, W., He, L., Yang, Z., Zhang, Z., et al. (2013). Subepicardial endothelial cells invade the embryonic ventricle wall to form coronary arteries. Cell Res. *23*, 1075–1090.

Tian, X., Pu, W.T., and Zhou, B. (2015). Cellular origin and developmental program of coronary angiogenesis. Circ. Res. *116*, 515–530.

Torii, Ma., Matsuzaki, F., Osumi, N., Kaibuchi, K., Nakamura, S., Casarosa, S., Guillemot, F., and Nakafuku, M. (1999). Transcription factors Mash-1 and Prox-1 delineate early steps in differentiation of neural stem cells in the developing central nervous system. Development *126*, 443–456.

Vishvanath, L., MacPherson, K.A., Hepler, C., Wang, Q.A., Shao, M., Spurgin, S.B., Wang, M.Y., Kusminski, C.M., Morley, T.S., and Gupta, R.K. (2016). Pdgfrβ+ mural preadipocytes contribute to adipocyte hyperplasia induced by high-fat-diet feeding and prolonged cold exposure in adult mice. Cell Metab. *23*, 350–359.

Vishvanath, L., Long, J.Z., Spiegelman, B.M., and Gupta, R.K. (2017). Do adipocytes emerge from mural progenitors? Cell Stem Cell *20*, 585–586.

Wang, Q.A., Tao, C., Gupta, R.K., and Scherer, P.E. (2013). Tracking adipogenesis during white adipose tissue development, expansion and regeneration. Nat. Med. *19*, 1338–1344.

Wigle, J.T., Chowdhury, K., Gruss, P., and Oliver, G. (1999). Prox1 function is crucial for mouse lens-fibre elongation. Nat. Genet. *21*, 318–322.

Zhang, H., Pu, W., Li, G., Huang, X., He, L., Tian, X., Liu, Q., Zhang, L., Wu, S.M., Sucov, H.M., and Zhou, B. (2016). Endocardium minimally contributes to coronary endothelium in the embryonic ventricular free walls. Circ. Res. *118*, 1880–1893.

Zhang, C., Chen, Y., Sun, B., Wang, L., Yang, Y., Ma, D., Lv, J., Heng, J., Ding, Y., Xue, Y., et al. (2017). m^6A modulates haematopoietic stem and progenitor cell specification. Nature *549*, 273–276.

Zhao, H., and Zhou, B. (2019). Dual genetic approaches for deciphering cell fate plasticity in vivo: more than double. Curr. Opin. Cell Biol. *61*, 101–109.

Please cite this article in press as: Han et al., A suite of new Dre recombinase drivers markedly expands the ability to perform intersectional genetic targeting, Cell Stem Cell (2021), https://doi.org/10.1016/j.stem.2021.01.007

STAR★METHODS

KEY RESOURCES TABLE

REAGENT or RESOURCE	SOURCE	IDENTIFIER
Antibodies		
tdTomato	Rockland	Cat# 600-401-379; RRID: AB_2209751
GFP	Nacalai Tesque	Cat# 04404-84; RRID:AB_10013361
CDH5	R&D	Cat# AF1002; RRID:AB_2077789
PDGFRa	R&D	Cat# AF1062;RRID:AB_2236897
PDGFRb	eBioscience	Cat# 14-1402-82; RRID:AB_467493
Troponin I	Abcam	Cat# AB56357; RRID:AB_880622
Prox1	Abcam	Cat# AB101851; RRID:AB_10712211
Prox1	R&D	Cat# AF2727; RRID:AB_2170716
HNF4a	Cell Signaling	Cat# 3113s; RRID:AB_2295208
UCP1	Sigma	Cat# u6382; RRID:AB_261838
METTL3	Abcam	Cat# AB195352; RRID:AB_2721254
FABP4	Abcam	Cat# AB13979; RRID:AB_1951817
E-cadherin	Cell Signaling	Cat# 3195; RRID:AB_355568
EpCAM	Abcam	Cat# ab92383; RRID:AB_301631
SMA	Sigma	Cat# F3777; RRID:AB_476977
Keratin 14	Covance	Cat# PRB-155P-100; RRID:AB_292096
Amylase	Sigma	Cat# A8273; RRID:AB_2772500
SM22	Abcam	Cat# AB14106; RRID:AB_443021
Lysozyme	Dako	Cat# A0099; RRID:AB_2341230
Ly6g	Abcam	Cat# AB25377; RRID:AB_470492
Endomucin	Santa Cruz	Cat# sc-65495; RRID:AB_2100037
Keratin 5	Covance	Cat# 905504; RRID:AB_10063444
T1a	DSHB	Cat# 8.1.1; RRID:AB_531893
Neun	Merck	Cat# MAB377X; RRID:AB_2149209
CD45	eBioscience	Cat# 11-0451; RRID:AB_469625
Connexin43	Sigma	Cat# C6219; RRID:AB_476857
ZsGreen	Clontech	Cat# 632474; RRID:AB_2491179
αA-crystallin (B-2)	Santa Cruz	Cat# sc-28306; RRID:AB_627304
PyMT	Abcam	Cat# ab15085; RRID:AB_301631
tdTomato	ChromoTek	Cat# ABIN334653; RRID:AB_2209751
Chemicals, peptides, and recombinant proteins		
Tamoxifen	Sigma-Aidrich	Cat# T5648
PBS	GIBCO	Cat# C10010500BT
Sucrose	Sigma-Aidrich	Cat# V900116
O.C.T.	Sakura	Cat# 4583
Triton X-100	Sigma-Aidrich	Cat# Sigma-X-100
Paraformaldehyde (PFA)	Sigma-Aidrich	Cat# P6148-1KG
Donkey serum	JIR	Cat# 017-000-001
Collagenase I	GIBCO	Cat# 17018029
Isoflurane gas	Jinan Shengqi Pharm. Co, Ltd.	Cat# 26675-46-7
HBSS	Invitrogen	Cat# 14175103
DNase I	Worthington	Cat# LS002139
RBC	eBioscience	Cat# 00-4333-57

(*Continued on next page*)

Please cite this article in press as: Han et al., A suite of new Dre recombinase drivers markedly expands the ability to perform intersectional genetic targeting, Cell Stem Cell (2021), https://doi.org/10.1016/j.stem.2021.01.007

Continued

REAGENT or RESOURCE	SOURCE	IDENTIFIER
Wheat Germ Agglutinin	invitrogen	Cat# W6748
DAPI	Sigma	Cat# D21490
RPMI 1640	invitrogen	Cat# 22400089
RIPA lysis buffer	Beyotime	Cat# P0013B
SYBR Green qPCR master mix	Thermo Fisher Scientific	Cat# 4367659
Trizol	invitrogen	Cat# 15596018
Critical commercial assays		
Tyramide signal amplification kit	PerkinElmer	NEL749B001KT
PrimeScript RT kit	Takara	Cat# R045A
Chromium Single Cell 3′ Library & Gel Bead Kit v3.1	10X Genomics	Cat# PN-1000121
Deposited data		
Single Cell RNA Sequencing	This paper	BioProject: PRJNA681924
Experimental models: organisms/strains		
Mouse: *Apln-DreER*	This paper	Shanghai Biomodel Organism Co., Ltd
Mouse: *Aplnr-DreER*	This paper	Shanghai Biomodel Organism Co., Ltd
Mouse: *Axin2-2A-DreER*	This paper	Shanghai Biomodel Organism Co., Ltd
Mouse: *Brachyury T-DreER*	This paper	Shanghai Biomodel Organism Co., Ltd
Mouse: *CCR2-2A-DreER*	This paper	Shanghai Biomodel Organism Co., Ltd
Mouse: *Cd11c-2A-DreER*	This paper	Shanghai Biomodel Organism Co., Ltd
Mouse: *CD45-Dre*	This paper	Shanghai Biomodel Organism Co., Ltd
Mouse: *Cdh1-2A-DreER*	This paper	Shanghai Biomodel Organism Co., Ltd
Mouse: *Cdh5-Dre*	This paper	Shanghai Biomodel Organism Co., Ltd
Mouse: *Cdh5-DreER*	This paper	Shanghai Biomodel Organism Co., Ltd
Mouse: *Cela1-2A-DreER*	This paper	Shanghai Biomodel Organism Co., Ltd
Mouse: *Clu-2A-DreER*	This paper	Shanghai Biomodel Organism Co., Ltd
Mouse: *Cx40-Dre*	This paper	Shanghai Biomodel Organism Co., Ltd
Mouse: *Cx40-DreER-GFP*	This paper	Shanghai Biomodel Organism Co., Ltd
Mouse: *Cx40-LSL-Dre*	This paper	Shanghai Biomodel Organism Co., Ltd
Mouse: *Cyp2e1-2A-DreER*	This paper	Shanghai Biomodel Organism Co., Ltd
Mouse: *Cyp2e1-DreER*	This paper	Shanghai Biomodel Organism Co., Ltd
Mouse: *Ela-DreER-GFP*	This paper	Shanghai Biomodel Organism Co., Ltd
Mouse: *Epcam-2A-DreER*	This paper	Shanghai Biomodel Organism Co., Ltd
Mouse: *F4/80-Dre*	This paper	Shanghai Biomodel Organism Co., Ltd
Mouse: *Flt3-2A-DreER*	This paper	Shanghai Biomodel Organism Co., Ltd
Mouse: *Gja1-2A-DreER*	This paper	Shanghai Biomodel Organism Co., Ltd
Mouse: *Gli1-DreER*	This paper	Shanghai Biomodel Organism Co., Ltd
Mouse: *Hcn4-DreER*	This paper	Shanghai Biomodel Organism Co., Ltd
Mouse: *Hey2-DreER*	This paper	Shanghai Biomodel Organism Co., Ltd
Mouse: *Hopx-2A-DreER*	This paper	Shanghai Biomodel Organism Co., Ltd
Mouse: *Ins-Dre*	This paper	Shanghai Biomodel Organism Co., Ltd
Mouse: *Ins-DreER*	This paper	Shanghai Biomodel Organism Co., Ltd
Mouse: *Isl1-Dre*	This paper	Shanghai Biomodel Organism Co., Ltd
Mouse: *K14-2A-DreER*	This paper	Shanghai Biomodel Organism Co., Ltd
Mouse: *K14-Dre*	This paper	Shanghai Biomodel Organism Co., Ltd
Mouse: *K19-2A-DreER*	This paper	Shanghai Biomodel Organism Co., Ltd
Mouse: *K19-DreER*	This paper	Shanghai Biomodel Organism Co., Ltd
Mouse: *K5-Dre*	This paper	Shanghai Biomodel Organism Co., Ltd

(*Continued on next page*)

Please cite this article in press as: Han et al., A suite of new Dre recombinase drivers markedly expands the ability to perform intersectional genetic targeting, Cell Stem Cell (2021), https://doi.org/10.1016/j.stem.2021.01.007

Continued

REAGENT or RESOURCE	SOURCE	IDENTIFIER
Mouse: *K5-DreER*	This paper	Shanghai Biomodel Organism Co., Ltd
Mouse: *K5-LSL-Dre*	This paper	Shanghai Biomodel Organism Co., Ltd
Mouse: *Kank1-2A-DreER*	This paper	Shanghai Biomodel Organism Co., Ltd
Mouse: *Lepr-2A-DreER*	This paper	Shanghai Biomodel Organism Co., Ltd
Mouse: *Lgr5-2A-DreER*	This paper	Shanghai Biomodel Organism Co., Ltd
Mouse: *Ly6g-2A-DreER*	This paper	Shanghai Biomodel Organism Co., Ltd
Mouse: *Lyz1-2A-DreER*	This paper	Shanghai Biomodel Organism Co., Ltd
Mouse: *Meox1-Dre*	This paper	Shanghai Biomodel Organism Co., Ltd
Mouse: *Ms4a3-2A-Dre*	This paper	Shanghai Biomodel Organism Co., Ltd
Mouse: *Ms4a3-2A-DreER*	This paper	Shanghai Biomodel Organism Co., Ltd
Mouse: *Msln-DreER*	This paper	Shanghai Biomodel Organism Co., Ltd
Mouse: *Myh11-2A-DreER*	This paper	Shanghai Biomodel Organism Co., Ltd
Mouse: *Myh11-Dre*	This paper	Shanghai Biomodel Organism Co., Ltd
Mouse: *Nppa-DreER*	This paper	Shanghai Biomodel Organism Co., Ltd
Mouse: *Nppb-DreER*	This paper	Shanghai Biomodel Organism Co., Ltd
Mouse: *Npr3-2A-DreER*	This paper	Shanghai Biomodel Organism Co., Ltd
Mouse: *P63-DreER*	This paper	Shanghai Biomodel Organism Co., Ltd
Mouse: *P63-LSL-Dre*	This paper	Shanghai Biomodel Organism Co., Ltd
Mouse: *Pax7-2A-DreER*	This paper	Shanghai Biomodel Organism Co., Ltd
Mouse: *Pdgfrb-Dre*	This paper	Shanghai Biomodel Organism Co., Ltd
Mouse: *Pdgfb-DreER*	This paper	Shanghai Biomodel Organism Co., Ltd
Mouse: *Pdgfrb-LSL-Dre*	This paper	Shanghai Biomodel Organism Co., Ltd
Mouse: *Plin1-dCreER*	This paper	Shanghai Biomodel Organism Co., Ltd
Mouse: *Plin1-2A-DreER*	This paper	Shanghai Biomodel Organism Co., Ltd
Mouse: *Prox1-RSR-2A-CreER*	This paper	Shanghai Biomodel Organism Co., Ltd
Mouse: *Prox1-2A-DreER*	This paper	Shanghai Biomodel Organism Co., Ltd
Mouse: *Rbfox3-2A-DreER*	This paper	Shanghai Biomodel Organism Co., Ltd
Mouse: *Sca1-2A-DreER*	This paper	Shanghai Biomodel Organism Co., Ltd
Mouse: *SiglecF-DreER*	This paper	Shanghai Biomodel Organism Co., Ltd
Mouse: *SMA-Dre*	This paper	Shanghai Biomodel Organism Co., Ltd
Mouse: *SMA-GFP-DreER*	This paper	Shanghai Biomodel Organism Co., Ltd
Mouse: *SMA-LSL-Dre*	This paper	Shanghai Biomodel Organism Co., Ltd
Mouse: *Snai1-LSL-Dre*	This paper	Shanghai Biomodel Organism Co., Ltd
Mouse: *Sox9-2A-DreER*	This paper	Shanghai Biomodel Organism Co., Ltd
Mouse: *Twist-LSL-Dre*	This paper	Shanghai Biomodel Organism Co., Ltd
Mouse: *Ucp1-Dre*	This paper	Shanghai Biomodel Organism Co., Ltd
Mouse: *Upk3b-Dre*	This paper	Shanghai Biomodel Organism Co., Ltd
Mouse: *Wnt1-Dre*	This paper	Shanghai Biomodel Organism Co., Ltd
Mouse: *Wt1-DreER*	This paper	Shanghai Biomodel Organism Co., Ltd
Mouse: *Zeb1-LSL-Dre*	This paper	Shanghai Biomodel Organism Co., Ltd
Mouse: *Pdgfra-DreER*	He et al., 2017a	N/A
Mouse: *Pdgfrb-CreER*	Gerl et al., 2015	N/A
Mouse: *R26-RSR-tdTomato*	Zhang et al., 2016	N/A
Mouse: *R26-GFP*	Zhang et al., 2016	N/A
Mouse: *R26-tdTomato*	Madisen et al., 2010	N/A

(*Continued on next page*)

Please cite this article in press as: Han et al., A suite of new Dre recombinase drivers markedly expands the ability to perform intersectional genetic targeting, Cell Stem Cell (2021), https://doi.org/10.1016/j.stem.2021.01.007

Continued

REAGENT or RESOURCE	SOURCE	IDENTIFIER
Mouse: *CAG-Dre*	Anastassiadis et al., 2009	N/A
Mouse: *Prox1-IRES-CreER*	Srinivasan et al., 2007	N/A
Mouse: *MMTV-PyMT*	Guy et al., 1992	N/A
Mouse: *NR1*	He et al., 2017b	N/A
Mouse: *Mettl3-flox*	Lin et al., 2017	N/A
Mouse: *Pparg-flox*	Akiyama et al., 2002	N/A
Mouse: *β-Catenin-flox*	Huelsken et al., 2001	N/A
Mouse: *Pten-flox*	Suzuki et al., 2001	N/A
Oligonucleotides for qRT-PCR		
Primer1 of β-actin: 5′-GATCATTGCTCCTCCTGAGC −3′	This paper	N/A
Primer2 of β-actin: 5′-ACTCCTGCTTGCTGATCCAC −3′	This paper	N/A
Primer1 of Pparg: 5′-GAGCTGACCCAATGGTTGCTGATT −3′	This paper	N/A
Primer2 of Pparg: 5′-TGGCCATGAGGGAGTTAGAAGGTT −3′	This paper	N/A
Primer1 of β-catenin: 5′-CCCAGTCCTTCACGCAAGAG −3′	This paper	N/A
Primer2 of β-catenin: 5′-CATCTAGCGTCTCAGGGAACA −3′	This paper	N/A
Primer1 of Pten: 5′-TGGATTCGACTTAGACTTGACCT −3′	This paper	N/A
Primer2 of Pten: 5′-GCGGTGTCATAATGTCTCTCAG −3′	This paper	N/A
Software and algorithms		
GraphPad Prism 6 software	GraphPad Software,Inc.	N/A
PhotoLine	https://www.pl32.com/	N/A
Cell Ranger (v.4.0.0)	10X Genomics	https://support.10xgenomics.com/

RESOURCE AVAILABILITY

Lead contact

Further information and requests for resources and reagents should be directed to and will be fulfilled by the Lead Contact, Bin Zhou, zhoubin@sibs.ac.cn.

Materials availability

Some of the new mouse lines reported in this study have been generated by and deposited to the Shanghai Model Organisms Company (https://www.modelorg.com/en/). The materials, reagents, mice lines, and original data could also be provided on reasonable request. Some materials would be provided upon completed Materials Transfer Agreement.

Data and code availability

The single cell RNA sequencing datasets that were generated for this manuscript are available under the SRA project accession number BioProject: PRJNA681924

Please cite this article in press as: Han et al., A suite of new Dre recombinase drivers markedly expands the ability to perform intersectional genetic targeting, Cell Stem Cell (2021), https://doi.org/10.1016/j.stem.2021.01.007

EXPERIMENTAL MODEL AND SUBJECT DETAILS

Mice generation and breeding

All mice used in this paper were utilized strictly in accordance with the guidelines of the Institutional Animal Care and Use Committee (IACUC) at the Institute of Biochemistry and Cell Biology, and the Institute for Nutritional Sciences, Shanghai Institutes for Biological Sciences, Chinese Academy of Science. Mice were raised on a standard rodent chow diet with 12-hour light and dark cycles. Tamoxifen (Sigma, T5648) was dissolved in corn oil (20 mg/ml) and administered by gavage at the indicated time points (0.2 mg per gram of mouse body weight). *CAG-Dre*, *Prox1-IRES-CreER*, *PDGFRa-DreER*, *R26-GFP, R26-tdTomato*, *PDGFRb-CreER*, *R26-RSR-tdTomato*, *Mettl3-flox*, *Pparg-flox*, *β-Catenin-flox*, *Pten-flox* mouse lines were described previously (Anastassiadis et al., 2009; Srinivasan et al., 2007; He et al., 2017a; Zhang et al., 2016; Gerl et al., 2015; Madisen et al., 2015; Lin et al., 2017; Akiyama et al., 2002; Huelsken et al., 2001; Suzuki et al., 2001). *Plin1-dCreER* mouse was generated by insertion of rox-CreER-rox into Plin1 gene start codon by homologous recombination using CRISPR/Cas9. In detail, a DNA cassette withtwo homologous arms spanning the left and right side of the ATG of Plin1 gene and containing rox flaned CreER followed with polyA sequence was used for homologous recombination using CRISPR/Cas9. *Prox1-RSR-CreER* mouse was generated by insertion of rox-Stop-rox-CreER into the translational stop codon of Prox1 gene by homologous recombination using CRISPR/Cas9. *Prox1-2A-CreER* was generated by crossing *Prox1-RSR-CreER* with CAG-Dre mouse, by which Dre-rox recombination removes RSR cassette in germline, thus generating *Prox1-2A-CreER* line in the next generation. For Dre, DreER, or LSL-Dre mouse lines, these genetic cassettes were targeted to 5′ UTR or 3′ UTR sites of endogenous genes by homologous recombination (Figures 1A and 1B). More detailed information for these newly generated Dre-related mouse lines, please refer to Table S1. For information on genotyping PCR primers, please refer to Table S2. All mice used were maintained on a C57BL6/ICR background.

METHOD DETAILS

Genomic PCR

Genomic DNA for genotyping was prepared from mice toes. Toes were lysed by Proteinase K and incubated overnight at 55°C, followed by centrifugation at maximum speed for 8 minutes to obtain supernatant with genomic DNA. DNA was precipitated by adding equal volume absolute ethyl alcohol then washed in 70% ethanol, and was finally dissolved in distilled H_2O. All mice were genotyped with specific primers that distinguish knock-in allele from wild-type allele. All genotype primers for new mice were included in Table S2. Any information regarding to the primers for Dre mouse lines would be provided upon request.

Cold exposure and skin wound injury model

For the cold exposure study, 10 week-old mice were maintained at 6°C and on a standard rodent chow diet with 12- hour light and dark cycles for 1-2weeks after the tamoxifen wash out. The mice were killed according to the standard protocols described previously (Tian et al., 2013). For the skin wound injury model, 8-10 week-old mice were anaesthetized with 2% isoflurane and oxygen flow in a plexiglass chamber. The back fur was removed and the skin was disinfected as described previously (Plikus et al., 2017). The mice were transferred onto a 37°C heat pad and maintained on anesthesia by inhalation of isoflurane with oxygen. A midline back skin incision was made as previously described (Plikus et al., 2017). Then the animals were placed on a warming pad for recovery. After the mice woke up, they were maintained in accordance with the IACUC guidelines.

Whole-mount fluorescence microscopy

Collected mouse tissue was washed in PBS and placed on agar for the whole-mount bright field and fluorescence imaging using the Zeiss (AxioZoom V16). To determine magnification of specific regions, we used the automated Z stack images acquired by the Zeiss stereo-scope (AxioZoom V16).

Whole-mount immunostaining

For embryos' skin whole-mount immunostaining, tissue was fixed in 4% paraformaldehyde (PFA) for 2 hours at room temperature, then tissues were washed in PBS 5 minutes for three times. Blocked in 5% normal donkey serum (Jackson Immunoresearch) and 0.1% Triton X-100 in PBS for at least 30 min at room temperature. Primary antibodies were incubated at 4°C for 48 hours in blocking buffer. After washing in PBS for 3 times, signals were developed with Alexa fluorescence antibodies (Invitrogen, 1:1000) for 2 hours, and nuclei were counterstained with 4'6-diamidino-2-phenylindole (DAPI, Vector lab). Immunostaining images were acquired by Zeiss confocal laser scanning microscope (LSM880), Nikon confocal laser scanning microscope (Nikon A1).

Section immunostaining

Immunostaining was performed according to the standard protocols described previously (Tian et al., 2013). In brief, tissues were dissected in PBS and fixed in 4% paraformaldehyde (PFA Sigma) at 4°C for 60-120 min. Afterward, tissues were washed in PBS for 3 minutes, three times, dehydrated in 30% sucrose overnight at 4°C. Following 1-5 hours of immersion in optimum cutting temperature (O.C.T., Sakura) at 4°C, the tissues were embedded in blocks and frozen at − In brief, tissues were dissected in PBS and fixed in 4% paraformaldehyde (PFA Sigma) at 4°C for 60-120 min. Afterward, tissues werimmunostaining, dried sections were washed in PBS for 6 min, three times and then blocked with 2.5% normal donkey serum (Jackson Immunoresearch) and 0.1% Triton

Please cite this article in press as: Han et al., A suite of new Dre recombinase drivers markedly expands the ability to perform intersectional genetic targeting, Cell Stem Cell (2021), https://doi.org/10.1016/j.stem.2021.01.007

X-100 in PBS for at least 30 min at room temperature. Sections were incubated with the primary antibodies overnight at 4°C. The following antibodies were used: tdTomato (Rockland, 600-401-379, 1:1000), GFP (Nacalai Tesque, 04404-84, 1:500), CDH5 (R&D, AF1002, 1:100), PDGFRa (R&D, AF1062, 1:500), PDGFRb (eBioscience, 14-1402-82, 1:500), Troponin I (Abcam, AB56357, 1:200), Prox1 (Abcam, AB101851), Prox1 (R&D, AF2727, 1:100), HNF4a (Cell Signaling, 3113s, 1:1000), UCP1 (Sigma, u6382, 1:200), METTL3 (Abcam, AB195352, 1:500), FABP4 (Abcam, AB13979, 1:500), E-cadherin (Cell Signaling, 3195, 1:500), EpCAM (Abcam, ab92383, 1:100), SMA (Sigma, F3777, 1:100). Keratin 14 (Covance, PRB-155P-100, 1:500), Amylase (Sigma, A8273, 1:1000), SM22 (Abcam, AB14106, 1:500), Lysozyme (Dako, A0099, 1:500), Ly6g (Abcam, AB25377, 1:200), Endomucin (Stnta Cruz, sc-65495, 1:500), Keratin 5 (Covance, 905504, 1:500), T1a (DSHB, 8.1.1, 1:100), NeuN (Merck, MAB377X,1:200), CD45 (eBioscience,11-0451,1:100), Connexin43 (Sigma, C6219, 1:500), ZsGreen (Clontech, 632474, 1:1000), PyMT (Abcam, ab15085, 1:200), tdTomato (ChromoTek, ABIN334653, 1:100), αA-crystallin(B-2) (Santa Cruz, sc-28306, 1:200). Signals were developed with Alexa fluorescence antibodies (Invitrogen), and nuclei were counterstained with 4'6-diamidino-2-phenylindole (DAPI, Vector lab). Immunostaining images were acquired by Zeiss stereomicroscope (AXIO Zoom, V16), Zeiss confocal laser scanning microscope (LSM880), Nikon confocal laser scanning microscope (Nikon A1) and Olympus confocal microscope (FV1200).

Inguinal stromal cell preparation

To generate single-cell suspensions, inguinal stromal cell isolated from wild-type male mice (8 weeks old) were further digested in collagenase I for 30-40 min as described. In detail, inguinal WAT was cut into small pieces, and these small pieces were digested by 2 mg/ml collagenase I (GIBCO, 17018029) in Hank's Balanced Salt Solution (HBSS) containing 5% FBS at 37°C for 30-40 minutes. During this process, inguinal WAT was frequent stirred to ensure full digestion. After sufficient digestion, cells were filtered through a 70-μm cell strainer (BD Biosciences), and the collected cells were centrifuged 5 min at 400 g speed. Subsequently, cell pellet was suspended in PBS or DEME for further experiments.

Single-cell RNA sequencing preparation and analysis

The cell suspense above was loaded in 10x Chromium controller to generate GEMs, which were further processed into single cell 3′ gene expression libraries using Chromium Single Cell 3′ Library Kit (v3.1 Chemistry). Sequencing was performed on Illumina Hiseq X Ten PE150 platform. Raw fastq files first were cleaned by Trim Galore with parameter "-q 20–phred33–stringency 3–length 20 -e 0.1." Trimmed fastq files were processed by CellRanger (v.4.0.0) pipeline. Further analysis was done by R package Seurat (v.3.2.0) with customized parameters. Notably, Pdgfra and Pdgfrb expression was imputed by Rmagic with setting "t = 'auto'." GO enrichment analysis was performed by Metascape using the genes upregulated in $Pdgfra^{+}Pdgfrb^{+}$ cells versus $Pdgfra^{+}$ cells.

H&E staining

10-30 μm-thick cryosections were incubated in Hematoxylin A solution for 10 min, washed with running tap water 2-3 times, rinsed in 1% concentrated hydrochloric acid diluted in 70% ethanol for 1 min and washed with water 2-3 times. Then the slides were incubated in 1% ammonia water for 1 min, washed in water 2-3 times, rinsed in 95% ethanol 10 s and then stained with Eosin-Y solution for 5-10 s, dehydrated in a series of ethanol and xylene, and lastly mounted with neutral balsam. All Image data were acquired using an Olympus microscope (Olympus, DP72).

Western blotting

Adipose tissues were collected at the indicated stages. All samples were homogenized in RIPA lysis buffer (Beyotime, P0013B) supplemented with protease inhibitors (Roche, 11836153001), incubated for 30 min on ice, and then centrifuged at maximum speed (22,000 g) for 15 min to isolate the central layer of protein. All samples were mixed with 5x loading buffer (Beyotime, p0015L), boiled for 10 min. Western blot analyses were performed with precast gradient gels (Beyotime, P0469M) and transferred onto polyvinylidenefluoride membranes (Millipore, IPVH00010) using a Mini Trans Blot system (Bio-Rad). Then the membranes were blocked with PBS-T (10mM Tris-HCl pH8.0, 150mM NaCl and 0.1% vol/vol Tween-20) and 5% BSA for 0.5 hour at room temperature. After that, membranes were probed with specific primary antibodies overnight at 4°C, washed for 3 times, and incubated with HRP-conjugated secondary antibodies for 1 hour at room temperature. Protein signals were detected via enhanced chemiluminescence kit (Pierce), according to manufacturer's protocol. All antibodies were commercially available: anti-PPARγ (Santa Cruz, sc-7273, 1:200), anti-β-CATENIN (Santa Cruz, sc-7199, 1:1000), anti-PTEN (Sangon Biotech, D155023, 1:500), anti-β-ACTIN (Proteintech, 60008-1-Ig, 1:5000), anti-β-ACTIN (Cell Signaling Technology, 3700, 1:1000), anti-α-TUBLIN (Sigma-Aldrich, T6199, 1:5000), Peroxidase AffiniPure Goat Anti-Rabbit IgG (Jackson ImmunoResearch, 111-035-047, 1:4000), Peroxidase AffiniPure Donkey Anti-Mouse IgG (Jackson ImmunoResearch, 715-035-150, 1:4000).

Quantitative real-time PCR (qRT-PCR) analysis

Adipose tissues were collected at the indicated stages. All samples were homogenized in TRIzol Reagent (Invitrogen, 15596018). RNA from adipose tissues was isolated according to the manufacturer's protocol. For each sample, 1 μg of total RNA was reverse transcribed by using PrimeScript RT reagent Kit with gDNA Eraser (Takara, RR047A). For qPCR, the SYBR Green PCR master mix (Thermo Fisher Scientific, 4367659) was used. And qPCR was carried out using the StepOnePlus real-time PCR system (Applied Biosystems). Gene expression was normalized to the endogenous control (*β-actin*). The following primers were used: *β-actin* (F: GATCATTGCTCCTCCTGAGC; R: ACTCCTGCTTGCTGATCCAC); *Pparg* (F: GAGCTGACCCAATGGTTGCTGATT; R: TGGCCATGAGGGAGTTAGAAGGTT);

Please cite this article in press as: Han et al., A suite of new Dre recombinase drivers markedly expands the ability to perform intersectional genetic targeting, Cell Stem Cell (2021), https://doi.org/10.1016/j.stem.2021.01.007

β-catenin (F: CCCAGTCCTTCACGCAAGAG; R: CATCTAGCGTCTCAGGGAACA); *Pten* (F: TGGATTCGACTTAGACTTGACCT; R: GCGGTGTCATAATGTCTCTCAG).

QUANTIFICATION AND STATISTICAL ANALYSIS

Statistics analysis

All data were collected from at least five individual biological samples. Data for two groups were analyzed by a two-sided unpaired Student's t test, whereas comparison between more than two groups was performed using an analysis of variance followed by Tukey's multiple comparison tests. Significance was accepted when $p < 0.05$. All data were presented as mean value ± SEM 3-5 individual biological samples were included in each experiment as indicated. Mice with indicated genotypes were assigned to groups randomly.

Cell Stem Cell, Volume *28*

Supplemental Information

A suite of new Dre recombinase drivers markedly expands the ability to perform intersectional genetic targeting

Ximeng Han, Zhenqian Zhang, Lingjuan He, Huan Zhu, Yan Li, Wenjuan Pu, Maoying Han, Huan Zhao, Kuo Liu, Yi Li, Xiuzhen Huang, Mingjun Zhang, Hengwei Jin, Zan Lv, Juan Tang, Jinjin Wang, Ruilin Sun, Jian Fei, Xueying Tian, Shengzhong Duan, Qing-Dong Wang, Lixin Wang, Ben He, and Bin Zhou

Supplemental Data

A Suite of New Dre-recombinase Drivers Markedly Expands the Ability to Perform Intersectional Genetic Targeting

Ximeng Han, Zhenqian Zhang, Lingjuan He, Huan Zhu, Yan Li, Wenjuan Pu, Maoying Han, Huan Zhao, Kuo Liu, Yi Li, Xiuzhen Huang, Mingjun Zhang, Hengwei Jin, Zan Lv, Juan Tang, Jinjin Wang, Ruilin Sun, Jian Fei, Xueying Tian, Shengzhong Duan, Qing-Dong Wang, Lixin Wang, Ben He, Bin Zhou

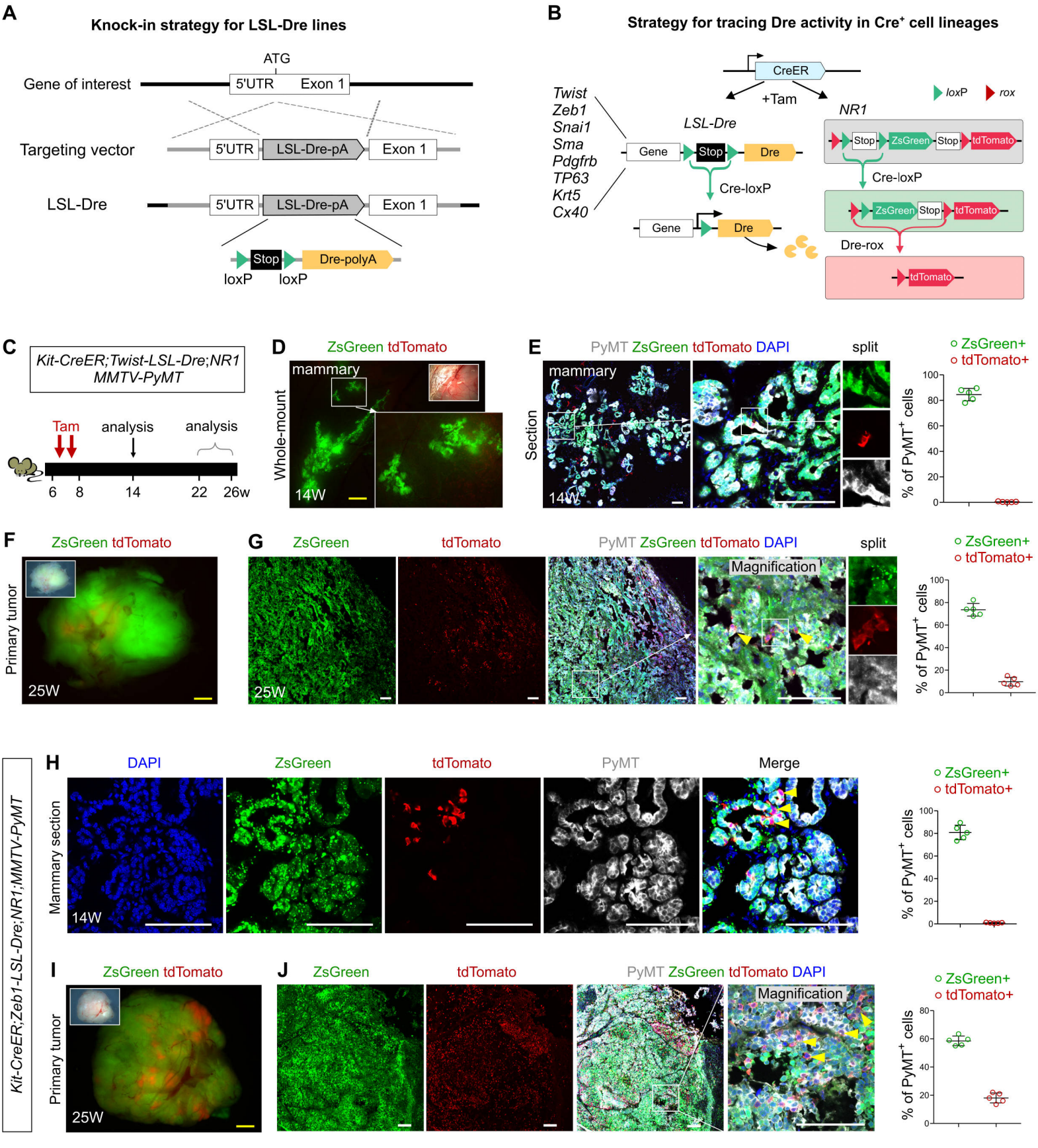

Figure S1. Generation of LSL-Dre mouse lines for Cre-induced Dre-mediated lineage tracing (Related to Figure 1)

(A) Schematic diagram illustrating knock-in strategy for LSL-Dre mouse lines by CRISPR/Cas9.

(B) Schematic diagram illustrating strategy for characterizing LSL-Dre using Cre drivers and dual nested reporter (*NR1*).

(C) Schematic diagram illustrating experimental design of tracing Twist gene activity specifically in Kit+ mammary epithelial cells during primary tumor growth. *Kit-CreER* is used to induce Dre expression under control of Twist gene. *MMTV-PyMT* is used to for endogenous mammary tumor formation.

(D,F) Whole-mount fluorescence images of mammary tissue at 14 weeks (14W, D) or 25W (F).

(E,G) Immunostaining for PyMT, ZsGreen, and tdTomato on mammary tissue sections at 14W (E) or 25W (G). Right panels show the percentage of PyMT+ cells expressing ZsGreen or tdTomato. Data are mean ± s.e.m.; n = 5.

(H-J) Examination of Zeb1 gene activity by Kit-CreER induced Dre lineage tracing during mammary tumor formation. Immunostaining for PyMT, ZsGreen, and tdTomato on mammary tumor sections at 14W (H) or 25W (J). Whole-mount fluorescence of tumors is shown in I. Right panels show the percentage of PyMT+ cells expressing ZsGreen or tdTomato. Data are mean ± s.e.m.; n = 5.

Scale bars, yellow, 2 mm; white, 100 μm. Each image is representative of 5 individual biological samples.

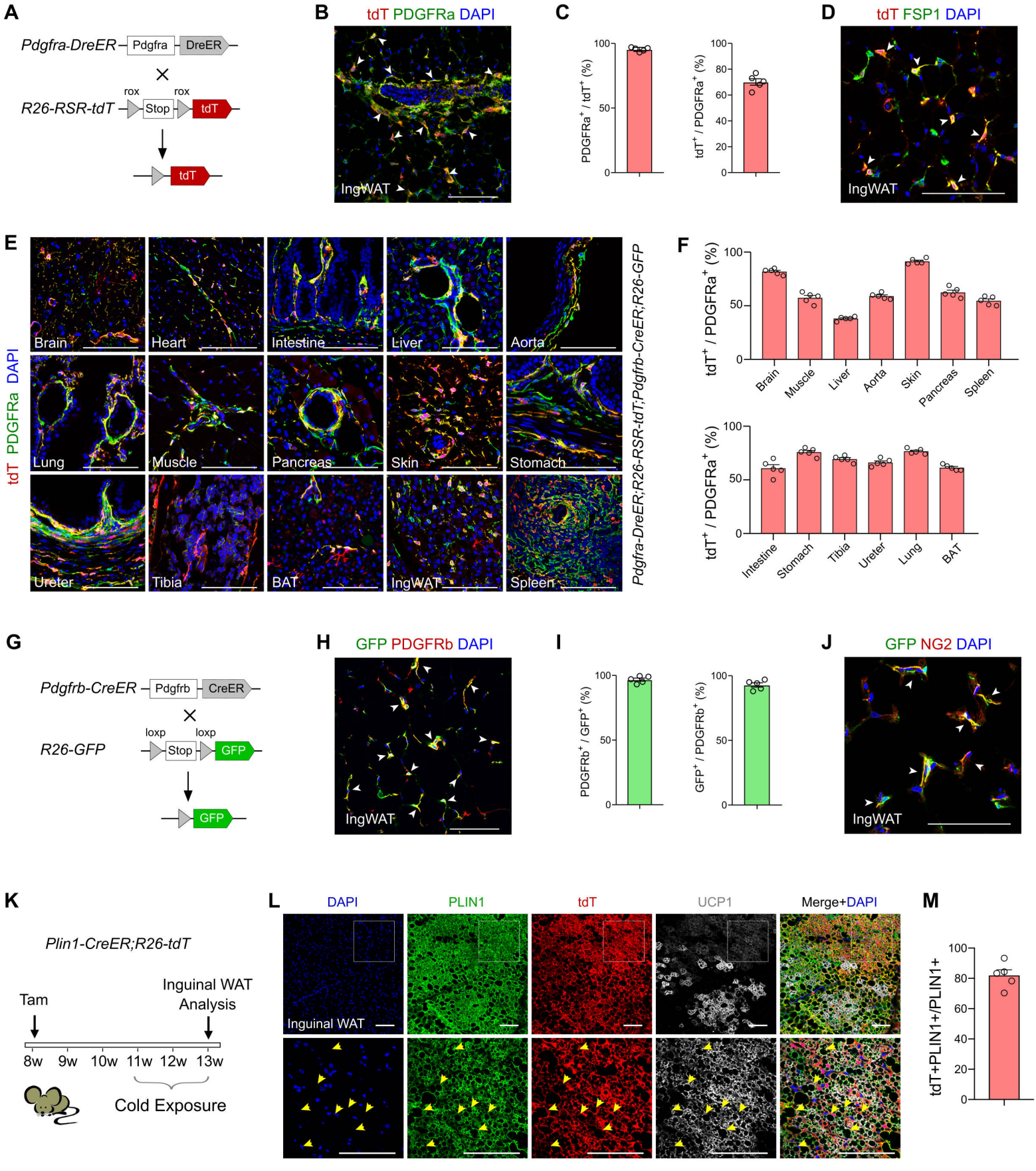

Figure S2. Labeling of PDGFRa+ and PDGFRb+ cells in adipose tissues, and tracing of adipocytes after cold exposure (Related to Figure 2,3)

(A) Schematic diagram illustrating strategies for genetic labeling of PDGFRa+ cells.

(B) Immunostaining for tdT and PDGFRa on inguinal white adipose tissue (IngWAT). Arrowheads, tdT+PDGFRa+ cells.

(C) Quantification of the percentage of tdT+ cells expressing PDGFRa (specificity) and the percentage of PDGFRa+ cells expressing tdT (efficiency).

(D) Immunostaining for tdT and FSP1 on IngWAT. Arrowheads, tdT+FSP1+ cells.

(E) Immunostaining for tdT and PDGFRa on sections collected from organs or tissues of *Pdgfra-DreER;R26-RSR-tdT;Pdgfrb-CreER;R26-GFP* mice treated with tamoxifen. These images were obtained from the same tissues in Figure 2, but with pseudo-color green for PDGFRa staining here.

(F) Quantification of the percentage of PDGFRa+ cells expressing tdT (efficiency) in different organs or tissues.

(G) Schematic diagram illustrating strategies for genetic labeling of PDGFRb+ cells.

(H) Immunostaining for GFP and PDGFRb on IngWAT. Arrowheads, GFP+PDGFRb+ cells.

(I) Quantification of the percentage of GFP+ cells expressing PDGFRb (specificity) and the percentage of PDGFRb+ cells expressing GFP (efficiency).

(J) Immunostaining for GFP and NG2 on IngWAT. Arrowheads, GFP+NG2+ cells.

(K) Schematic diagram illustrating the experimental design.

(L) Immunostaining for tdT, PLIN1, and UCP1 on inguinal WAT sections. Yellow arrowheads, tdT+PLIN1+UCP1+ adipocytes.

(M) Quantification of percentage of adipocytes contribute majority to adipocytes after cold exposure.

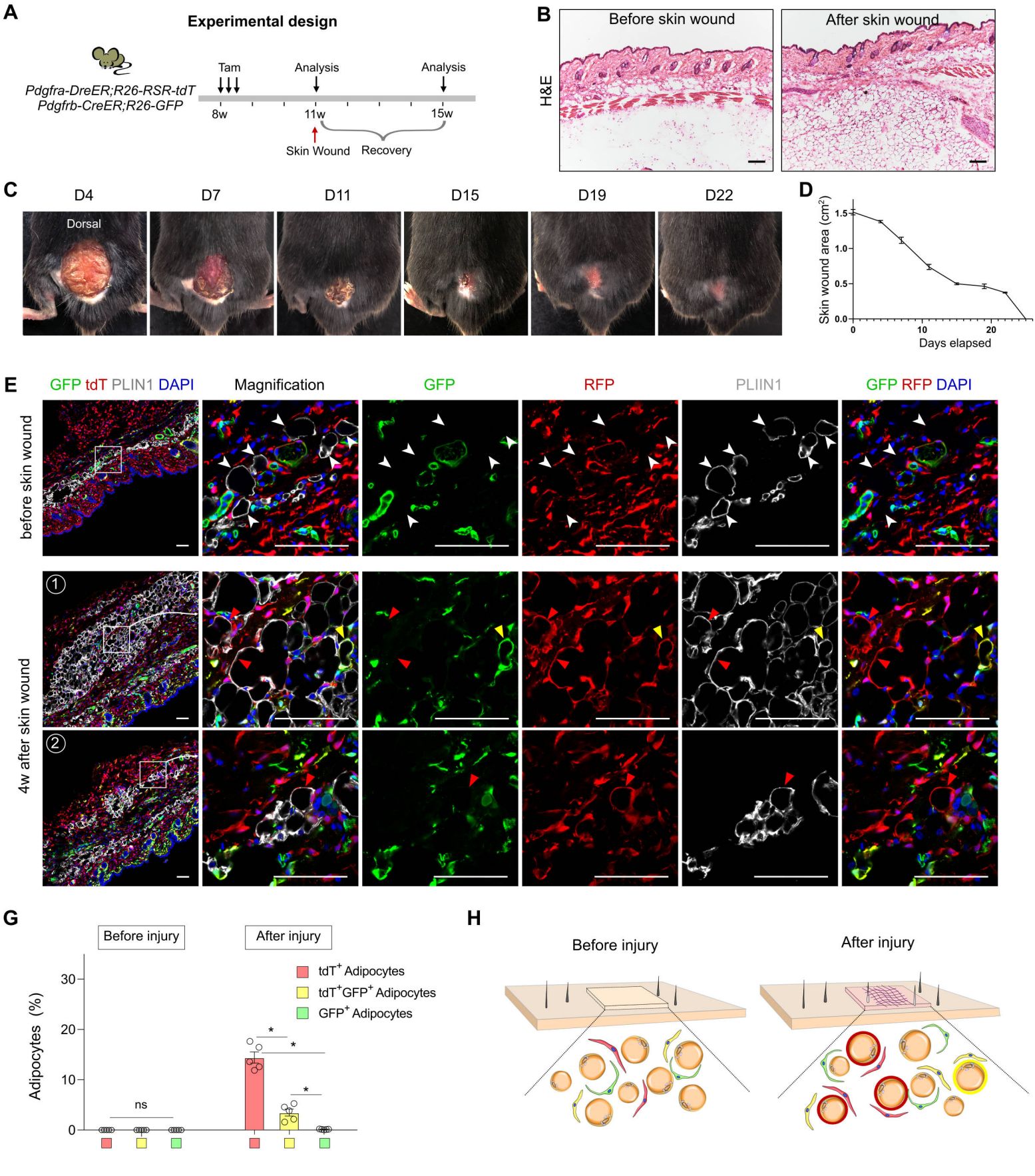

Figure S3. Perivascular stem cells contribute to adipogenesis after skin wound injury (Related to Figure 3)
(A) Schematic diagram illustrating the experimental design.
(B) H&E staining for skin sections of before and after skin wound injury.
(C) A time-course study of repair process of skin puncture wounds. D, days post skin wound injury.
(D) Quantification of the wound area of the mice at different days after skin wound injury.
(E) Immunostaining for tdT,GFP, and PLIN1 on back skin sections from mice before and after skin wound injury. White arrowheads, fluorescence-negative adipocytes; red arrowheads, tdT+ adipocytes; yellow arrowheads, tdT+GFP+ adipocytes.
(G) Quantification of percentage of adipocytes expressing tdT, GFP, or both in skin samples before injury and after injury. Data are mean ± SEM; n = 5; *P < 0.05; ns, non-significant.
(H) Cartoon image showing adipocytes from perivascular stem cells after skin wound injury.
Scale bars, 100 μm. Each image is representative of 5 individual biological samples.

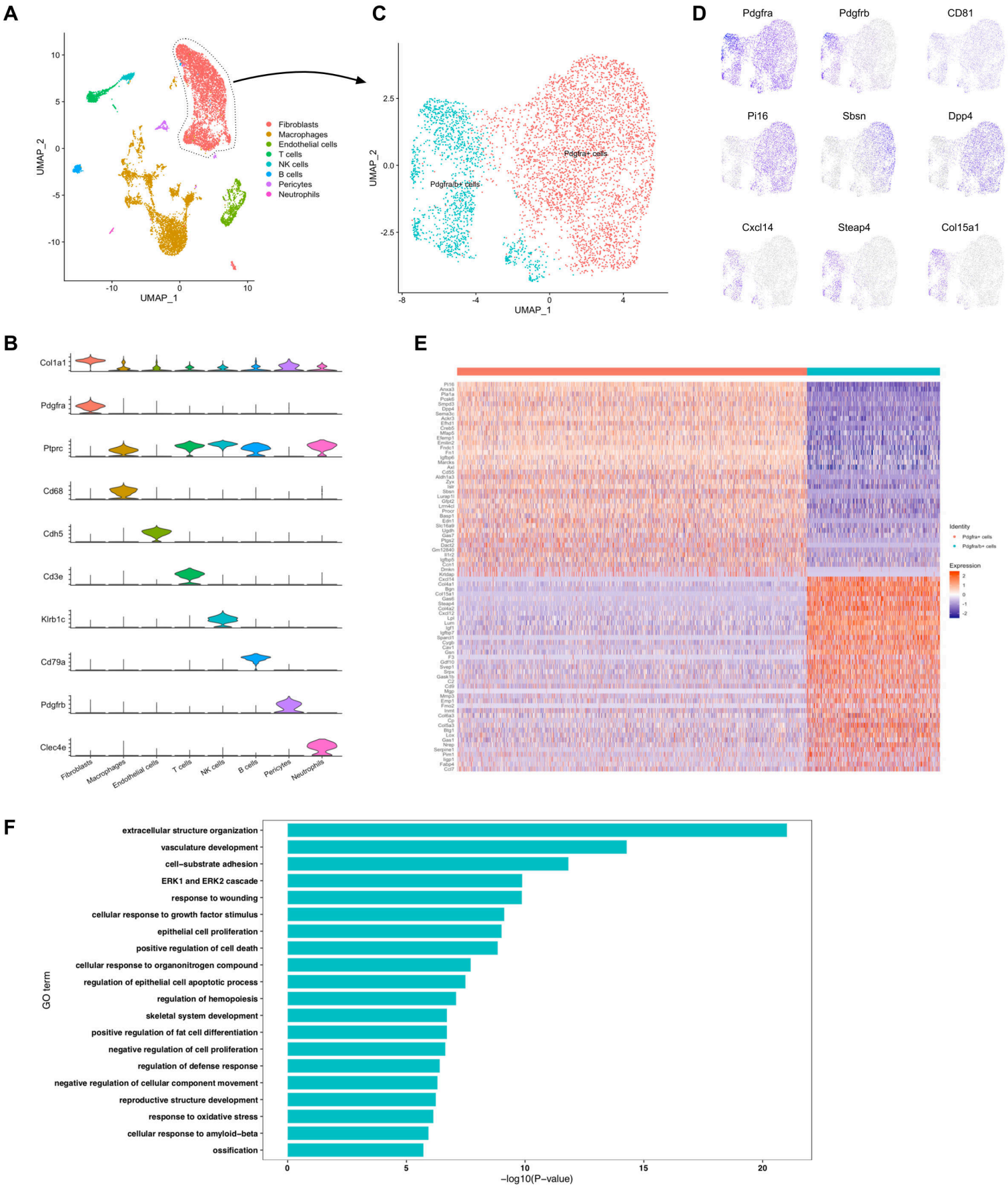

Figure S4. Single-cell RNA sequencing analysis of cells collected from adipose tissue (Related to Figure 3)
(A) Unsupervised Louvain clustering and UMAP plot of cells isolated from inguinal WAT.
(B) Violin plot of ten representative maker genes expressed across clusters.
(C) Re-UMAP of 5,044 fibrobalsts circled by dash line in (A).
(D) Relative expression of Pdgfra and Pdgfrb imputed by Magic and selected genes in fibroblasts.
(E) scRNA-seq heatmap of top 40 differential expressed genes for Pdgfra+ cells versus Pdgfra+Pdgfrb+ cells
(F) GO enrichment pathway analysis of up-regulated genes in Pdgfra+Pdgfrb+ cells, compared with those in Pdgfra+ cells.

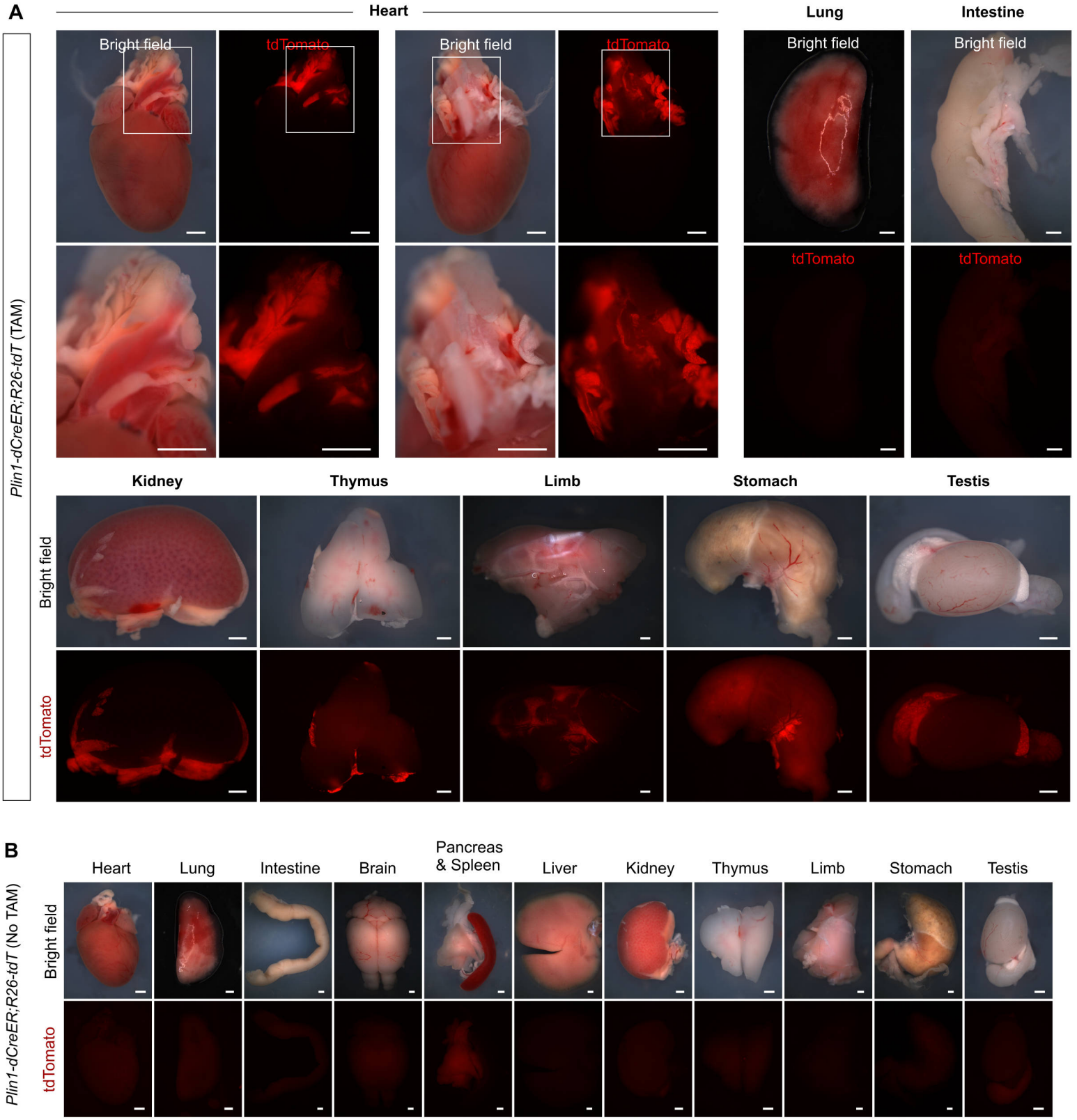

Figure S5. Characterization of *Plin1-dCreER* mouse line (Related to Figure 4)
(A) Whole-mount fluorescence images of different organs collected from *Plin1-dCreER;R26-tdT* mice treated with tamoxifen (Tam). The visceral fat tissues on the organ surface could be detected as tdT+.
(B) Whole-mount fluorescence images of different organs collected from *Plin1-dCreER;R26-tdT* mice treated without tamoxifen (No Tam).
Scale bars, 1 mm. Each image is representative of 5 individual biological samples.

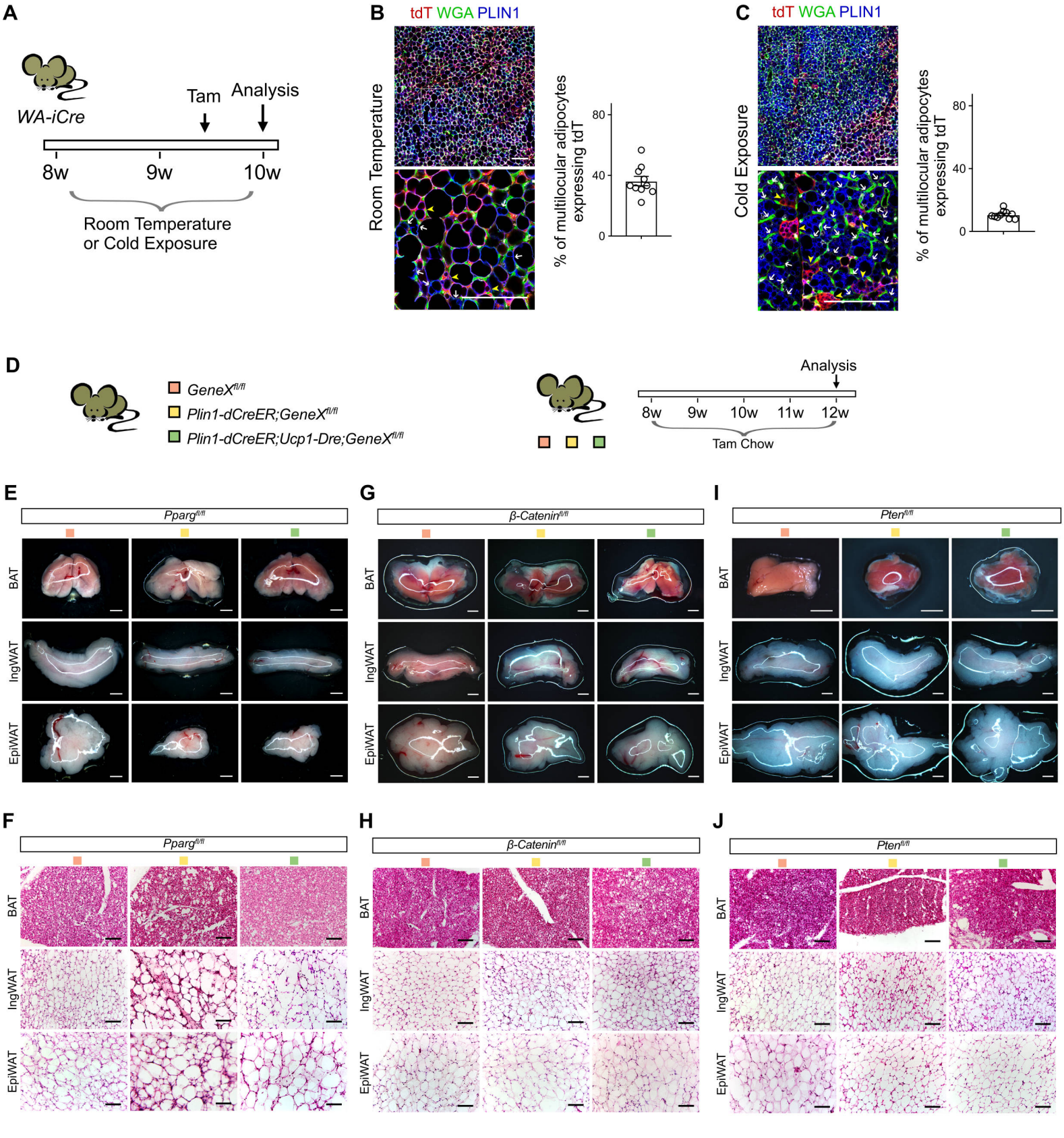

Figure S6. Multilocular adipocytes in the inguinal WAT and Phenotype of specific gene knockout by *WA-iCre* (Related to Figure 5)

(A) Schematic diagram illustrating the experimental design of *WA-iCre* mice in room temperature and cold exposure.

(B,C) Immunostaining for tdT, WGA, and Perilipin 1 (PLIN1) on inguinal WAT sections from mice in room temperature (B) or housed at cold exposure (C) for 2 weeks. White arrows, tdT^{-}PLIN1^{+} multilocular adipocytes; yellow arrowheads, tdT^{+}PLIN1^{+} multilocular adipocytes. Quantification of percentage of multilocular adipocytes expressing tdT (devoid UCP1-Dre) at ambient temperature (B) or at cold exposure (C). Data are mean ± SEM; n = 10.

(D) Schematic diagram illustrating the experimental design.

(E,G,I) Whole-mount views of BAT, IngWAT, and EpiWAT from three flox homozygous mice (*Pparg$^{fl/fl}$, β-Catenin$^{fl/fl}$, or Pten$^{fl/fl}$*) containing no Cre, *Plin1-dCreER*, or *WA-iCre* allele.

(F,H,J) H&E stained tissue sections of BAT, IngWAT, and EpiWAT from three flox homozygous mice (*Pparg$^{fl/fl}$, β-Catenin$^{fl/fl}$, or Pten$^{fl/fl}$*) containing no Cre, *Plin1-dCreER*, or *WA-iCre* allele.

Scale bars, 2mm in F,H,J; 100μm in others. Each image is representative of at least 5 individual biological samples.

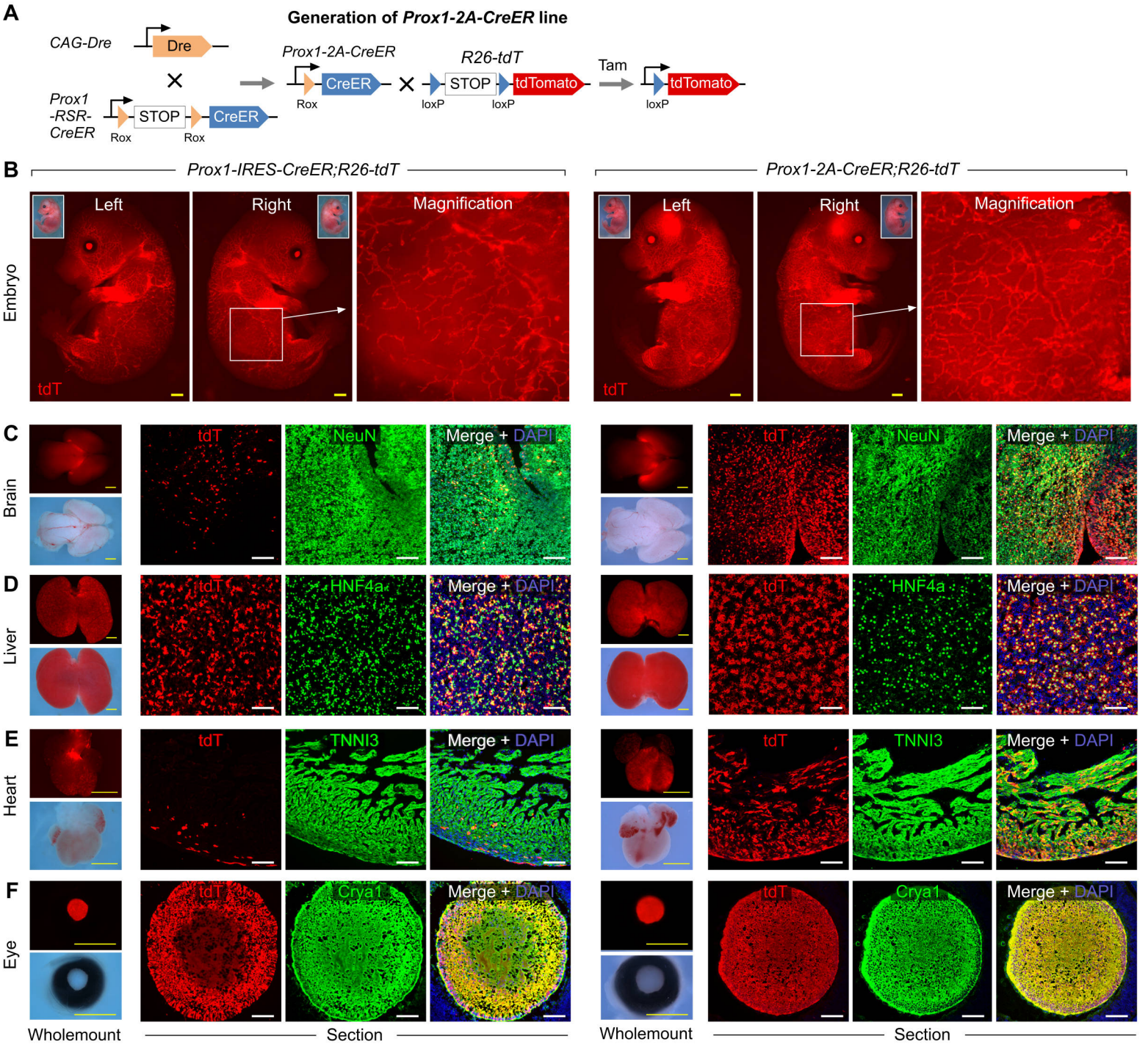

Figure S7. Comparison of *Prox1-IRES-CreER* and *Prox1-2A-CreER* mice (Related to Figure 6)

(A) Schematic figure showing experimental strategy for generation of *Prox1-2A-CreER* line.

(B) Whole-mount fluorescent images of E16.5 *Prox1-IRES-CreER;R26-tdT* (left panel) and *Prox1-2A-CreER;R26-tdT* (right panel) embryos. Inserts, bright field images. Tamoxifen was induced at E12.5.

(C-F) Whole-mount fluorescence and bright-field images of brain, liver, heart, and eye. Immunostaining for tdT and difference cell lineage markers NeuN, HNF4a, TNNI3, and Crya1 on tissue sections from *Prox1-IRES-CreER;R26-tdT* (left) and *Prox1-2A-CreER;R26-tdT* (right).

(G-H) Immunostaining for tdT and cell lineage markers on tissue sections of E16.5 embryos treated with tamoxifen (Tam) or without tamoxifen (No Tam). Scale bars, yellow 1mm; white, 100 μm. Each image is representative of 5 individual biological samples.

Table S1. Newly Generated Transgenic Dre Mouse Lines, Related to Figure 1

Mouse Line Name	Gene locus	Dre/DreER	Targeting tissues	Biomodel Stock#	Targeting Method
Npr3-2A-DreER	Npr3	DreER	Endocardial cells	NM-KI-190015	Cas9
Cd11c-2A-DreER	Cd11c	DreER	Monocytes, granulocytes, dendritic cells	NM-KI-190032	Cas9
Aplnr-DreER	Aplnr/Apj	DreER	Vascular endothelial cells, sinus venosus	NM-KI-00132	ES cell
Ins-DreER	Ins2	DreER	Islet beta cells of pancreas	NM-KI-190039	Cas9
Sox9-2A-DreER	Sox9	DreER	Duct cells, intestinal stem cells, bone cells, neurons		Cas9
SMA-GFP-DreER	SMA	DreER	Smooth muscle cells, myofibroblast		Cas9
Cdh1-2A-DreER	Cdh1	DreER	Epithelial cells	NM-KI-190031	Cas9
Lyz1-2A-DreER	Lyz1	DreER	Intestine paneth cells	NM-KI-190033	Cas9
Plin1-2A-DreER	Plin1	DreER	Adipocytes	NM-KI-190034	Cas9
Ly6g-2A-DreER	Ly6g	DreER	Monocytes, granulocytes, neutrophils	NM-KI-190036	Cas9
K19-DreER	K19	DreER	Epithelial cells, duct cells, luminal cells, limbal cells		Cas9
Pdgfb-DreER	Pdgfb	DreER	Endothelial cells, natural killer cells, angioblasts, pericytes		Cas9
P63-DreER	P63	DreER	Basal epithelial cells, keratinocytes, limbal epithelial cells	NM-KI-190029	Cas9
Gli1-DreER	Gli1	DreER	Mesenchymal stromal cells, chondrocytes		Cas9
Hopx-2A-DreER	Hopx	DreER	Alveolar type 1 cells, intestine stem cell, choroid plexus cells	NM-KI-190035	Cas9
K5-DreER	K5	DreER	Basal epithelial cells, keratinocytes, outer root sheath cells		Cas9
K19-2A-DreER	K19	DreER	Epithelial cells, duct cells, luminal cells, limbal cells		Cas9
Hey2-DreER	Hey2	DreER	Oligodendrocyte procursors, Retinal progenitors, cardiomyocytes		Cas9
Rbfox3-2A-DreER	Rbfox3	DreER	Neuronal cells	NM-KI-190103	Cas9
Sca1-2A-DreER	Sca1	DreER	Hematopoietic cells, mesenchymal progenitors, endothelial cells		Cas9
Kank1-2A-DreER	Kank1	DreER	Endocardial cells, oligodendrocyte procursors, chondrocytes	NM-KI-190040	Cas9
Flt3-2A-DreER	Flt3	DreER	Granulocyte-monocyte progenitors, B or dendritic cell progenitors	NM-KI-190115	Cas9
Cyp2e1-DreER	Cyp2e1	DreER	Perivenous hepatocytes		Cas9
Wt1-DreER	Wt1	DreER	Mesothelial cells, epicardium		Cas9
K14-Dre	K14	Dre	Basal epithelial cells, keratinocytes, bulge stem cells		Cas9
Cx40-DreER-GFP	Cx40	DreER	Aortic endothelial cells, cardiomyocytes, Purkinje fiber, His bundle		ES cell
Myh11-Dre	Myh11	Dre	Vascular smooth muscle cells, ovarian mesenchymal stromal cells		Cas9
Nppb-DreER	Nppb	DreER	Cardiomyocytes of myocardial trabecula		Cas9
Epcam-2A-DreER	Epcam	DreER	Epithelial cells, epithelial progenitors, gastrointestinal carcinomas		Cas9
Lgr5-2A-DreER	Lgr5	DreER	Intestine stem cells, bulge stem cells, ductal cells, hepatocytes,	NM-KI-200178	Cas9
Prox1-2A-DreER	Prox1	DreER	Lymphocytes, cardiomyocytes, hepatocytes, neurons, epithelial cells		Cas9
Cela1-2A-DreER	Cela1	Dre	Exocrine cells, duct cells, lens vesicle cells, proerythroblasts	NM-KI-190094	Cas9
Cyp2e1-2A-DreER	Cyp2e1	DreER	Perivenous hepatocytes		Cas9
K14-2A-DreER	K14	DreER	Basal epithelial cells, keratinocytes, bulge stem cells	NM-KI-190125	Cas9
Gja1-2A-DreER	Gja1	DreER	Cardiomyocytes, corneal epithelial cells, nueral crest cells	NM-KI-200026	Cas9
Pax7-2A-DreER	Pax7	DreER	Myobalst, muscle satellite cells, neural progenitors, dermomyotome cells	NM-KI-190124	Cas9
K5-Dre	K5	Dre	Basal epithelial cells, keratinocytes, outer root sheath cells		Cas9
Myh11-2A-DreER	Myh11	DreER	Vascular smooth muscle cells, ovarian mesenchymal stromal cells	NM-KI-190037	Cas9
Ela-DreER-GFP	Ela	DreER	Placenta, cardiac cells		Cas9
Clu-2A-DreER	Clu	DreER	Billiary epithelial cells, brain, testis, ovary, liver and pancreas	NM-KI-200025	Cas9
Cdh5-Dre	Cdh5	Dre	Endothelial cell, lymphatic endothelial cell		Cas9
Cdh5-DreER	Cdh5	DreER	Endothelial cell, lymphatic endothelial cell		Cas9
Lepr-2A-DreER	Lepr	DreER	Bone marrow stromal cells, dermal papilla cells, choroid plexus cells		Cas9
Axin2-2A-DreER	Axin2	DreER	Praxial mesoderm cells, Wnt responsive cells in liver, intestine, lung, skin		Cas9
SiglecF-DreER	SiglecF	DreER	Adipcotyes, lung macrophages, intestine, spleen, heart		Cas9
Hcn4-DreER	Hcn4	DreER	Sinoatrial node cells, atriventricular node cells		Cas9
Msln-DreER	Msln	DreER	Mesothelial cells, meningeal cells, granulosa cells		Cas9

K5-LSL-Dre	K5	Dre	Basal epithelial cells, buldge stem cells, basal cells, keratinocytes	Cas9
Snai1-LSL-Dre	Snail	Dre	Transcription factors in multiple tissues, EMT factors	Cas9
Twist-LSL-Dre	Twist	Dre	Transcription factors in multiple tissues, EMT factors	Cas9
Pdgfrb-LSL-Dre	Pdgfrb	Dre	Mesenchymal stem cells, pericytes, adipose mural cells, epicardial cells	ES cell
SMA-LSL-Dre	SMA	Dre	Vascular, airway smooth muscle cells, mesenchymal stem cells, pericytes	Cas9
Cx40-LSL-Dre	Cx40	Dre	Purkinje fiber cells, His bundle cells, arterial endothelial cells	Cas9
P63-LSL-Dre	P63	Dre	Basal cells, keratinocytes, trachea progenitor cells	Cas9
Zeb1-LSL-Dre	Zeb1	Dre	Transcription factors in multiple tissues, EMT factors	Cas9
CD45-Dre	CD45	Dre	Hematopoietic cells, circulating endothelial progenitors, bone marrow cells	Cas9
Ms4a3-2A-DreER	Ms4a3	DreER	Hematopoietic cells, monocytes, granulocytes	Cas9
Isl1-Dre	Isl1	Dre	Motor neurons, heart tube cells, cardiomyocyte progenitor cells	Cas9
Wnt1-Dre	Wnt1	Dre	Roof or floor plate cells, dopaminergic neurons, neural crest cells	Cas9
Meox1-Dre	Meox1	Dre	Atrioventricular node cells, intermediate mesoderm cells, muscle progenitors	Cas9
Upk3b-Dre	Upk3b	Dre	Mesothelial cells, viceral white adipocytes, extraembryonic angioblasts	Cas9
Ucp1-Dre	Ucp1	Dre	Brown or beige adipocytes	Cas9
Cx40-Dre	Cx40	Dre	Aortic endothelial cells, cardiomyocytes, Purkinje fiber, His bundle	Cas9
F4/80-Dre	F4-80	Dre	Macrophages, granulocytes, Kupffer cells, Hofbauer cells	Cas9
Ms4a3-2A-Dre	Ms4a3	Dre	Hematopoietic cells, monocytes, granulocytes	Cas9
CCR2-2A-DreER	CCR2	DreER	Monocytes, dendritic cells, hematopoietic bone marrow cells	Cas9
Brachyury T-DreER	Brachyury T	DreER	Notochord, mesoderm, endoderm in early development	Cas9
Ins-Dre	Insulin	Dre	Islet beta cells of pancreas	Cas9
Apln-DreER	Apln	DreER	Vascular endothelial cells	Cas9
Nppa-DreER	Nppa	DreER	Atrial cardiomyocytes, trabecular cardiomyocytes	Cas9
SMA-Dre	SMA	Dre	Vascular, airway smooth muscle cells, mesenchymal stem cells, pericytes	Cas9
Pdgfrb-Dre	Pdgfrb	Dre	Mesenchymal stem cells, pericytes, adipose mural cells, epicardial cells	ES cell

Table S2. Genotyping Primers for Nwly Generated Transgenic Dre Mouse Lines, Related to Figure 1

Mouse	Primers (Mutant)	Primers (Willd Type)
Mouse: *Apln-DreER*	Primer1: 5'-AGAGAGTTTTTGCCGCCGAC-3'	Primer1: 5'-GAAGCATTCTCTCTAACAGCCTGG-3'
	Primer2: 5'-CAGACATCCTCATCAGGGTGTTG-3'	Primer2: 5'-ACGCACTCACCTCCACAAACTG-3'
Mouse: *Aplnr-DreER*	Primer1: 5'-AGAGAGTTTTTGCCGCCGAC-3'	Primer1: 5'-GAAGCATTCTCTCTAACAGCCTGG-3'
	Primer2: 5'-CAGACATCCTCATCAGGGTGTTG-3'	Primer2: 5'-ACGCACTCACCTCCACAAACTG-3'
Mouse: *Axin2-2A-DreER*	Primer1: 5'-CTCAGAAAGAGGGGGAAAGAGTG-3'	Primer1: 5'-TGTTGGGTTGGGAGAGAGACTTAG-3'
	Primer2: 5'-CAGGCTCACAGACTTGTCATCAGAC-3'	Primer2: 5'-ATTTCGTGGCTGTTGCGTAGGC-3'
Mouse: *Brachyury T-DreER*	Primer1: 5'-CCACATCTCATCATAGCTCATTTGC-3'	Primer1: 5'-CCACATCTCATCATAGCTCATTTGC-3'
	Primer2: 5'-GAAGTACTCCCTAGCCATCTCAGG-3'	Primer2: 5'-CAACAAGGGAGGACATTAGAGGTG-3'
Mouse: *CCR2-2A-DreER*	Primer1: 5'-TTGTTCTCTTCTTGACCACCTTCC-3'	Primer1: 5'-CTTGGGTGGTGGCTGTGTTT-3'
	Primer2: 5'-CCTTCCTAATCCTGTGACCCTTT-3'	Primer2: 5'-CTCAGGGTGTTAGGGGCGTA-3'
Mouse: *Cd11c-2A-DreER*	Primer1: 5'-GCCCCTCTCTTCTTTCTACCACTC-3'	Primer1: 5'-GCCCCTCTCTTCTTTCTACCACTC-3'
	Primer2: 5'-TACTCCTTGCCGATGTTCCTCAGG-3'	Primer2: 5'-TTGCCCAGATGCTTCCTTGCTG-3'
Mouse: *CD45-Dre*	Primer1: 5'-GAAACTTGCTCCCCATCTGATAAG-3'	Primer1: 5'-GAAACTTGCTCCCCATCTGATAAG-3'
	Primer2: 5'-CCCAGGCATCGCTAAAAATCTTC-3'	Primer2: 5'-TGTGTCCAGAAGGGCAAATCC-3'
Mouse: *Cdh1-2A-DreER*	Primer1: 5'-CCTTACGACTCTCTGTTGGTGTTCG-3'	Primer1: 5'-CCTTACGACTCTCTGTTGGTGTTCG-3'
	Primer2: 5'-AGACATCCTCATCAGGGTGTTGTAG-3'	Primer2: 5'-ATTAGTGAGGTGTGAGGGGCTTGG-3'
Mouse: *Cdh5-Dre*	Primer1: 5'-GATGGTGCCTATCCTCTTTCCC-3'	Primer1: 5'-GATGGTGCCTATCCTCTTTCCC-3'
	Primer2: 5'-ATGAAGTTCTCAGCAGCCTCCTGG-3'	Primer2: 5'-CGCACCACCAATGATAACCAATC-3'
Mouse: *Cdh5-DreER*	Primer1: 5'-CCTTGGCTTGGTCCCTTACA-3'	Primer1: 5'-GATGGTGCCTATCCTCTTTCCC-3'
	Primer2: 5'-CTGGTACTCCTTGCCGATGT-3'	Primer2: 5'-CGCACCACCAATGATAACCAATC-3'
Mouse: *Cela1-2A-DreER*	Primer1: 5'-CTCCTCCCCATTTTCACTTGTG-3'	Primer1: 5'-CTCCTCCCCATTTTCACTTGTG-3'
	Primer2: 5'-ACTCCTTGCCGATGTTCCTCAG-3'	Primer2: 5'-TCCTACATTGTTGCTGCTGCC-3'
Mouse: *Clu-2A-DreER*	Primer1: 5'-AACCCCGGGGATTTTACTTTC-3'	Primer1: 5'-AACCCCGGGGATTTTACTTTC-3'
	Primer2: 5'-ACTGACCCGGCTATTATCCTTGTT-3'	Primer2: 5'-CTCTCAGGGTGTTAGGGGCGTAGG-3'
Mouse: *Cx40-Dre*	Primer1: 5'-CATCTCCCACACCAAGACCATC-3'	Primer1: 5'-TGTGAGCCCGCAAGAAACT-3'
	Primer2: 5'-CACCCAGGCATCGCTAAAAATC-3'	Primer2: 5'-ATGCGGAAAATGAACAGGAC-3'
Mouse: *Cx40-DreER-GFP*	Primer1: 5'-GAACGGCATCAAGGTGAACTTC-3'	Primer1: 5'-CAGCCTCTAGAAAGTAGTAGG-3'
	Primer2: 5'-CGGAAAATGAACAGGACAGTGAG-3'	Primer2: 5'-CGGAAAATGAACAGGACAGTGAG-3'
Mouse: *Cx40-LSL-Dre*	Primer1: 5'-GCTACGTCCCTTCGGCCCTCAATC-3'	Primer1: 5'-TGTGAGCCCGCAAGAAACT-3'
	Primer2: 5'-TCTGCAGTACCCAATAACGAATGT-3'	Primer2: 5'-ATGCGGAAAATGAACAGGAC-3'
Mouse: *Cyp2e1-2A-DreER*	Primer1: 5'-CATCTCCCACACCAAGACCATC-3'	Primer1: 5'-GGGTCAGCCTTTGAAATGATAGC-3'
	Primer2: 5'-CACCCAGGCATCGCTAAAAATC-3'	Primer2: 5'-GGTTGATACCAGCCAGGATACACC-3'
Mouse: *Cyp2e1-DreER*	Primer1: 5'-GGGTCAGCCTTTGAAATGATAGC-3'	Primer1: 5'-GGGTCAGCCTTTGAAATGATAGC-3'
	Primer2: 5'-ATGAAGTTCTCAGCAGCCTCCTGG-3'	Primer2: 5'-GGTTGATACCAGCCAGGATACACC-3'
Mouse: *Ela-DreER-GFP*	Primer1: 5'-GCACAGATACTGCGATTTACAGACG-3'	Primer1: 5'-CGGACAGATACTGCGATTTACAGAC-3'
	Primer2: 5'-CAGACATCCTCATCAGGGTGTTG-3'	Primer2: 5'-AGACCCAGAAGCACAAACAGGC-3'
Mouse: *Epcam-2A-DreER*	Primer1: 5'-TCCTCATCCTCTCCCACATCAG-3'	Primer1: 5'-ACCCTGTTTCCTCCTCTGTTGC-3'
	Primer2: 5'-ACTATCAAAGCAGTAACCCTTCGC-3'	Primer2: 5'-ACTATCAAAGCAGTAACCCTTCGC-3'
Mouse: *F4/80-Dre*	Primer1: 5'-CCTGGAAAAAGCCTGAGACACTG-3'	Primer1: 5'-AGGGAAGGAAATGGAGAGAAAGAC-3'
	Primer2: 5'-AAATGAAAGCCATACGGGAAGC-3'	Primer2: 5'-CCAAGGTAAAGTTTGCTGTGTGC-3'
Mouse: *Flt3-2A-DreER*	Primer1: 5'-GTGCACACTTGCGCACATAA-3'	Primer1: 5'-GTGCACACTTGCGCACATAA-3'
	Primer2: 5'-GTAGAGGCCAGGTCAGCATC-3'	Primer2: 5'-TCCTCAGAGGCGAGGCTAAT-3'
Mouse: *Gja1-2A-DreER*	Primer1: 5'-AGCAAGCCAGCGAGCAAAAC-3'	Primer1: 5'-AGCAAGCCAGCGAGCAAAAC-3'
	Primer2: 5'-AGACATCCTCATCAGGGTGTTGTAG-3'	Primer2: 5'-CACGGGAACGAAATGAACACC-3'
Mouse: *Gli1-DreER*	Primer1: 5'-GGCTGCTTCTGCCCACTCTT-3'	Primer1: 5'-GGCTGCTTCTGCCCACTCTT-3'
	Primer2: 5'-GCGTAGGCTCCCTGGTCATT-3'	Primer2: 5'-CCAGGTCTTTGAATGGGGAATA-3'
Mouse: *Hcn4-DreER*	Primer1: 5'-CGGGCCCGGGAGGAGGTG-3'	Primer1: 5'-AGCGAAGGACGCGTCCTCACTG-3'
	Primer2: 5'-GGTAGAGGCCAGGTCAGCATCGTG-3'	Primer2: 5'-ACCGTTGGTGCTGGACTTGCCG-3'
Mouse: *Hey2-DreER*	Primer1: 5'-GCGGGGCCTGGAGAGTG-3'	Primer1: 5'-CACGCCTCTGCCAACGCCTCTCG-3'
	Primer2: 5'-CATGGCGTAGTGCTTGTCG-3'	Primer2: 5'-TCCAGTCCAGCTCCCTTCCAGTCG-3'
Mouse: *Hopx-2A-DreER*	Primer1: 5'-AACCTTCCCAGCATCCTTTGCG-3'	Primer1: 5'-AACCTTCCCAGCATCCTTTGCG-3'
	Primer2: 5'-TCATCAGTGTCTCAGGCTTTTTCC-3'	Primer2: 5'-GCCAAGCCATCACTTTACACAGAAC-3'
Mouse: *Ins-Dre*	Primer1: 5'-AAGATACTAGGTCCCCAACTGCAAC-3'	Primer1: 5'-AAACAGCAAAGTCCAGGGGG-3'
	Primer2: 5'-TTCAGCATGGCGTAGTGCTTGTCG-3'	Primer2: 5'-ATGGGTGTGTAGAAGAAGCCACGC-3'
Mouse: *Ins-DreER*	Primer1: 5'-CCTCTCTTACGTGAAACTTTTGCTATCCTC-3	Primer1: 5'-GATCCGCTACAATCAAAAACCATCAGC-3'
	Primer2: 5'-TCAGACAGAGGAGGCAGGCCA-3'	Primer2: 5'-TCCCGGGCCTCCACC-3'

Mouse: *Isl1-Dre*	Primer1: 5'-GGCGATGGAGCTGAGTTGG-3'	Primer1: 5'-AGGAAGAGAGGTGCCCCGA-3'
	Primer2: 5'-TGCTTGTCGATGGTGGTAGAGG-3'	Primer2: 5'-GCAGCAACAACAACAACAAAAGG-3'
Mouse: *K14-2A-DreER*	Primer1: 5'-TTGGACCTTCTAATGCGTTTGG-3'	Primer1: 5'-TTGGACCTTCTAATGCGTTTGG-3'
	Primer2: 5'-AGACATCCTCATCAGGGTGTTGTAG-3'	Primer2: 5'-TAGGGACAATACAGGGGCTCTTCC-3'
Mouse: *K14-Dre*	Primer1: 5'-ATGGGAAAGTGTAGCCCGC-3'	Primer1: 5'-GACGAGAAAGCCCAAAACACTTC-3'
	Primer2: 5'-CTCAGGGTGTTAGGGGCGTAG-3'	Primer2: 5'-ATAGCCACCTCCAATCCCACAG-3'
Mouse: *K19-2A-DreER*	Primer1: 5'-AGTATTACATCACGGGGGAGGC-3'	Primer1: 5'-GAAGCCCACTACAACAATCTGCC-3'
	Primer2: 5'-CTCTCTGAAGGGGAAACAAGATTG-3'	Primer2: 5'-CCAATCCGAAGAGAGAACAATGG-3'
Mouse: *K19-DreER*	Primer1: 5'-CAATCCAGCGGACCTTCCTT-3'	Primer1: 5'-ATACCCGCCCCTTCAACATC-3'
	Primer2: 5'-TGTCCAAGTAGGAGGCGAGA-3'	Primer2: 5'-AAACACCCCCTGACCCAATG-3'
Mouse: *K5-Dre*	Primer1: 5'-CATCTCCCACACCAAGACCATC-3'	Primer1: 5'-CATGCCCAGCCCACTAATCA-3'
	Primer2: 5'-CACCCAGGCATCGCTAAAAATC-3'	Primer2: 5'-TCCCTCCACCTTTGTTCAGC-3'
Mouse: *K5-DreER*	Primer1: 5'-CATGCCCAGCCCACTAATCA-3'	Primer1: 5'-CATGCCCAGCCCACTAATCA-3'
	Primer2: 5'-ATGGCGTAGTGCTTGTCGAT-3'	Primer2: 5'-TCCCTCCACCTTTGTTCAGC-3'
Mouse: *K5-LSL-Dre*	Primer1: 5'-AGCCCCACAGATGGACAGAAAC-3'	Primer1: 5'-AGCCCCACAGATGGACAGAAAC-3'
	Primer2: 5'-TGCCTGGAATCCCAACAACTCG-3'	Primer2: 5'-TTTTGGAGCCCCCCACATTG-3'
Mouse: *Kank1-2A-DreER*	Primer1: 5'-CCCACTCACCGAGGTTCTTTTG-3'	Primer1: 5'-CCCACTCACCGAGGTTCTTTTG-3'
	Primer2: 5'-TCTGCCAGGTTGGTCAGTAAGC-3'	Primer2: 5'-TTCAGCCGCTCCTTGACTCTTC-3'
Mouse: *Lepr-2A-DreER*	Primer1: 5'-GGTTGGATGAGCTTTTGGAA-3'	Primer1: 5'-GGTTGGATGAGCTTTTGGAA-3'
	Primer2: 5'-CCAGGCTCACAGACTTGTCA-3'	Primer2: 5'-GTCTCCCACATCCACAACAA-3'
Mouse: *Lgr5-2A-DreER*	Primer1: 5'-GCCTTAGTATCCTTTACCCACGC-3'	Primer1: 5'-GCCTTAGTATCCTTTACCCACGC-3'
	Primer2: 5'-ACTCCTTGCCGATGTTCCTCAG-3'	Primer2: 5'-ACCCATTGAGTCATCCAACGAG-3'
Mouse: *Ly6g-2A-DreER*	Primer1: 5'-CTTCTGTTCAGCCTGGTTTCAGTC-3'	Primer1: 5'-CTTCTGTTCAGCCTGGTTTCAGTC-3'
	Primer2: 5'-ACTCCTTGCCGATGTTCCTCAG-3'	Primer2: 5'-TCAAGAGCAGCAAGCCACAAC-3'
Mouse: *Lyz1-2A-DreER*	Primer1: 5'-ACACAGGGCACAGATTTCAACC-3'	Primer1: 5'-ACACAGGGCACAGATTTCAACC-3'
	Primer2: 5'-TGTCTCAGGCTTTTTCCAGGTG-3'	Primer2: 5'-TGCTGACTGACAAGGGAGACTTTG-3'
Mouse: *Meox1-Dre*	Primer1: 5'-CCGGGAAGGGCTTGTCAGTAT-3'	Primer1: 5'-TTGCCTGCTCGGGTTTTGGTTGG-3'
	Primer2: 5'-GTAGAGGCCAGGTCAGCATCGTG-3'	Primer2: 5'-TGGGGGCTGGGGGTTCCTCA-3'
Mouse: *Ms4a3-2A-Dre*	Primer1: 5'-TCTGAGAACCTGAACACTCAGC-3'	Primer1: 5'-TCTGAGAACCTGAACACTCAGC-3'
	Primer2: 5'-CCGGTTCTCTCTCCCTTCTC-3'	Primer2: 5'-AAGGGGAACAAGCGAAGATT-3'
Mouse: *Ms4a3-2A-DreER*	Primer1: 5'-TCACCTCCTAATTCTGTGGAGTC-3'	Primer1: 5'-TCACCTCCTAATTCTGTGGAGTC-3'
	Primer2: 5'-GTGGTGATGGTCTTGGTGTG-3'	Primer2: 5'-GTGTGCTTGCATGTGCCTAT-3'
Mouse: *Msln-DreER*	Primer1: 5'-AGTGCTCCTGGTACAAACGG-3'	Primer1: 5'-AGTGCTCCTGGTACAAACGG-3'
	Primer2: 5'-GAACACCAGCCTCAGGTCTC-3'	Primer2: 5'-GGCCTAGGGATCATTCCTGC-3'
Mouse: *Myh11-2A-DreER*	Primer1: 5'-AGAAGAAATGGACGCTCGGG-3'	Primer1: 5'-AGAAGAAATGGACGCTCGGG-3'
	Primer2: 5'-AGACATCCTCATCAGGGTGTTGTAG-3'	Primer2: 5'-GGGCTCTGCTGTCGTTTAGTGTTC-3'
Mouse: *Myh11-Dre*	Primer1: 5'-TGACCCCATCTCTTCACTCCACAG-3'	Primer1: 5'-TGACCCCATCTCTTCACTCCACAG-3'
	Primer2: 5'-CACCCAGGCATCGCTAAAAATC-3'	Primer2: 5'-CCATTTTCCACCAACTCCACG-3'
Mouse: *Nppa-DreER*	Primer1: 5'-ACTGATAACTTTAAAAGGGCATCT-3'	Primer1: 5'-ACTGATAACTTTAAAAGGGCATCT-3'
	Primer2: 5'-AGGTCAGCATCGTGCAGCTGAAGG-3'	Primer2: 5'-GCCAGCGAGCAGAGCCCTCAGTTT-3'
Mouse: *Nppb-DreER*	Primer1: 5'-GCACCGTTGTTGAAGACACCAG-3'	Primer1: 5'-CCCACAATGAATACTCCACACAGG-3'
	Primer2: 5'-ACTCCTTGCCGATGTTCCTCAG-3'	Primer2: 5'-TGAATCCCCCATCCTTCCATAG-3'
Mouse: *Npr3-2A-DreER*	Primer1: 5'-TATCAAACCTAACCCAGATGTCCC-3'	Primer1: 5'-CCCGTCCTTTGGTAATCTTCAGTG-3'
	Primer2: 5'-TACTCCTTGCCGATGTTCCTCAGG-3'	Primer2: 5'-GGACGCAGCAGACTTTCAAGAC-3'
Mouse: *P63-DreER*	Primer1: 5'-CTATTGCTTCCCGTATGGCTTTCA-3'	Primer1: 5'-ACAGCCACAGTACACGAACC-3'
	Primer2: 5'-GTGTTGTAGGGGCTGGTGGACGAG-3'	Primer2: 5'-GCATATACAGCACCTCCTAA-3'
Mouse: *P63-LSL-Dre*	Primer1: 5'-GAGGCACCTGAATTCTGTTATCTT-3'	Primer1: 5'-TGCGCGGGACGTCCTTCTGCTAC-3'
	Primer2: 5'-CTCTACTTCCGCTGCTGCTCTTAT-3'	Primer2: 5'-CTCTACTTCCGCTGCTGCTCTTAT-3'
Mouse: *Pax7-2A-DreER*	Primer1: 5'-GCAGGTGTGTAAAGGGAAGACATTG-3'	Primer1: 5'-GCAGGTGTGTAAAGGGAAGACATTG-3'
	Primer2: 5'-AGACATCCTCATCAGGGTGTTGTAG-3'	Primer2: 5'-ATAAGGGGACTGAGGTGAGGAGAC-3'
Mouse: *Pdgfrb-Dre*	Primer1: 5'-CATCTCCCACACCAAGACCATC-3'	Primer1: 5'-GGGTGGGACTTTGGTGTAGAGAAG-3'
	Primer2: 5'-CACCCAGGCATCGCTAAAAATC-3'	Primer2: 5'-GGAACGGATTTTGGAGGTAGTGTC-3'
Mouse: *Pdgfb-DreER-GFP*	Primer1: 5'-GCTAGACGCCTTGGCTGGTT-3'	Primer1: 5'-GCTAGACGCCTTGGCTGGTT-3'
	Primer2: 5'-CACACACCTTCTAGGACACT-3'	Primer2: 5'-GAAGTTCTCAGCAGCCTCCT-3'
Mouse: *Pdgfrb-LSL-Dre*	Primer1: 5'-GAAGAACGGCATCAAGGTGAAC-3'	Primer1: 5'-GGGTGGGACTTTGGTGTAGAGAAG-3'
	Primer2: 5'-CAGCAGAGAGGAAGGAAGAGCG-3'	Primer2: 5'-GGAACGGATTTTGGAGGTAGTGTC-3'
Mouse: *Plin1-2A-DreER*	Primer1: 5'-CTTCTTCCGGCCCAGCGTCAT-3'	Primer1: 5'-CTGCCCCGGCCTGGACGACA-3'
	Primer2: 5'-CTCTCAGGGTGTTAGGGGCGTAGG-3'	Primer2: 5'-CCCTTAAAAATTGGTTCTGATGGT-3'
Mouse: *Prox1-2A-DreER*	Primer1: 5'-ACTGCCTACAAGAACTCCTTCACG-3'	Primer1: 5'-ATGTCTCCTCTGAAACCCACGG-3'
	Primer2: 5'-CAGACATCCTCATCAGGGTGTTG-3'	Primer2: 5'-TCCCTTCTCCTGAAAACCAACC-3'

Mouse: *Rbfox3-2A-DreER*	Primer1: 5'-AAACTTGCTAAGAACGCCAGTCC-3'	Primer1: 5'-AAACTTGCTAAGAACGCCAGTCC-3'
	Primer2: 5'-AGACATCCTCATCAGGGTGTTGTAG-3'	Primer2: 5'-TTCCGATGCTGTAGGTTGCTGTGG-3'
Mouse: *Sca1-2A-DreER*	Primer1: 5'-GCAATGTAGCAGTTCCCAATGG-3'	Primer1: 5'-GCAATGTAGCAGTTCCCAATGG-3'
	Primer2: 5'-TCATCAGTGTCTCAGGCTTTTTCC-3'	Primer2: 5'-CCCAGATACTTATGTGTGGATGGTG-3'
Mouse: *SiglecF-DreER*	Primer1: 5'-CAAATGCTACAGTTCAGGAGTGGAG-3'	Primer1: 5'-CAAATGCTACAGTTCAGGAGTGGAG-3'
	Primer2: 5'-CAGGCTCACAGACTTGTCATCAGAC-3'	Primer2: 5'-TGAGAGCGAATAACCGTCCG-3'
Mouse: *SMA-Dre*	Primer1: 5'-CATCTCCCACACCAAGACCATC-3'	Primer1: 5'-CCAAGAACCCTGTCTGTGGG-3'
	Primer2: 5'-CACCCAGGCATCGCTAAAAATC-3'	Primer2: 5'-CTTGTCCTCTCCGCGTTCAA-3'
Mouse: *SMA-GFP-DreER*	Primer1: 5'-GCCTGTGACACTCCCGCTCTT-3'	Primer1: 5'-GCCTGTGACACTCCCGCTCTT-3'
	Primer2: 5'-TGCTGTCTTCCTCTTCAC-3'	Primer2: 5'-CTTCGGGCATGGCGGACTTGA-3'
Mouse: *SMA-LSL-Dre*	Primer1: 5'-CCAAGAACCCTGTCTGTGGG-3'	Primer1: 5'-CCAAGAACCCTGTCTGTGGG-3'
	Primer2: 5'-CGGGTTCCTTCCGGTATTGT-3'	Primer2: 5'-CTTGTCCTCTCCGCGTTCAA-3'
Mouse: *Snai1-LSL-Dre*	Primer1: 5'-GTGACCCCGACTAGGTAGGT-3'	Primer1: 5'-TGGATCCCAACTGCCAAGAC-3'
	Primer2: 5'-ACTTGCCCCTTGCTCCATAC-3'	Primer2: 5'-AGTTGACTACCGACCTTGCG-3'
Mouse: *Sox9-2A-DreER*	Primer1: 5'-TCCCAAAACCGACGTGCAAG-3'	Primer1: 5'-TCGCAATACGACTACGCTGACC-3'
	Primer2: 5'-GCTGAAGTTAGTAGCTCCGCTTCC-3'	Primer2: 5'-AACTCTGAAGGAGACAAGCCCCTC-3'
Mouse: *Twist-LSL-Dre*	Primer1: 5'-CACGGAGGTATAAGAGCCGC-3'	Primer1: 5'-GCCCGCACGGAGGTATAAGA-3'
	Primer2: 5'-ACTTGCCCCTTGCTCCATAC-3'	Primer2: 5'-TTGCTCAGGCTGTCGTCGG-3'
Mouse: *Ucp1-Dre*	Primer1: 5'-CCTCTGGGCATAATCAGGAACTG-3'	Primer1: 5'-CCTCTGGGCATAATCAGGAACTG-3'
	Primer2: 5'-TAGTGCTTGTCGATGGTGGTAGAG-3'	Primer2: 5'-GCAGGCTCCAAACACCTAAACAAG-3'
Mouse: *Upk3b-Dre*	Primer1: 5'-TTTCCTGTTCTCCTGGCAGTCC-3'	Primer1: 5'-TTTCCTGTTCTCCTGGCAGTCC-3'
	Primer2: 5'-TAGTGCTTGTCGATGGTGGTAGAG-3'	Primer2: 5'-TGGCTAAGGGCATCCATTGC-3'
Mouse: *Wnt1-Dre*	Primer1: 5'-CGGCCCGCCTCCAGACTTATTA-3'	Primer1: 5'-CGGCCCGCCTCCAGACTTATTA-3'
	Primer2: 5'-CAGCCTTGCCCACCTTGAAAA-3'	Primer2: 5'-CTCATGGCCAGGCTCACAGACT-3'
Mouse: *Wt1-DreER*	Primer1: 5'-TATTACATCACGGGGGAGGCAGAG-3'	Primer1: 5'-GACACCGAGGGGACTCATTACTTAC-3'
	Primer2: 5'-CTGGCATCAGGAAGGAACAGAC-3'	Primer2: 5'-CTGGCATCAGGAAGGAACAGAC-3'
Mouse: *Zeb1-LSL-Dre*	Primer1: 5'-GCCTCGAGTGTCGTAAACCA-3'	Primer1: 5'-GCCTCGAGTGTCGTAAACCA-3'
	Primer2: 5'-ACTTGCCCCTTGCTCCATAC-3'	Primer2: 5'-GCTTTCTGCGCTTACACCTG-3'
Mouse: *Pdgfra-DreER*	Primer1: 5'-CCCAGGCATCGCTAAAAATCTTC-3'	Primer1: 5'-CCATCTTCTCCTTCCTTGCTGTAAG-3'
	Primer2: 5'-CAGTGGCTTTCTGTTTGGCTAATG-3'	Primer2: 5'-CAGTGGCTTTCTGTTTGGCTAATG-3'
Mouse: *Pdgfrb-CreER*	Primer1: 5'-AAGACTCACACGATACAACA-3'	N/A
	Primer2: 5'-TTGCGAACCTCATCACTCGTT-3'	N/A
Mouse: *R26-RSR-tdTomato*	Primer1: 5'-ACGGGTGTTGGGTCGTTTGTTC-3'	Primer1: 5'-CCGAAAATCTGTGGGAAGTC-3'
	Primer2: 5'-TTCTTGTAATCGGGGATGTCGGCG-3'	Primer2: 5'-GGCATTAAAGCAGCGTATCC-3'
Mouse: *R26-GFP*	Primer1: 5'-CAGCGACTTCTTCATCCAGAGC-3'	Primer1: 5'-AAGGGAGCTGCAGTGGAGTA-3'
	Primer2: 5'-AAAGCAGCGTATCCACATAGCG-3'	Primer2: 5'-CCGAAAATCTGTGGGAAGTC-3'
Mouse: *R26-tdTomato*	Primer1: 5'-GGCATTAAAGCAGCGTATCC-3'	Primer1: 5'-AAGGGAGCTGCAGTGGAGTA-3'
	Primer2: 5'-CTGTTCCTGTACGGCATGG-3'	Primer2: 5'-CCGAAAATCTGTGGGAAGTC-3'
Mouse: *CAG-Dre*	Primer1: 5'-ACTCCTTGCCGATGTTCCTCAG-3'	N/A
	Primer2: 5'-TTGTCCCAAATCTGGCGGAG-3'	N/A
Mouse: *Prox1-IRES-CreER*	Primer1: 5'-CACACACACACACGCTTGC-3'	Primer1: 5'-CACACACACACACGCTTGC-3'
	Primer2: 5'-GCCAGAGGCCACTTGTGTAG-3'	Primer2: 5'-GTGGAAAGGAGCGTACACTGA-3'
Mouse: *MMTV-PyMT*	Primer1: 5'-GGAAGCAAGTACTTCACAAGGG-3'	Primer1: 5'-CAAATGTTGCTTGTCTGGTG-3'
	Primer2: 5'-GGAAAGTCACTAGGAGCAGGG-3'	Primer2: 5'-GTCAGTCGAGTGCACAGTTT-3'
Mouse: *NR1*	Primer1: 5'-GCCTCTGCTAACCATGTTCATGC-3'	Primer1: 5'-TTGGAGGCAGGAAGCACTTG-3'
	Primer2: 5'-ATGTTTCAGGTTCAGGGGGAGGTG-3'	Primer2: 5'-TGGAGAAAAAGGAGAGAGGCATTC-3'
Mouse: *Mettl3-flox*	Primer1: 5'-TGCTGTGCCTTTCTTAGTTGTC-3'	Primer1: 5'-TGCTGTGCCTTTCTTAGTTGTC-3'
	Primer2: 5'-AGGCTCAGTCCTCCTCACAA-3'	Primer2: 5'-AGGCTCAGTCCTCCTCACAA-3'
Mouse: *Pparg-flox*	Primer1: 5'-TGTAATGGAAGGGCAAAAGG-3'	Primer1: 5'-TGTAATGGAAGGGCAAAAGG-3'
	Primer2: 5'-TGGCTTCCAGTGCATAAGTT-3'	Primer2: 5'-TGGCTTCCAGTGCATAAGTT-3'
Mouse: *β-Catenin-flox*	Primer1: 5'-AGAATCACGGTGACCTGGGTTAAA-3'	Primer1: 5'-AGAATCACGGTGACCTGGGTTAAA-3'
	Primer2: 5'-CAGCCAAGGAGAGCAGGTGAGG-3'	Primer2: 5'-CAGCCAAGGAGAGCAGGTGAGG-3'
Mouse: *Pten-flox*	Primer1: 5'-CTCCTCTACTCCATTCTTCCC-3'	Primer1: 5'-CTCCTCTACTCCATTCTTCCC-3'
	Primer2: 5'-ACTCCCACCAATGAACAAAC-3'	Primer2: 5'-ACTCCCACCAATGAACAAAC-3'
Mouse: *Plin1-dCreER*	Primer1: 5'-TGTGAAAGACAAGCCTGCGG-3'	Primer1: 5'-TGTGAAAGACAAGCCTGCGG-3'
	Primer2: 5'-TGCGAACCTCATCACTCGTTGC-3'	Primer2: 5'-CATTCCTATCCTTCTCTCCACGG-3'
Mouse: *Prox1-RSR-2A-CreER*	Primer1: 5'-TCCTTGTATCAGCAGGTTCCAGAG-3'	Primer1: 5'-ATGTCTCCTCTGAAACCCACGG-3'
	Primer2: 5'-ATGTTTCAGGTTCAGGGGGAGGTG-3'	Primer2: 5'-TCCCTTCTCCTGAAAACCAACC-3'